UNIVERSITY OF DURBAN - WESTVILLE

A STUDY OF HIGH VOLTAGE DIRECT CURRENT CONDUCTOR CORONA IN A PURPOSE BUILT CORONA CAGE

BY

GARY CHARLES SIBILANT,

BSC (MATHEMATICS AND APPLIED MATHEMATICS)

BSC (ELECTRICAL ENGINEERING)

A THESIS SUBMITTED IN PARTIAL FULFILLMENT OF THE REQUIREMENTS FOR THE DEGREE OF MASTER OF SCIENCE IN ELECTRICAL ENGINEERING AT THE UNIVERSITY OF DURBAN-WESTVILLE

SUPERVISORS:

PROFESSOR N.M. IJUMBA, PHD, PRENG, CENG

MR. A.C. BRITTEN, MSC, PRENG

MARCH 2003

ACKNOWLEDGEMENTS

I would like to thank The Lord, Jesus Christ, who is my God for giving me the strength and ability to have been able to complete this work. With Him by my side I know all things are possible. Even though I have often faltered, he has always been there for me.

I am eternally en-debited to my family who have given me the opportunities that they never had, especially my Mother and Father who have sacrificed so much to get me to where I am today. I will always be proud of you.

To Professor Nelson Ijumba who has guided me through this thesis, your valuable help and assistance is appreciated.

To Mr. A.C. Britten, who has always been there offering insight and forcing me to think in new directions, you have helped me more than you could imagine.

I would also like to thank the following people for their contribution to my work and who have given me the opportunity to work on this project, Arthur Burger, Mashudu Mulaudzi, Trevor Dudley.

I thank Logan Pillay of ESKOM resources and strategy for his role in keeping the HVDC project afloat.

Dr JP Holtzhausen, and the rest of the staff at the Stellenbsch University, High Voltage Laboratory.

Administrative and support staff at the university of Durban Westville, thank you for providing me with assistance during the construction of the Cage as well as during testing.

ABSTRACT

The main aim of this study was concerned with the design and commissioning of a corona cage, which could be used under Direct Current (DC) conditions. The cage was designed based on empirical formulas and equations as well as electric field simulations. The designed cage was then fabricated. The commissioning of the cage was undertaken in the High Voltage Direct Current (HVDC) laboratory at the University of Durban - Westville (UDW).

Tests to determine the effects of a silicone coating as well as wind on the corona performance of conductors were undertaken. The tests were done in order to determine ways of improving the corona performance of conductors under HVDC potential. The tests were carried out using various conductor surface conditions. The wind tests were made possible by using a powerful fan. A silicone coating was also used to determine the effects that it would have in mitigation of corona activity on HVDC conductors. The conductors were tested without the coating, with half of their length coated and then fully coated.

Results showed that the effect of wind on corona generation in a corona cage is minimal. The effect of the silicone coating was that it increased the corona currents measured in the corona cage. The conductors with no coating generated the lowest currents, the half coated conductors generated the second highest measured currents and the fully coated conductors generated the most corona.

Analysis of the increased currents showed that the increase in corona currents due to the silicone coating could be attributed to three factors. Firstly the coating caused an increase in conductor to cage capacitance. Secondly, partial discharges could have occurred in the silicone due to microscopic air particles and lastly, the increase in corona currents could be ascribed to the effect of the boundary conditions on the boundary between the conductor and the coating.

TABLE OF CONTENTS

LIST OF FIGURES

LIST OF TABLES

CHAPTER 1

INTRODUCTION

1.1 BACKGROUND AND RATIONALE

Corona performance is one of the more important criterion when it comes to the design and construction of a transmission line. The high voltages at which modern transmission lines operate have increased the corona problem to the point to which they have become a concern to the power industry. Consequently, these lines are now designed, constructed and maintained so that during dry conditions they will operate below the corona-inception voltage, meaning that the line will generate a minimum of corona-related phenomena. In foul weather conditions, however, water droplets, fog and snow can produce corona discharges. With the advent of line compaction, more time will have to be spent on determining the corona performance of the conductors to be used on that specific line, as under normal operating conditions the conductor surface gradient will be very close to the corona inception gradient for that specific conductor.

It therefore becomes clear that a tool, which can either predict the corona performance of a future line or generate corona data, which can be used in the design of a new line, would be invaluable. Several such tools exists, a corona cage is one such tool.

Corona cage tests are often used as a convenient and inexpensive means of obtaining the excitation functions defining the corona performance of AC conductor bundles, which in turn is used to predetermine the corona performance of a proposed AC transmission line design using the same conductor bundle. The main requirement is that the surface electric field and adjacent electric fields existing in the vicinity of the conductor bundle are accurately replicated when using the corona cage for testing.

Due to differences in space charge conditions existing between AC and DC transmission lines, with respect to the presence of corona on the conductors, corona on conductors under DC in cage conditions is not properly understood as yet.

Conductor corona performance (including Corona loss, Radio interference and Audible noise) as mentioned, is an important criterion when it comes to the design and construction of transmission lines. On Eskoms only HVDC line (The Cahora-Bassa line), the losses incurred are not clearly known as yet. The design, construction and testing of a small corona cage will help in quantifying and analyzing these losses.

The research for this thesis was conducted in such a manner that on completion, the following questions have been answered:

- What size cage should be used to accurately model field effects on the Cahora-Bassa Line?

  Under this question the following questions arise:

  - Will it be feasible to design a corona cage to test conductor bundles?
  - What should the length and radius of the cage be?

- Is a corona cage under DC conditions an accurate representation of corona effects on the line itself?
- What effect will the space charge phenomenon have on the fields in the cage?
- How does changing the surface condition of the conductor affect corona performance in a cage?

Once this project has been completed it is expected that Eskom will have a better understanding of DC corona performance. Technological expertise with regards to HVDC will be available within the confines of Eskom itself. As it is known that HVDC transmission will greatly increase in the next ten to twenty years, this expertise will greatly assist Eskom in the design of future HVDC lines as well as improving its current HVDC line (The Cahora-Bassa line).

A working HVDC laboratory has been established at the University of Durban Westville a former disadvantaged university in South Africa. This laboratory contains a small corona cage designed to allow corona to be studied under DC and AC conditions. This makes small-scale fundamental corona research possible at both undergraduate as well as postgraduate level. It will also be utilized by industry wishing to do corona research.

1.2 STUDY PROCEDURE

These are the procedures that were followed in order to complete this research.

- **A literature survey** was carried out which served as the foundation to my knowledge on corona and corona cages.

  Here the (Electrical Power Research Institute) EPRI books were thoroughly studied and assimilated. This was carried out at Megwattparks' as well as the TSI library in Gauteng

- **Contact was made** with various entities that have HVDC knowledge and expertise.

  This was done in an effort to establish what work has been done with respect to corona studies under DC conditions.

- **Visits to corona cages** were undertaken.

  A visit to the Stellenbosch corona cage as well as several visits to Eskom's corona cage at Megawatt Park was undertaken.

- **Design data** of the towers and conductors used was obtained from the Cahora-Bassa line.

  This was used to calculate the various parameters required for accurate modeling in a corona cage.

- **Electric field calculations** were performed to determine the dimensions of the corona cage to be used. The optimum cage size and conductor configuration design was thus found.

- **Tests** were performed in the HVDC laboratory at the University of Durban Westville. This was done under the supervision of Professor Nelson Ijumba and Mr. Tony Britten.

- **Simulations** of the fields were also done using computer software packages.

  This complimented the field calculations as well as the test results.

The literature that was reviewed covered the following topics:

- The use of corona cages for AC and DC conditions.
- Field effects on AC and DC lines.

- AC and DC corona cage design criterion.
- The effects of corona on AC and DC lines.
- Simulation of corona on DC lines using software packages.
- Radio interference on AC and more specifically DC lines.
- Audible noise levels on HV transmission lines with the emphasis on DC lines.

The following references have proven to be the most useful with regards to this research:

- IEEE Transactions on Power Apparatus and Systems
- EPRI Transmission Line Reference Book.
- EPRI HVDC Transmission Line Reference Book.

CHAPTER 2

CORONA

In this chapter the phenomenon of Corona is discussed.

- **Corona:** Corona is discussed under general AC conditions and then more specifically under DC conditions. Various corona modes as well as corona formation and mechanisms are presented.
- **Corona Loss:** Corona loss is expounded. The corona loss on AC and DC lines will be compared to each other. The factors which influence corona losses arfe discussed with specific attention being given to the factors influencing DC corona losses.
- **Radio Interference:** Radio interference is defined. The differences between AC and DC radio interference are discussed. The levels of RI on the Cahora Bassa line are stated.
- **Audible Noise:** Audible Noise will be discussed and defined. Differences between AC and DC audible noise levels will be discussed.

2.1 CORONA

The environmental effects produced by corona discharges on conductors play an important role in the design and operation of high-voltage transmission lines. Corona Loss (CL), Radio Interference (RI) and Audible Noise (AN) are the principal environmental consequences of corona on both AC and DC lines, while corona-generated space charge environment is also important in the case of DC lines.

In layman's terms corona can be described as the faint glow on the surface of electrical conductors under high voltages. This glow is caused by electrical discharges that occur when the electric fields strength on the surface of the conductor exceeds the electrical breakdown strength of air.

According to the IEEE Standard Dictionary of Electrical and Electronic Terms, corona is described as: " A luminous discharge due to ionization of the air

surrounding a conductor caused by a voltage gradient exceeding a certain critical value."

Corona discharges form at the surface of a transmission-line conductor when the electric-field intensity on the conductor surface exceeds the breakdown strength of air, which is about 30 kV/cm at standard temperature and pressure levels. This occurs when the conductor surface has irregularities, such as conductor nicks, air-borne particles (insects, weed and grass seeds, dust, etc.), or water-drops, all of which enhance the local electric field. This breakdown strength is controlled by a host of various conditions such as [11, 169]:

- Air pressure
- Electrode material
- Presence of water vapor
- Incident photo ionization
- and Voltage

Corona on power lines is mainly a statistical phenomenon. Scratches, displacement of strands, water droplets and dirt can cause corona discharges to start at a considerably lower surface gradient than that determining breakdown in air. Any irregularity on a conductor's surface causes a voltage gradient concentration that may become the point source for a discharge. The result of this breakdown of air in this region generates the following:

- Light
- Audible noise
- Radio noise
- Conductor vibration
- Ozone and other by products.

Generally, corona on high voltage (HV) lines causes losses, interference with telecommunication lines and radio receivers in the vicinity of the lines. For the purposes of this study, only Radio Interference, Audible Noise and Corona Loss will be considered. Pictures of corona activity are shown in figures 2.1 to 2.3.

Figure 2.1: Corona Activity on Conductor Hardware

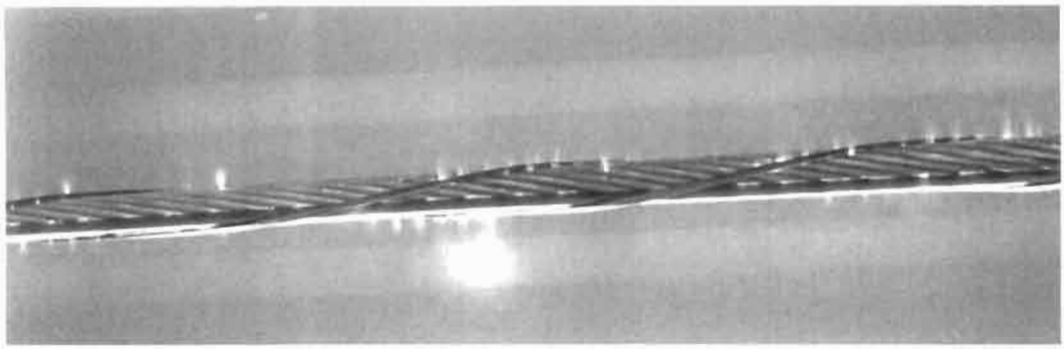

Figure 2.2: Corona Activity on a Conductor with Adlash

Figure 2.3: Corona Activity on Conductor Terminal Fittings

Corona is a member of a family of discharges called Partial Discharges (PD's). These discharges do not propagate the entire distance between two electrodes and therefore they are called partial discharges. They are limited to only a part of the dielectric material [8].

2.1.1 Basic Ionization Processes

If the levels of conductor surface electric fields are high enough, complex ionization processes take place in the air surrounding the high voltage transmission line conductors which results in the discharge known as corona.

Atmospheric air is the most important insulating material used on high voltage transmission lines. Although insulators are used for structural support, ambient air is the main insulating medium between high voltage conductors and their grounded support structures and the ground plane.

Atmospheric air consists mainly of water vapor and a number of gasses [4, 55]. The volume percentage of this water vapor depends on the ambient temperature and is highest at the equator and decreases towards the poles. The volume percentage of the gaseous content of dry air remains the virtually the same from part of the earth to another [4, 55].

Under normal conditions, the gaseous and water vapor molecules in air are electrically neutral, that is no electrons are either removed from or added to them. Naturally occurring phenomena however, prevents the air from staying electrically neutral. These phenomena are: [4, 56]

- Gamma rays produced by radioactive decay processes in the soil.
- Cosmic radiation
- Ultra-violet light.

2.1.1.1 Ionization and Excitement

An atom consists of a nucleus of neutrons and protons, surrounded by electrons in orbital motion. The number of electrons, which equal the number of protons in the nucleus, is different for each element. The number of neutrons in the nucleus determines the atomic mass of the element. The electrons occupy different orbits, characterised by different permissible energy states. The highest energy of the atom is found when the electron is in an orbit furthest from the nucleus and the lowest energy is found when the electron is in an orbit nearest the nucleus.

If enough energy is imparted on the atom to allow the electron in the outermost orbit to jump to the next permissible higher energy level, the atom is said to be excited. If enough energy is imparted on the atom so that the orbiting electron is dislodged

sufficiently far away from the atom, so that it will not return to its original state, then the atom is said to be ionized. The energy required for this ionization of an atom may be supplied in a number of ways. Depending on the amount of energy transferred, the atom may be either excited or ionized as described by the following equations: [4, 57]

$$A + e \Rightarrow A^{*} + e \qquad \{\text{Excitation}\}$$

$$A + e \Rightarrow A^{+} + e + e \qquad \{\text{Ionization}\}$$

In actual gas discharges, the electron energy distribution has to be taken into account in order to get an estimate of the process of ionization by electric collision. In view of this, Townsend defined a Coefficient (α) as follows:

This is defined as the number of ionization collisions that take place during a unit length movement of one electron. [17, 23]. This is sometimes referred to as Townsend's first ionization coefficient. From the above definition the following differential equation can be derived.

$$dn = n(x) \cdot \alpha \cdot dx$$

Where: dn is the number of new electrons freed.

n(x) is the number of electrons.

dx is the distance travelled.

Solving this equation over the distance between the electrodes gives the following solution.

$$n = n_0 \cdot \exp(\alpha x)$$

Where: n_0 is the number of electrodes at the negative electrode.

The solution shows that the number of positive and negative ions increases exponentially. This type of discharge is called an avalanche.

The coefficient α, changes with field strength, gas pressure and other conditions that influence the production of electron pairs [11, 170].

Ionization by positive ion impact is an improbable process except at energies much higher than those likely to be encountered in corona discharges. The energy required for excitation or ionization may also be derived from electromagnetic energy in the form of light, or from a photon with an energy level of $\boldsymbol{h\nu}$ where ν is the frequency of

radiation and h is Planck's constant. Photo-excitation and photo-ionization may be described by the following equations.

$$A + h\nu \Leftrightarrow A^{*} \qquad \text{(photo-excitation or photon emission)}$$

$$A + h\nu \Leftrightarrow A^{+} + e \qquad \text{(photo-ionization)}$$

Ionization by electron collision as well as by absorption of light play important roles in corona discharges. Other processes such as thermal ionization and shock ionization also occur, but do not affect corona discharges.

The ionization phenomenon is the major contributor to the corona power loss process. When discussing this phenomenon, two zones of activity must be defined. The first is the ionization zone, which is a very thin circumferential layer surrounding the conductor surface. The second zone encompasses the electrode and inter-electrode space and the region between each conductor and the ground plane. Within the ionization zone the high field strength causes high velocity particles to collide with air molecules. These collisions cause the Townsend's coefficient of ionization (α) to exceed the coefficient of electron attachment (η). Electrons are therefore removed from the atomic structure of the air molecules and are accelerated away from the negative conductor and toward the positive conductor. These high-velocity electrons then collide with other air molecules releasing additional electrons in an avalanche process. Ionization of air molecules occurs during this process. Ions carrying the same charge as the adjacent conductor are repelled from the ionization zone at initial velocities of about 1.4 cm/s for positive ions and 1.8 cm/s for negative ions for every V/cm of field strength [12, 18].

2.1.1.2 Electron Emission from Conductor Surfaces

Electron emissions from conductor surfaces is an important factor in gap discharges, especially in corona discharges in air. The electrons at the peripheral layer of atoms on the metal surface are free to move within the metal. These electrons must gain sufficient energy, however, in order to escape from the metal surface. [4, 60].

The energy needed to facilitate electron emission from a conductor surface may be supplied by different physical mechanisms, the more important of which include:

- Thermionic emission;
- Electron emission by positive ion impact;

- Field emission;
- Photo-electric emission.

Thermionic emission occurs at very high temperatures and is important in vacuum tubes. Field emission occurs at very high values of surface electric field and is important mainly in vacuum breakdown phenomena. Both these mechanisms do not play a role in gas discharges at normal atmospheric pressure and temperature.

2.1.2 Discharge Phenomenon

The basic ionization phenomenon which has been described in the preceding sections will be useful in understanding the various discharge phenomenon which occurs in gases.

Figure 2.4 shows a uniform electric field arrangement. A voltage, U is assumed to be applied between the electrodes, which are separated by a distance d, this produces an electric field of E = U/d.

At the cathode, free electrons are produced either by natural ionization processes or by artificial illumination with ultraviolet light. [4, 65].

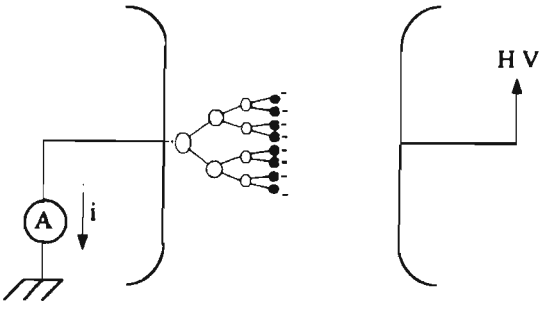

Figure 2.4: Gas Discharge in a Uniform Field Electrode Arrangement [4]

As the voltage is increased, the typical voltage current curve shown in figure 2.5 is obtained. This can be divided into three regions as follows [4]:

- For a voltage below U_0, the current increases, in a linear fashion, with the voltage in the beginning and then it saturates gradually as it approaches U_0. At lower voltages the current is produced by the movement of the free electrons, created either naturally or artificially, due to the electric field in the gap.

- As the voltage increases to a level above U_0, the current starts to increase exponentially. This current increases occurs as a result of the electrons gaining sufficient energy from the higher electric field in the gap to ionize the neutral gas molecules and create new electron-positive-ion pairs. These newly created electrons also gain sufficient energy to ionize other gas molecules, leading to a process known as cumulative ionization. This exponential rise in the number of electrons is known as an electron avalanche, this is shown in figure 2.6.
- Above a voltage U_1, the current increases very rapidly until flashover or electrical breakdown occurs at the voltage U_2. This rapid increase in the current is attributed to a process known as secondary ionization, which creates additional electrons at the cathode capable of initiating new electron avalanches.

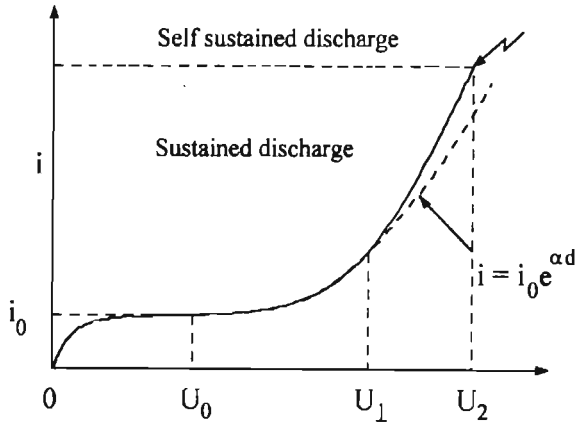

Figure 2.5: Voltage-Current Characteristic of the Discharge [4]

2.1.3 Corona Modes

Corona modes can be categorized into positive and negative polarity modes. For DC conditions, the conductor will exhibit either the negative or positive mode, depending on its polarity.

For the same polarity, corona can manifest itself in one or more modes depending on, the voltage applied, electrode shape and surface conditions. Each of these corona modes has different characteristics like, current shape, magnitude and frequency of pulses.

2.1.3.1 Negative DC Corona Processes

When the stressed conductor is at a negative potential, electron avalanches are initiated at the cathode and develop in a continuously decreasing field towards the anode. Free electrons which, can move much faster than ions in an applied field, are thus concentrated at the tip of the avalanche. A concentration of positive ions thus forms in the region of the gap between the cathode and the boundary surface S_0 [4, 67]. This is seen in figure 2.6.

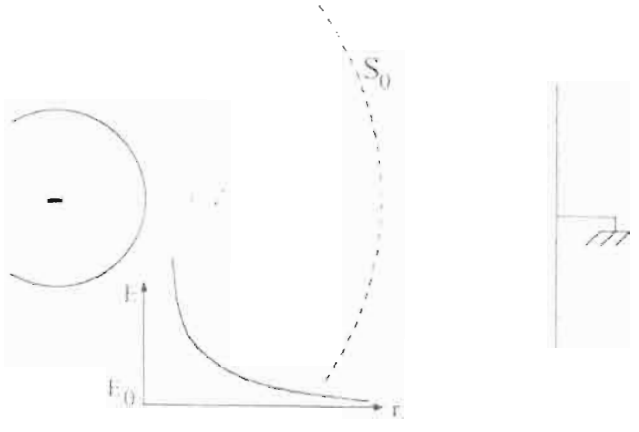

Figure 2.6: Electron Avalanche at the Cathode [4, pg 68]

As can be seen from figure 2.6 free electrons continue to migrate across the gap. Beyond the surface S_0 the free electrons quickly attach themselves to the oxygen molecules to form negative ions, which due to their low drift velocity accumulate in the gap beyond S_0. Once the development of the first electron avalanche has been completed there are two ion space charges in the gap as shown in figure 2.7.

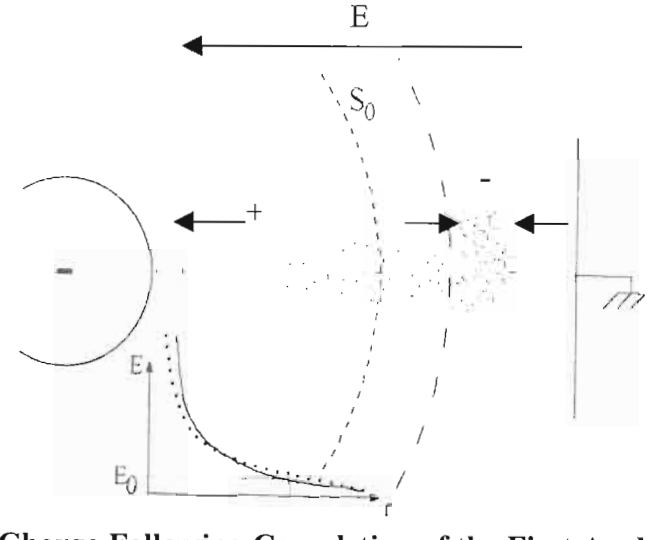

Figure 2.7: Space Charge Following Completion of the First Avalanche [4, pg 68]

From figure 2.7 it can be seen that the ion space charges in the gap produces a slight increase in the field near the cathode and a corresponding increase in the field towards the anode. A reduction in the field occurs in the middle of the gap. The effect of the space charge is such that it actually conditions the development of the discharge, producing three different modes of corona discharge with distinct electrical, physical and visual properties [4, 68].

These modes in order of increasing field intensity are [4, 69]:

- Trichel pulses
- Negative pulseless glow discharge
- Negative streamer discharge.

Trichel Streamer Discharge:

This discharge mode follows a regular pulsating pattern in which the streamer is initiated, develops and is then suppressed. A short dead time follows before the cycle is repeated. The duration of an individual streamer is short, about a few hundred nanoseconds, while the dead time varies from a few microseconds to a few milliseconds or more. The resulting discharge current consists of regular negative pulses of small amplitude and short duration, succeeding one another at the rate of a few thousand pulses per second. The streamer repetition rate is basically a function of the applied field. It increases linearly with the applied voltage. At high electric fields however the pulse repetition rate is reduced as a result of the establishment of a short-duration stable discharge system [4, 69].

Figure 2.8: Trichel Streamer Discharge [4, 69]

Negative Pulseless Glow Discharge:

If the voltage is now increased further, trichel pulses, after reaching a critical frequency, change over into a new mode of corona called a pulseless glow. The shift

is accompanied by a change in the visual manifestation of the discharge. The wandering of the discharge on the cathode terminates and it becomes fixed at one point. Pulseless glow corona exhibits typical features of a glow discharge. It is easily distinguishable by a bright spherical negative glow followed by a luminous conical positive column stretching outward from the point. The different parts of the discharge are separated by two dark spaces [4, 70]. With an increase in the voltage, the steady corona current increases continuously until, close to breakdown, it changes back to negative streamers.

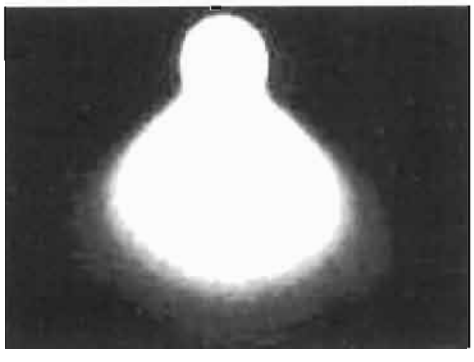

Figure 2.9: Negative Pulseless Glow [4, 70]

Negative Streamers:

As the voltage increases further, Negative streamers appear. The conical positive column reaches out with little branching. The current consists of pulses superimposed on a quasi-steady state current. The rise times of these pulses are in the order of $0.5*10^{-6}$s. The glow discharge characteristics observed at the cathode imply that this corona mode also depends largely on electron emission from the cathode by ionic bombardment while the formation of the streamer channel characterized by intensive ionization denotes even more effective space charge removal by the field [4, 71].

Figure 2.10: Negative Streamer [4, 71]

2.1.3.2 Positive DC Corona Processes

When the stressed electrode is positive in polarity, the electron avalanche is initiated at a point on the boundary surface S_0 and develops, in a continuously increasing field towards the anode. This is shown in figure 2.11 below.

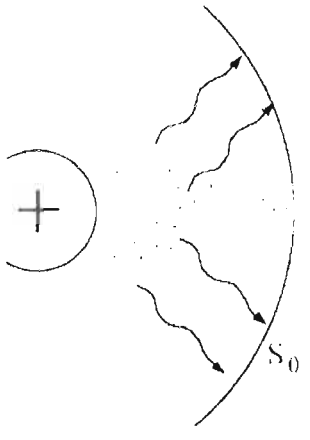

Figure 2.11: Avalanche Development Near Anode [4, 71]

This causes the highest ionization activity to occur at the anode. A positive ion space charge is left behind along the path of development of the avalanche, once again due to the lower ion mobility. Since there is a high electric field intensity near the anode, the effect of electron attachment is less than in negative corona, and the majority of free electrons that are created, are absorbed in the anode. Negative ions will be formed mainly away from the anode in the low field region.

Due to the presence of the positive ion space charge near the anode, a field enhancement in the gap is produced. This can be seen in figure 2.12. Photons released by excited molecules in the primary avalanche give rise to secondary electrons, which are accelerated in the enhanced field region and create secondary avalanches [4, 72]. This promotes radial propagation of the discharge in the gap, along a streamer channel.

There are four different corona discharge modes, each having distinct electrical, physical and visual characteristics which can be seen at the anode prior to the breakdown of the gap.

These modes in order of increasing field intensity are [4, 72]:

- Burst Corona
- Onset Streamer discharge

- Positive Glow discharge
- Breakdown Streamer Discharge

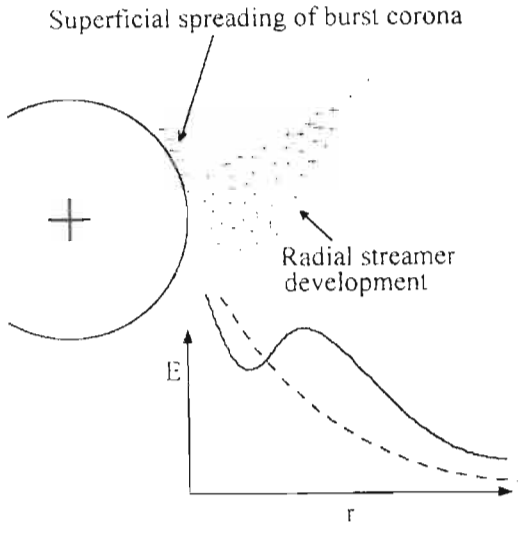

Figure 2.12: Successive Stages of Avalanche Development Near Anode [4, 72]

Burst Corona:

This discharge results from the ionization activities at the anode surface. These activities allow the highly energetic incoming electrons to lose their energy before their absorption by the anode. Positive ions are created, during this process, in the area directly next to the anode. They build up cumulatively and form a positive space charge that suppresses the discharge. The discharge current, which results from this, consists of small positive pulses, each corresponding to the spread of the ionization over a small area of the anode, and its ensuing suppression by the positive space charge produced [4, 73].

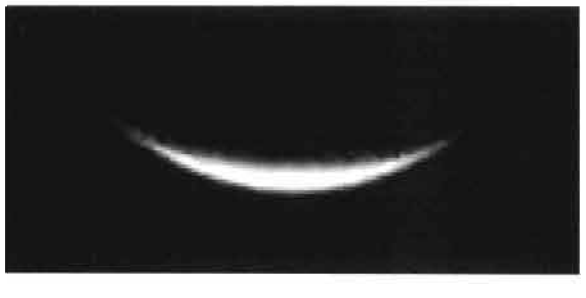

Figure 2.13: Burst Corona [4, 73]

Onset Streamer Discharge:

This mode of corona discharge results from the radial development of the discharge. The positive ion space charge formed adjacent to the anode surface causes, field

enhancement in its immediate vicinity and attracts subsequent electron avalanches. A streamer channel develops in the radial direction, which results in the onset streamer discharge. Onset pulses appear as streamers in a stem with some branching. They have a high branching repetition rate, which gives them a brush-like appearance. During the streamer development a considerable amount of space charge ion is formed in the low field region. The successive electron avalanches results and absorption of free electrons at the anode results in the formation of space charge in front of the anode. The electric field at the anode drops below the critical value for ionization and causes the suppression of the streamer discharge. In order for the applied field to remove the positive ion space charge and to restore the conditions necessary for the development of a new streamer, a dead time is required. As this discharge, develops in a pulsating mode, it produces a positive current pulse of large amplitude and relatively low amplitude [4, 73].

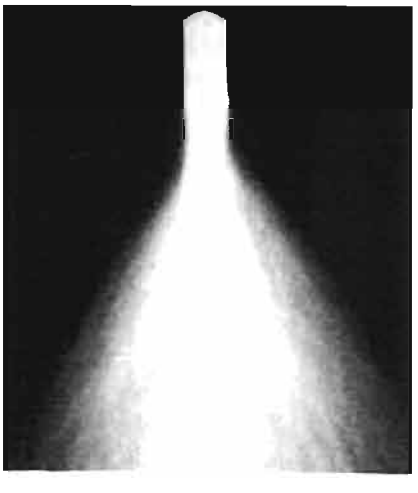

Figure 2.14: Onset Streamer [4, 74]

Positive Glow Discharge:

In this mode, ionization activity over the anode surface results in a thin luminous layer immediately adjacent to the anode surface, where intense ionization activity takes place. The discharge current is mainly a direct current. Over this current a small pulsating current component with a high repetition rate is superimposed. The development of this type of discharge can be interpreted as being a result of a particular combination of the rate of removal and creation of positive ions in the gap. The positive space ion is renewed from the anode, thus promoting surface ionization

activity. The negative ions mainly contribute by supplying the necessary triggering electrons to sustain ionization activity at the anode [4, 74].

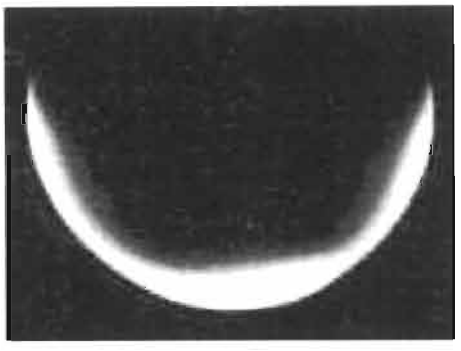

Figure 2.15: Positive Glow [4, 75]

Breakdown Streamer Discharge:

Breakdown streamers resemble onset streamers, but they get displaced from the axial position by the negative space charge. Positive streamers have velocities, which range from 20 to 20000 cm/μs. These streamers advance much faster than negative streamers due to photo ionization. The streamer discharge rise times are usually in the nanosecond range. The development of a breakdown streamer is directly related to the effective removal of the positive space charge by the high field intensity [4, 75].

2.1.3.3 AC Corona Modes

The electric field at the highly stressed electrode, the conductor, varies continuously with time, both in intensity and polarity under alternating voltages. Different corona modes occur in the same cycle of applied voltage. The corona mode, which occurs, can be easily identified by the discharge current.

For short gaps the ion space charge is created and absorbed by the electrodes in the same half cycle. The same corona modes that develop near onset voltages can be observed in the two half-cycles [4, 75].

- Trichel streamers
- Positive onset streamers
- Burst corona

For long gaps, the ion space charge created in one half cycle is not absorbed by the electrodes, but is drawn back to the region of high field intensity in the following half cycle and can influence the development of the discharge.

On practical conductors with a large diameter, it is more common to see, during the positive half cycle, onset streamers than the glow discharge. On very thin and clean wires only the glow mode of corona, sometimes referred to as ultra corona, occurs. This phenomenon has been exploited to obtain higher breakdown voltages of air gaps. Studies have been carried out on stranded conductors which were wrapped with thinner wires to eliminate pulsative corona and therefore reduce problems of RI and AN [4, 76].

2.2 Corona Loss

The literature on corona loss goes back to the beginning of the century, if not earlier. Corona loss is a power loss that occurs as a result of corona current that flows from the conductors of one polarity to the conductors of the opposite polarity or to ground.

The power transmission efficiency of a transmission line is decreased by corona loss since it adds to the resistance loss (RI^2) caused by the load current. [10, 3-149] Corona loss occurs only when there is corona activity on the transmission line or electrical conductor that is being considered. However the selection of conductor parameters is rarely affected by corona loss as, it is generally only a small fraction of the (RI^2) losses. In absolute values however, corona loss can be extremely high. For example an average yearly loss of about 25 W/m can be expected for a ±500 kV line. In the case of the Cahora Bassa line, which is about 1400km long, the losses incurred due to corona loss will be 35 MW per year.

2.2.1 Factors Influencing Corona Loss

In 1956 it was discovered that airborne substances such as insects, dust, vegetation, spider webs, bird droppings and other non-metal materials and not the imperfections on conductors as generally assumed, that produced fair weather corona loss on high voltage lines.

If care is taken to prevent the conductor being scratched during stringing, fair weather corona discharges are seldom experienced, except on non-metal projections on the line, after about one year of weathering. The metal protrusions, which remain after the first year, will produce only the glow type of corona discharge at or below the system operating voltage [11, 180].

Discharges can also occur when a small foreign particle like a speck of dust or snowflake or raindrop passes the conductor and initiates a discharge from conductor to particle. The discharge normally starts before the particle comes in contact with the conductor. This leads to an increase in corona loss.

The effect of water on conductor corona performance is quite significant. Water in the form of rain or drizzle, forms small drops on the upper surface of a conductor it comes in contact with. After some time the water runs down the strands forming a layer of water around the conductor. This eliminates many smaller drops on the top and leaves suspended drop at the bottom. As the water accumulates, drops will eventually form on the bottom and fall off due to gravity [11, 181].

Two extreme conditions may exist with regards to the degree of wetness that occurs on a conductor. They are:

- Hydrophilic
- Hydrophobic

If a surface is hydrophilic it implies that the surface "allows" the water to spread uniformly over it. On the other hand a hydrophobic surface would cause the water to bead up in small droplets, similar to water on a waxed surface.

Hydrophobicity has the effect of increasing the surface tension between the conductor and the water droplets. Local points of electric field intensification occur around these water droplets formed. This has the effect of decreasing the corona inception gradient and increasing corona loss.

The hydrophilic condition will decrease the surface tension between the conductor and the water. This leads to a decrease in electric field intensity around the water droplets and consequently a decrease in corona loss.

2.2.2 Differences Between AC and DC Corona Loss

Corona current of an HVDC line is dependent on line geometry; particularly pole spacing, this is as a result of the space charge. For an HVAC line, the corona loss is a function only of the conductor dimensions and of the corona-free surface gradient. This means that a change in the surface gradient on AC conductors has the same effect on the AC corona loss whether it is achieved by changing the voltage or by

changing the phase spacing. For HVDC lines on the other hand, the corona loss depends also directly on the pole spacing even if the corona-free conductor surface gradient is kept the same. In fact, a pole spacing that increases the corona-free surface gradient to the same value as an increase in the voltage has more of an effect on corona loss.

Another important difference between HVAC and HVDC corona loss is the change in loss due to the weather conditions. For example, 345 kV and 500 kV AC lines have negligible corona loss in fair weather; foul weather corona loss can be 100 or more times greater than fair weather corona loss [10, 3-150; 1]. On the other hand, fair weather DC corona loss is not negligible; but the increase in loss in the passing of weather conditions from fair weather to foul weather may not be as dramatic as for AC. It has been noted in some cases that foul weather DC corona is only 2-3 times larger than fair weather DC corona. [10, 3-150; 1]. Other tests have shown that the mean foul weather losses are 2-4 times more than fair weather losses [12, 19].

2.2.3 Factors Influencing Corona Loss on DC lines

Under both unipolar and bipolar operating conditions, conductor polarity has little significant effect on the corona losses incurred. The main differences occur under fair and rainy weather conditions.

The atmospheric variable with the largest impact on the corona loss is wind flow. Tests have shown that wind flowing perpendicular to the line has the largest effect on the corona current distribution at ground level, especially under bipolar lines. Laboratory tests have shown that corona loss increases with magnitude of the perpendicular component of the wind applied [4, 205]. Tests have shown that wind can increase the corona loss and RI by between 2 and 4 times [29].

After the creation of an ion by an electron – air particle collision, positive ions could attain a velocity of as high as 1.4 cm/s and negative ions up to 1.8 cm/s for every V/cm of field strength [12, 18]. It is known that the electric field strength rapidly attenuates with distance from the conductor and therefore the ion velocity is decreased by one or two orders of magnitude. Typical wind velocities are in the same range and will thus tend to move ions from the electric field lines, thus inducing a random dispersion of charged particles downwind from the line.

The wind will also remove ions from the ion cloud that forms around the energized DC conductor at gradients above corona onset. Under no wind conditions this ion cloud has the effect of creating a stable atmosphere around the conductor. The formation of this ion cloud of the same polarity around the conductor causes a suppression of further ion formation at the conductor surface. The wind, which removes this ion cloud, will move some of these ions to the opposite polarity field surrounding the other conductor. As a result of this the ion balance is disturbed and the conductor produces more ions in an attempt to restore the equilibrium.

As wind velocities increase, more ions are moved away from the conductors this causes, the corona current and the corona losses to increase [12, 31].

The effects of wind in corona cage conditions will be tested and documented in chapter seven.

2.3 Radio Interference

2.3.1 Definition of Radio Interference

One of the consequences of transmission line corona discharges is radio interference. Radio interference is a rather general term, which, by definition, refers to any unwanted disturbance within the radio frequency band, such as undesired electric waves in any transmission channel or device. This is also known as radio noise.

Pulses of current and voltage are produced on transmission line conductors by corona discharges, which are pulsating in nature. These pulses are characterized by rise and decay-time constants, in the order of a few nanoseconds to tens or hundreds of nanoseconds, and by repetition rates, which may be in the MHz range. As a result of this, the frequency spectra of these pulses can cover a considerable portion of the radio frequency band. The electromagnetic fields resulting from the corona discharges may, therefore, create unwanted disturbances in the operation of a transmission channel or device over a wide range of frequencies.

In theory transmission line radio interference can interfere with any radio frequency communication. This is dependent on factors such as, the distance from the transmission line to the communication-receiving device, the orientation of the receiving antenna, the transmission line geometry, and the weather conditions. The

level of interference may be such that the reception of the desired information is practically unaffected; or it may be such that reception is rendered completely unintelligible; or, it may range between these two extremes.

2.3.2 Differences Between AC and DC Radio Interference

Much radio interference research has been devoted to AC transmission lines and the design considerations for AC are similar to DC, however there are a few important differences.

Under AC conditions the highest levels of RI occur during wet weather conditions. Under DC conditions the highest RI levels occur during fair, dry weather. During wet weather conditions rain drops on the surface of the electrical conductors cause local field enhancements, due to their shape. This produces corona at electrical fields, which are much lower than the conductor electric field that exists in corona free conditions.

As a result of this there is an intense ionization of the air near the surface of the DC conductor and a large amount of space charge is produced. Due to this space charge there is an increase in corona loss and air ions. Space charge also has the effect of producing a fairly uniform ion cloud around the conductor and of maintaining the conductor surface electric field at the value of the rain - drop corona onset field.

Raindrop corona is not very impulsive under the above conditions, compared to most corona in fair weather conditions. This type of corona is more of a glow. Glow corona corresponds to steady noiseless charge emission from conductors into space. This does not occur on AC lines, due to the nature of the alternating electric field on the surface of the conductor that prevents the formation of a uniform ion cloud of the same polarity. As a result of this phenomenon, RI generation on DC lines is higher in fair weather than in wet weather [4].

The positive pole of a bipolar DC line produces more RI than the negative pole to such an extent that the RI produced by the negative pole can be ignored. This implies that, whereas AC-RI occurs on all conductors, DC-RI is limited to specific conductors. The reason for the positive pole producing more RI than the negative pole lies in the fundamental differences in the corona processes, which occur at these poles. Current pulses caused by corona have higher magnitudes and longer decay

times on a positive polarity conductor than on a negative polarity conductor. Consequently, corona on the positive polarity affects broadcast bands more than the negative pole [4]. Figure 2.16 below shows the lateral profile of RI under AC and DC conditions.

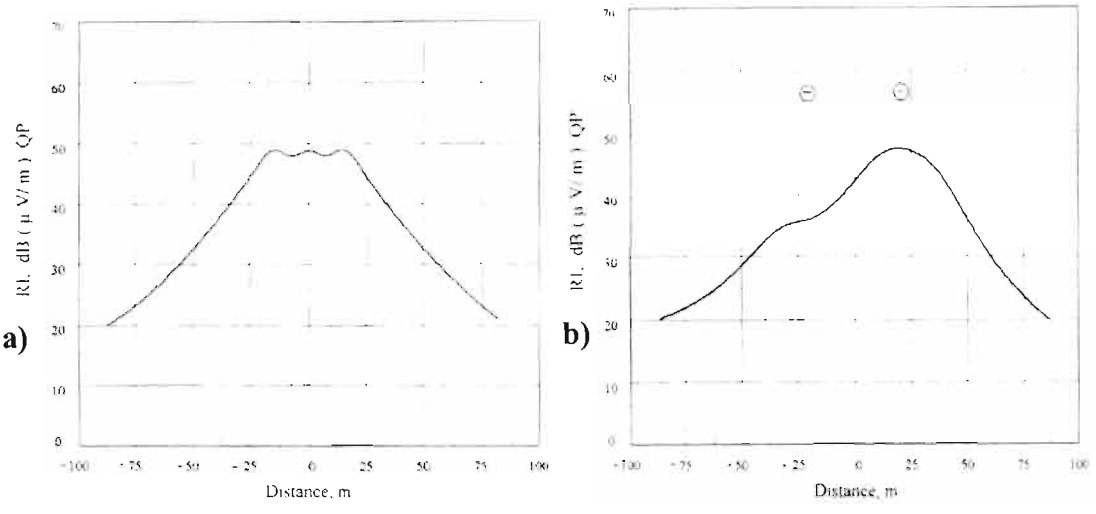

Figure 2.16: Lateral Profile of RI: a) AC, b) DC [4]

The measured levels of RI on the Cahora Bassa line are as follows:

- Negative Polarity 350 kV = -65 dBm.
- Positive Polarity 350 kV = -70 dBm.

These levels were measured on the shield wire of the Cahora Bassa line, using a Wandel and Golterman selective voltmeter.

2.4 AUDIBLE NOISE

2.4.1 Causes of Audible Noise

The Audible Noise (AN), emitted from high-voltage lines is caused by the discharge of energy that occurs when the electrical field strength on the conductor surface is greater than the 'breakdown strength' (the field intensity necessary to start a flow of electric current) of the air surrounding the conductor. AN can also be produced by intermittent flashovers of insulators in transmission line insulator strings.

AN from transmission lines, which is corona generated is very different from other environmental noises to which the public may be exposed to. Compared to traffic and aircraft noises, AN levels are generally lower but cover a much wider frequency

spectral range. The AN frequency spectrum also varies in level and shape depending on the weather conditions.

2.4.2 Differences between AC and DC Audible Noise

DC lines have the highest levels of AN under fair, dry weather conditions, compared to AC lines which experience higher AN levels under wet weather conditions. In wet weather conditions, ionization on DC lines is so high that irregularities on the surface of the conductor are surrounded by a high amount of space charge, which reduces the electric field at the conductor surface, as well as reducing the intensity of the corona current pulses. This results in audible noise generation on DC lines being less during wet weather than in dry weather.

[10] States: " The audible noise generated by each noise source on the conductor surface is a function of the characteristics of the source (its corona inception field), and of the electric field at the source. The electric field at the source, in turn, depends on the space charge generated by the source itself and by other corona sources that are nearby. This space charge reduces the electric field at the surface of the conductor below the nominal (corona-free) conductor surface field. If enough space charge is produced, the surface field is reduced below the corona inception field of the source and the source ceases to be in corona, until the space charge is driven by the electric field sufficiently away from the source. The time between bursts of corona from HVDC conductors, i.e. the 'relaxation time of HVDC corona' can vary from zero (practically continuous corona emission) to several seconds. HVAC corona is quite different from this phenomenon as the surface electric field varies at the applied frequency. The shape of the sources change due to erosion and dehydration caused by corona."

HVDC emissions that are almost continuous occur when the corona inception of the source is significantly lower than the corona free conductor field. In this case the corona current is either continuous or occurs in small pulses that do not produce audible noise. This occurs under wet weather conditions when raindrops decrease the inception field.

All of this means that HVDC AN, is a rather complex function of the nature and number of corona sources. Both, a source free conductor and a conductor with many

sharp (low corona inception field) sources, produces no or very little AN. The worst conditions occur with a critical number of critical sources per unit length.

The figure below compares the effect of rain on HVDC corona to that on HVAC corona.

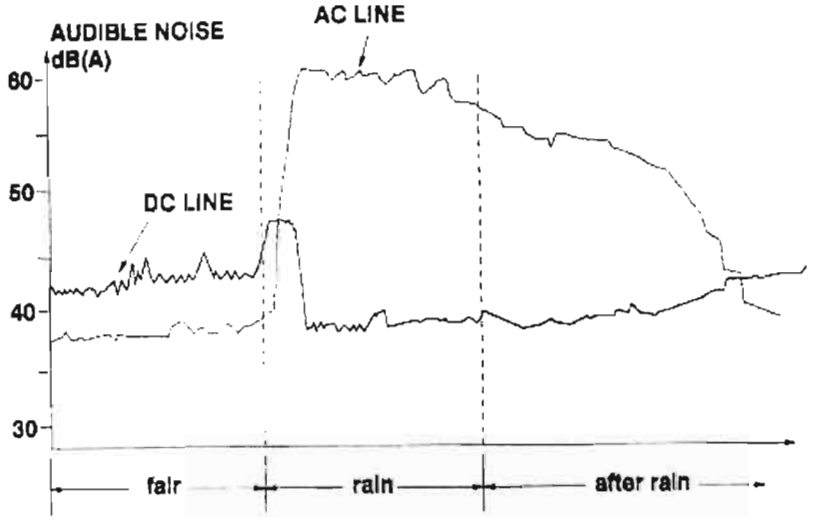

Figure 2.17: Differences Between AC and DC Audible Noise [10].

Once again, the positive polarity pole of a bipolar HVDC line produces more audible noise than the negative pole. AN generated by the negative pole can be ignored. On the positive pole pulses, caused by corona, have higher magnitude and larger decay times than on the negative polarity.

2.5 SUMMARY

Corona is a result of the voltage gradient, of a conductor or any voltage carrying equipment, exceeding a certain critical value. This critical value is dependent upon factors, such as

- Air pressure
- Electrode material
- Presence of water vapor
- Incident photo ionization and
- Voltage level

The phenomenon of corona results in the generation of various discharges, the main ones being:

- Light

- Audible Noise
- Radio Noise

Corona modes can be characterized under positive and negative polarity modes.

Negative DC polarity modes in order of increasing field intensity are as follows:

- Trichel pulses
- Negative pulseless glow discharge
- Negative streamer discharge

Positive DC polarity modes in order of increasing field intensity are as follows:

- Burst corona
- Onset streamer discharge
- Positive glow discharge
- Breakdown streamer discharge

Different corona modes occur in the same half cycle of applied voltage under AC conditions. The same corona modes that develop near onset voltages can be observed in the half cycles, namely:

- Trichel streamers
- Positive onset streamers
- Burst corona

The efficiency of transmission lines is decreased by corona loss, which adds to the RI^2 losses incurred by the line. Corona loss is influenced by a host of factors such as scratches, nicks and airborne substances.

HVDC corona current which, causes corona loss is dependent upon line geometry, particularly pole spacing, due to the effect of space charge. On HVAC lines however, corona loss is a function only of the conductor dimensions and the corona free surface gradient.

AC corona loss is negligible in fair, dry weather conditions while the same cannot be said for DC lines. AC wet, foul weather losses may be many times higher than the AC fair, dry weather losses. DC wet, foul weather losses may only be about 2-3 times as large as the wet, foul weather DC losses.

DC radio interference is more severe on the positive pole than on the negative pole. It is therefore limited to specific conductors only. The highest levels of DC radio interference occurs during fair, dry weather. The worst AC radio interference occurs during wet, foul weather conditions.

DC lines also experience the highest levels of audible noise under fair, dry conditions compared to AC lines that experience higher levels of AN under wet, foul weather conditions.

CHAPTER 3

CORONA TEST METHODS

This chapter describes the various methods, which are employed for corona testing.

There are normally two main objectives for experimental corona studies on conductors. These are:

- To gain a better understanding of the physical mechanisms involved in corona discharges as well as the resulting corona effects.
- To generate experimental data that can be used to develop prediction methods for the corona performance of transmission lines. [4, 238]

Since the discovery that conductor size has an influence on the current carrying capacity as well as the corona losses, laboratory as well as outdoor test methods, have been used to study different aspects of corona performance. The main corona test methods employed are as follows:

- Laboratory test cages
- Outdoor test cages
- Outdoor test lines
- Operating lines

3.1 Laboratory Test Cages

Laboratory studies have been carried out using a variety of electrode geometry's such as; point-plane, sphere-plane and concentric-spherical, in order to understand the physics of corona discharges. Studies of corona on cylindrical conductors have been mostly made in a configuration commonly known as a corona "cage". This configuration consists mainly of a test conductor placed concentrically inside another metallic cylinder with a much larger radius. The outer cylinder may be made out of a thin metallic sheet, but it is often made of some wire mesh. It is due to this wire mesh that it is called a corona cage.

Applying sufficient voltage between the conductor and the cage generates high conductor surface electric fields. Generally, voltage is applied to the conductor and the cage is maintained at close to zero potential by connecting it to ground via a small measuring impedance. In special cases, where fast-rising corona current pulses are to be measured, this may be reversed with the conductor being grounded and the voltage being applied to the cage.

The main benefit of the cage setup is that the conductor surface electric field distribution can be determined quickly and accurately. Early corona research was mainly carried out in laboratory corona cages. These cages have also been used to study the basic physics of corona discharges on cylindrical conductors at alternating as well as direct voltages. Corona characteristics studied in the laboratory include conditions for the occurrence of different AC and DC corona modes, corona pulse characteristics such as amplitude, pulse shape, repetition rate etc., corona loss (CL), radio interference (RI), audible noise (AN) and ozone generation.

For a cage of finite length, the electric field distribution in the longitudinal direction is uniform over the central section of the conductor and becomes non-uniform towards both ends. By adding a guard section of the cage at both ends, a central section of the cage may be selected to obtain a fairly uniform electric field distribution along the length of the conductor. The central section is used for corona measurements by connecting it to ground through appropriate measuring impedances. The two guard end sections will be connected directly to ground.

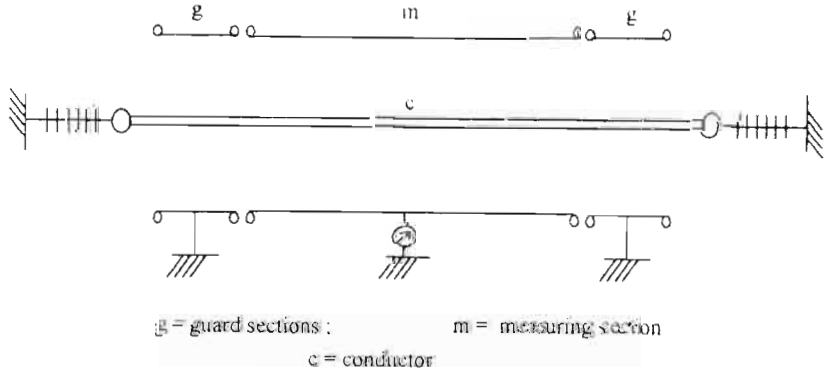

Figure 3.1: Electrical Diagram of Corona Cage [4, 239]

An important criterion for the design of any cage setup is to have an adequate margin between the breakdown and corona onset voltages. For the largest conductor to be tested the cage diameter should be small enough to obtain corona at a sufficiently low

voltage. This is due to the fact that the largest conductor in the cage will result in the lowest electric field gradient measured for the same applied voltage in the cage as when compared to a smaller diameter conductor. At the same time the air gap clearance between the cage and the conductor should be large enough so that the breakdown voltage is higher than the onset voltage. A margin of at least 50% between these two voltages permits studies to be carried out at different conductor surface gradients above corona onset.

Smooth as well as stranded conductors may be tested in laboratory cages. Conductor surface imperfections and water drops can also be simulated within the laboratory, using different types of metallic protrusions. Artificial contaminants, such as grease and sand have been used to simulate low values of conductor surface roughness factor and to study the corona performance of polluted conductors.

3.2 Outdoor Test Cages

To test conductor bundle configurations commonly used on transmission lines; the cage dimensions have to be much larger than what those of laboratory cages are. An outdoor cage also permits the experimental data collection to be obtained under natural weather conditions.

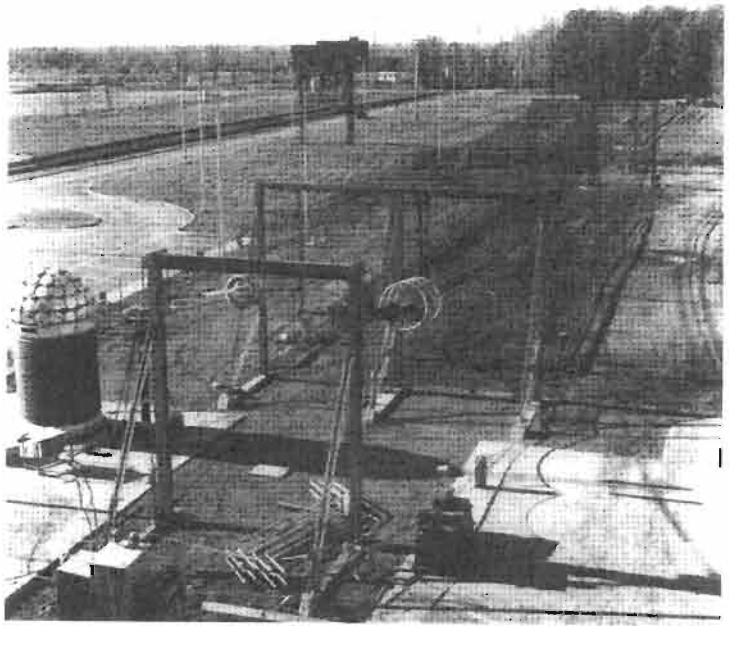

Figure 3.2: Outdoor Corona Cage [4]

An outdoor test cage arrangement consists essentially of conductor configurations placed at the center of a wire mesh enclosure that is either circular or square in cross

section. Outdoor corona cages are usually square because of difficulties in fabricating cylindrical cage enclosures of a large diameter. Conductor lengths in the order of hundreds of meters are required to properly simulate fair weather corona performance in cages whereas shorter conductor lengths are needed for to simulate foul weather corona performance. Outdoor cages have generally been used mainly to determine the corona performance under heavy rain conditions, by using artificial rain.

3.3 Outdoor Test Lines

Outdoor test lines are essentially short sections of full-scale transmission lines. They are used to obtain the statistical all weather corona performance of certain conductor configurations.

For AC corona studies, either three-phase or single-phase test lines can be used. Three phase test lines accurately reproduce the electric field conditions of normal transmission lines. Single-phase test lines are relatively less expensive to build and it is comparatively easier to use the test results for predicting the performance of long three-phase lines. An example of an outdoor test lines is shown in figure 3.3 below.

The entire inter-electrode region of DC transmission line is filled with space charge, which has an important effect on corona performance, therefore a single conductor test line can be used to study unipolar corona while a two conductor test line is necessary for bipolar corona studies [4].

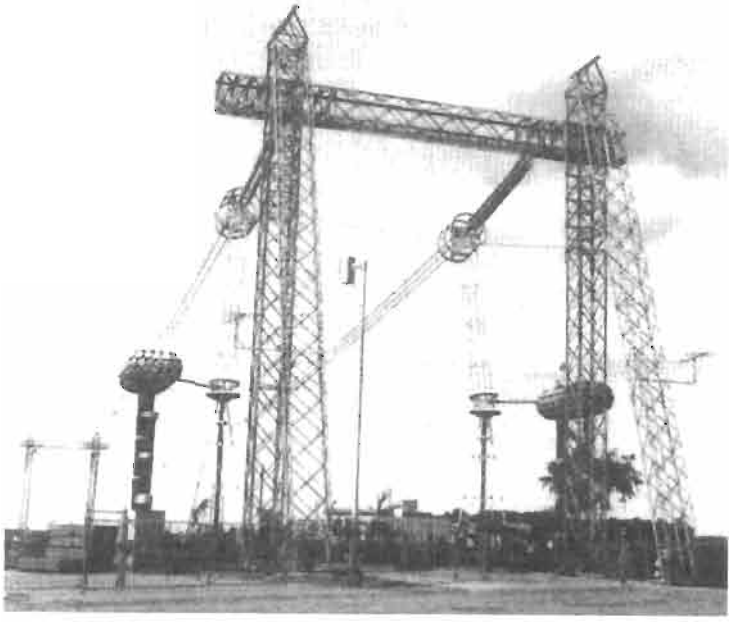

Figure 3.3: Outdoor Test Line [4]

3.4 Operating Lines

Corona performance measurements of operating high voltage AC and DC transmission lines are very useful for developing methods for prediction as well as for checking the validity of empirical methods. The instrumentation and methods used for measuring RI and AN from operating lines are similar to those for test lines. For the measurement of CL, however, the best source of data is from test lines and corona cages. For long-term measurements of RI and AN from operating lines it is also necessary to make simultaneous measurements of the weather variables.

Figure 3.4: A transmission line

3.5 Summary

Several corona test methods exist for corona studies. The choice of which method to use depends on a variety of factors. For the purposes of this study it was decided to use a laboratory corona cage. This was done due mainly to the following:

- The conductor surface electric field can be easily determined.
- Uniform field distribution.
- The effect of surface changes on the conductor can be easily tested.

This will be discussed in more detail in the following chapter.

CHAPTER 4

CORONA CAGE DESIGN

This chapter covers the design and construction of the Corona Cage in the High Voltage Direct Current (HVDC) laboratory.

The criteria used for the design of AC and DC corona cages are discussed. The design techniques used and associated calculations are presented here. The corona inception voltage for HVDC lines is discussed and calculated for the Cahora Bassa line.

The criterion used for the design of this specific cage is discussed, as well as the design techniques and constraints, which were considered during the design and construction process.

Cages were first built in the 1960's, primarily to study RI and CL. Audible noise only became an issue in the late 1960's. Ozone became an issue about a decade later. [7]

4.1 Electric Field Modeling

Electric field modeling of the cage and the conductor to be used was done with a software package called QUICKFIELD©. The corona cage can easily be modelled in any finite element simulation package, since its symmetrical properties simplify it to a one-dimensional problem. QUICKFIELD© was used to simulate a corona cage [23]. A very simple model was implemented and used. The results of which can be seen in figure 4.1. As is expected, the highest field intensity occurs around the conductors' surface while the lowest intensity occurs near the cage walls. It is this effect which allows corona studies to take place in a corona cage. We can obtain a very high electric field gradient on the surface of the conductor by using a relatively low applied voltage.

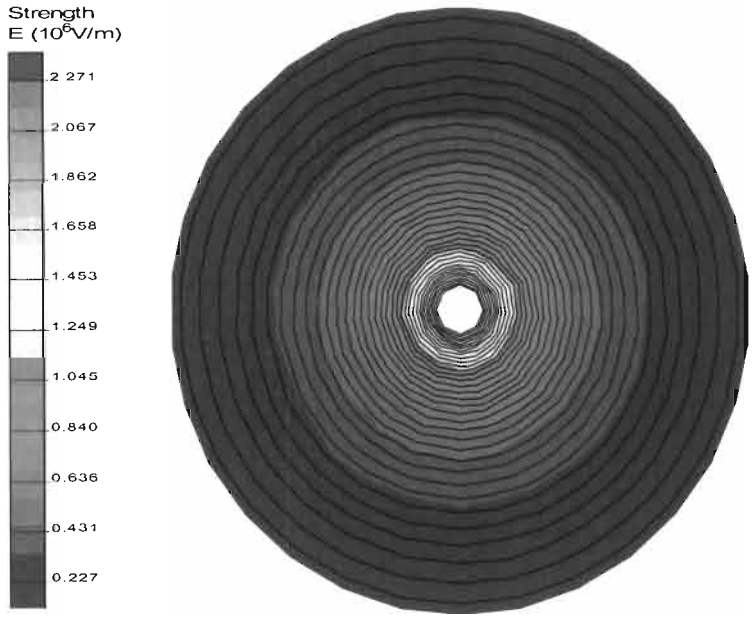

Figure 4.1: Electric Field Modeling of Conductor and Corona Cage

Figure 4.2 below shows the electric field model of the corona cage from a side view with a conductor strung up in the middle. The orange region is the field within the cage, the blue region is outside the cage. This shows the effect that the guard rings have on the field distribution in the cage. The ends of the cage shows how the field is non-uniform in that region, in the center of the cage we see that the field is totally uniform, with no fringing effects present at all. We only have slight field changes in the area where the outer rings are attached to the inner ring. These are the little yellow/green spots on the top and bottom of the orange region.

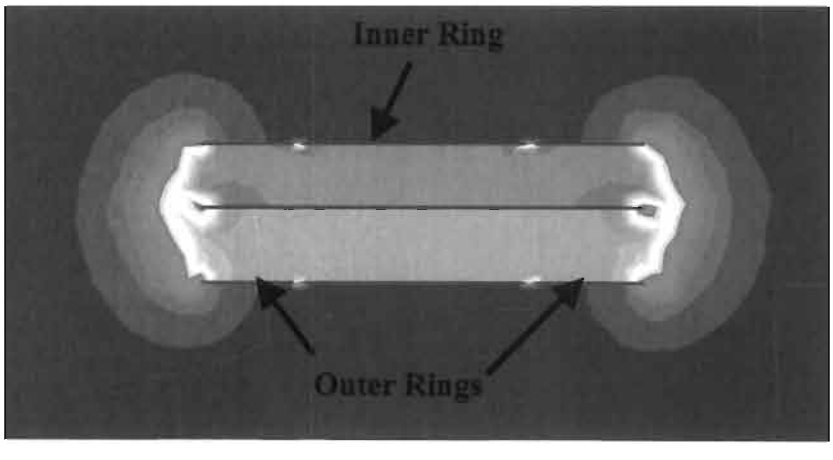

Figure 4.2: The elimination of the fringing effects on the inner ring

4.2 CORONA CAGE DESIGN

The main questions, which have to be answered in the design of a corona cage, are as follows:

- What size cage should be used to accurately model field effects, e.g. on the Cahora-Bassa Line? Under this question the following questions arise:
  - Will it be feasible to design a corona cage to test conductor bundles?
  - What should the length and radius of the cage be?

Secondary questions that arise with this specific DC cage are as follows:

- What size cage will be needed under the prevailing conditions, e.g. space constraints and source voltage limitations?
- What effect will the space charge phenomenon have on the fields in the cage?

4.2.1 Type of Cage

In order to determine what type of cage we need, we have to know the dimensions of the Cahora Bassa HVDC transmission line. This is shown in figure 4.3.

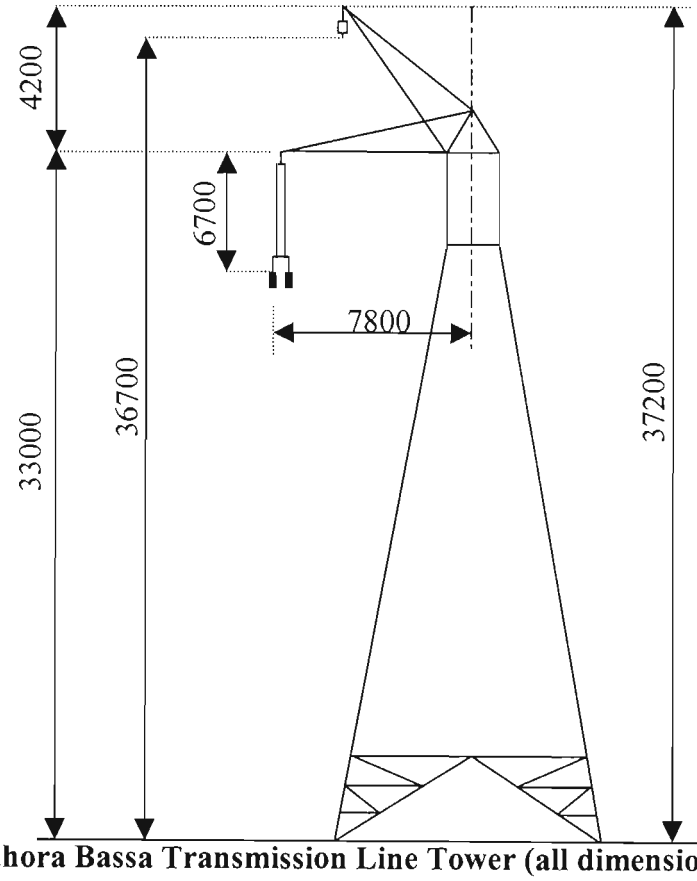

Figure 4.3: Cahora Bassa Transmission Line Tower (all dimensions in mm).

PARAMETER	DIMENSION
Minimum Ground Clearance	8.55m
Maximum Sag	16.25m
Spacing at Midspan	11m

Table 4.1: Cahora Bassa Transmission Line Data

Table 4.1 shows the clearances and sag that occurs on the line itself, this information is necessary for calculating the conductor surface gradients. The Cahora Bassa line uses a four-bundled conductor configuration. Which can be seen in figure 4.4.

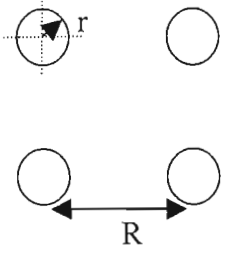

Figure 4.4: Cahora Bassa Conductor Bundle Configuration

Where: r = Sub-Conductor radius = 1.59cm.

R = Sub-Conductor spacing = 45 cm

4.2.2 Bundled Conductors

Bundled conductors are generally used, instead of single conductors, when the receiving end has a high power requirement. Bundled conductors, also reduces the electric field gradient, which a single conductor may experience.

The equivalent radius of bundled conductors is given by the following formula: [11, 22]

$$R_{eq} = \frac{A}{2}\sqrt[n]{\frac{n \cdot d}{A}} \qquad (4.1)$$

Where: A is the sub-conductor bundle diameter = $\sqrt{(2R)^2}$

n is the number of sub-conductors.

d is the diameter of each sub-conductor = 2r.

For the Cahora-Bassa line,

$$A = \sqrt{(2 \cdot 45)^2} \quad = 63.64cm$$

n = 4 and d = 3.18cm.

So,

$$R_{eq} = \frac{63.64}{2}\sqrt[4]{\frac{4 \cdot 3.18}{63.64}} = 21.276cm$$

We can take this value to be 21.3cm.

Peeks formula gives us the corona onset gradient which is independent of applied voltage:

$$E_c = E_0 \cdot m \cdot \delta\left[1 + \frac{K}{\sqrt{r \cdot \delta}}\right] \quad (4.2)$$

Where: m = roughness factor (we will assume this to be 0.8 for simplification)

δ = Correction factor also known as Relative Air Density

r = conductor radius in centimeters (R_{eq} in this case)

E_0 and K are constants.

Constant	AC	Positive DC	Negative DC
E_0 (kV/cm)	31	33.7	31
K	0.308	0.24	0.308

Table 4.2: Corona Inception Constants

$$\delta = \frac{p}{760} \cdot \frac{293}{(273 + t)} \quad (4.3)$$

Where: p = prevailing atmospheric pressure in mm of mercury

t = ambient temperature in degrees Celsius.

So for the Cahora-Bassa line: At 1800m the atmospheric pressure is given by:

$$760 - \frac{1800}{120} \times 10 = 610mmHg$$

So:

$$\delta = \frac{610}{760} \cdot \frac{293}{(273 + 25)} = 0.789$$

And E_c for positive polarity DC can now be calculated as follows:

$$E_c = 33.7 \cdot 0.8 \cdot 0.789\left[1 + \frac{0.24}{\sqrt{1.59 \cdot 0.789}}\right] = 25.83 kV/cm$$

This shows that for the particular conductor used the corona inception gradient is 25.83 kV/cm. This value is lower than the breakdown strength of air (which is 30 kV/cm). Under certain conditions this inception gradient may decrease, and then the line may go into corona.

From Literature [12, 22] we find an equation to calculate the maximum surface gradient which monopolar lines may experience.

$$g_{max} = \frac{2V(1+B)}{nd \ln \frac{2H}{R_{eq}}} kV/cm \qquad (4.4)$$

Where: V = voltage of one conductor (kV)

n = number of sub-conductors

d = diameter of sub-conductors (cm)

H = Line to ground clearance (Ave. height)(cm)

B = "influence" of charges on other sub-conductors comprising the bundle or bundling coefficient

Since the Cahora Bassa line uses a four-conductor bundle,

$$B = \frac{4.242d}{2c} \qquad (4.5)$$

Where: c = distance between sub-conductors in cm

d = diameter of sub-conductor in cm

Now:

- $B = 0.15$
- $V = 533$ kV
- $n = 4$
- $d = 3.18$ cm
- $c = 45$ cm
- $H = 1497$ cm (Height – 2/3 of the sag).

The inception gradient is not very close to the maximum operating surface gradient, so under normal operating conditions the Cahora Bassa line will not go into corona. However the actual roughness factor could be lower than the roughness factor of 0.8 used to calculate the inception gradient. This would decrease the corona inception gradient, which could lead to the operating gradient being much closer and even above the corona inception gradient. The table below gives the inception gradient for the Cahora Bassa line configuration for various conductor surface roughness factors.

Table 4.3 shows that as the surface roughness factor decreases, so the chances, of the conductor, going into corona increases. It is important to keep in mind that the maximum conductor surface gradient that the line will experience under normal conditions is 19.49 kV/cm. The table shows that if the roughness factor of the conductor drops to 0.6 or below, the conductor will go into corona.

CONDUCTOR SURFACE ROUGHNESS FACTOR	CORONA INCEPTION GRADIENT
1	32.29
0.7	22.60
0.6	19.37
0.5	16.15
0.4	12.92

Table 4.3: Corona Inception Gradient for Different Roughness Factors

4.2.3 Cage Required to Model Bundled Conductors

The cage diameter required to accurately model corona conditions that occur on the Cahora Bassa line, can be determined as follows: using the formula for calculating the gradient of concentric cylinders, which is as follows:

$$E_c = \frac{V}{a \cdot \ln\left(\frac{b}{a}\right)} \qquad (4.6)$$

Where: V is the applied voltage

a is the inner radius

b is the outer radius

Now making b the subject of the formula we get:

$$b = a \cdot \exp\left[\frac{V}{a \cdot E_c}\right]$$

Using a = 21.3cm (this is R_{eq} for the Cahora Bassa line which was calculated earlier) and V = 200kV and E_c = 25.83kV/cm (which is the positive corona inception gradient calculated for the Cahora Bassa line) we find that b = 30.64cm. This means that the diameter of the cage should be about 62cm.

In order to ensure that the cage accurately models the in-service conditions of the conductors on the Cahora Bassa line, it is has been said that the corona cage diameter has to be at least 3 - 5 times the sub-conductor spacing. This means that the cage will have to have a minimum diameter of 1.35m - 2.25m. As well as having a large diameter, the length of the cage would have to be about 18m. This length was derived using the ESKOM corona cage as a reference and scaling according to the diameter. The length of the cage needs to be sufficient in order to eliminate any fringing, which may occur, as well as to ensure electric field uniformity along the conductor.

It is interesting to note that the results of the calculations presented above, contradict the diameter having to be 3 - 5 times the sub-conductor radius. The necessity of having a large conductor to cage wall distance could be attributed to the phenomenon of flashover. A large enough spacing will prevent flashovers from occurring. This was, demonstrated by Tomkins in his thesis [26].

To ensure that a uniform field distribution along the central section of the conductor is obtained, the length of the cage has to be fairly long, at least 3 - 5 times the diameter. However with the use of end rings (as discussed in chapter 3), this criterion is greatly reduced. We can now obtain a uniform field distribution with a much shorter length of cage.

Due to the weight of the bundled conductors a hydraulic tensioning system would have needed to be included in the cage design, to ensure that the conductors are accurately tensioned and strung. This design would mean that the cage would have to be installed in an outdoor location. Due to space constraints in the laboratory at the

University of Durban Westville as well as the cost of constructing such a cage, it was decided that it was not feasible to further pursue the design of this type of cage.

As the cage needs to fulfill the added role of being a teaching tool, it was more feasible to design a single conductor cage. If a cage were designed to test bundled conductors it may not have been accessible to undergraduate students for experimentation purposes due to the costs and labor intensity of stringing conductors up in the cage. Due to these factors, a single conductor corona cage was instead decided upon and designed.

From here on all calculations and designs presented will refer to a single conductor corona cage. The source voltage was assumed to be 200 kV at sea-level as at the time of the design, the source voltage was not known, therefore a conservative estimate of 200 kV was chosen.

4.3 Electric Field Calculations For A Single Conductor Corona Cage

A corona cage that is used for testing a single conductor can be accurately modeled as a co-axial cylinder. The formula for maximum surface gradient in such a configuration is the same equation as 4.6 which, is as follows:

$$E_{max} = \frac{V}{a \cdot \ln\left(\frac{b}{a}\right)} \qquad (4.7)$$

Where: V = applied voltage in kV.

a = inner radius in cm.

b = outer radius in cm.

Each conductor will have a different corona inception gradient, which is dependent upon its diameter r, its surface roughness factor m, and the Relative air density (RAD) δ. Peek's formula gives us the relationship between the corona inception gradient and these factors.

Peeks formula is as follows: [12]

$$E_c = 33.7 \cdot m \cdot \delta \cdot \left(1 + \frac{0.24}{\sqrt{r \cdot \delta}}\right) \qquad (4.8)$$

Now assuming m = 0.8 and δ = 1 (RAD at sea level) and using r = 1.59cm,

$$E_c = 32.10 kV/cm$$

This clearly shows that the corona inception gradient for this type of conductor at sea level is at 32.10 kV/cm. So in order to simulate corona conditions in the cage, a conductor surface gradient of at least 33 kV/cm will have to be obtained using this particular conductor.

To determine the cage diameter necessary to simulate this condition accurately, simulations were carried out. The simulation was carried out as follows. Equation 4.7 was used and the cage diameter varied to see which diameter would be optimal, the results of this is shown in figure 4.5. These tests were conducted assuming RAD = 1, surface roughness factor = 0.8 and supply voltage = 200 kV.

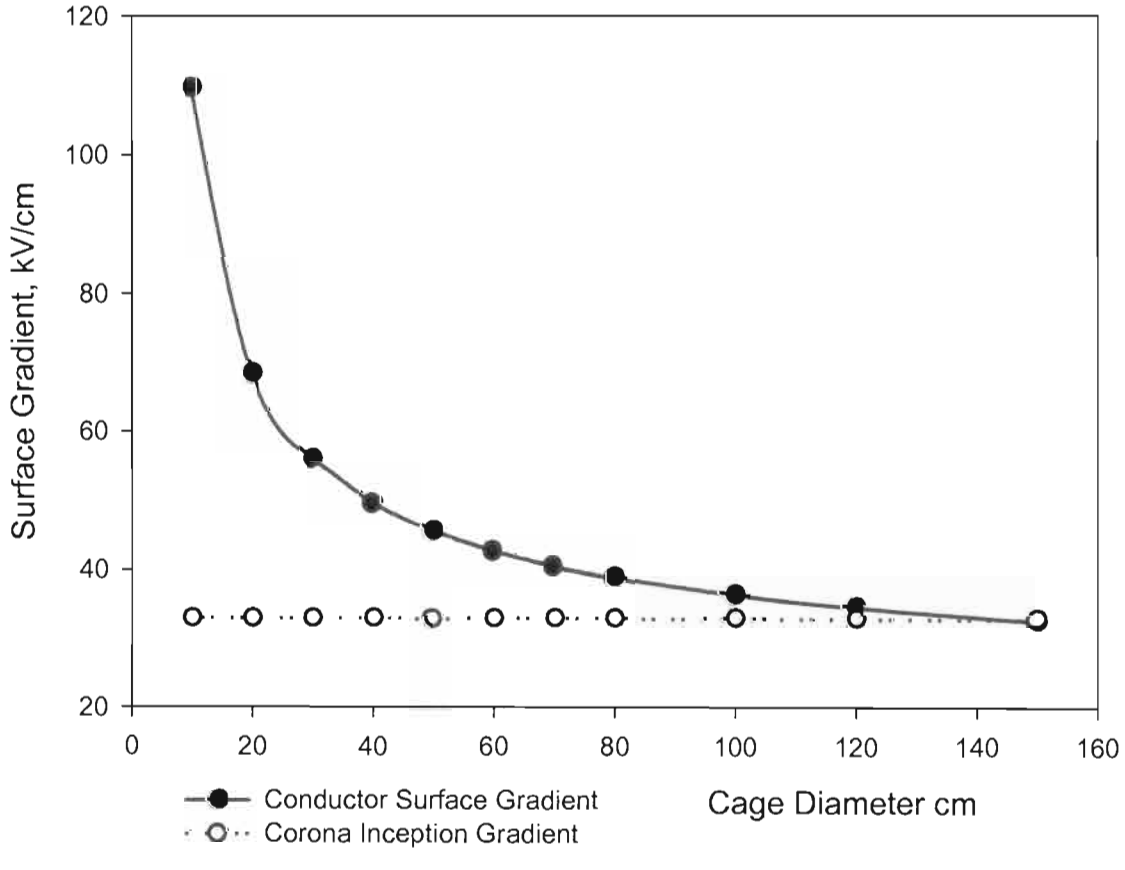

Figure 4.5: Conductor Surface Gradient for Cahora Bassa Conductor with Varying Cage Diameters.

From the figure above we can see that the surface gradient of the conductor, for the range of cage diameters used will safely exceed the corona inception gradient of the conductor.

A diameter of 150cm was chosen. This would ensure that the inception gradient would be exceeded while providing the largest conductor to cage distance. However

the corona cage should also be able to test conductors of different radii. This is to ensure its viability. A varying diameter cage was also discussed after a visit to Stellenbosch University's high voltage laboratory where such a cage is in use. However due to complications with regards to the construction of such a cage a decision was made to have one with a fixed diameter.

A second test was performed to determine the feasibility of a cage with a diameter of 150 cm. In this simulation the cage diameter and all other values were kept constant, while the conductor diameter was varied. The graphical results of these simulations are shown in figure 4.6. The figure shows that a corona cage with a diameter of 150cm can be used to test corona phenomenon on all conductor diameters from 0.1cm up to about 4cm. The conductor surface gradient induced by the cage exceeds the corona inception gradient for conductors with diameters in the given range. This ensures that the cage can be used to test most conductors used by ESKOM both for DC and AC voltages. It should be noted that under DC conditions the conductor will be monopolar with the cage connected to earth.

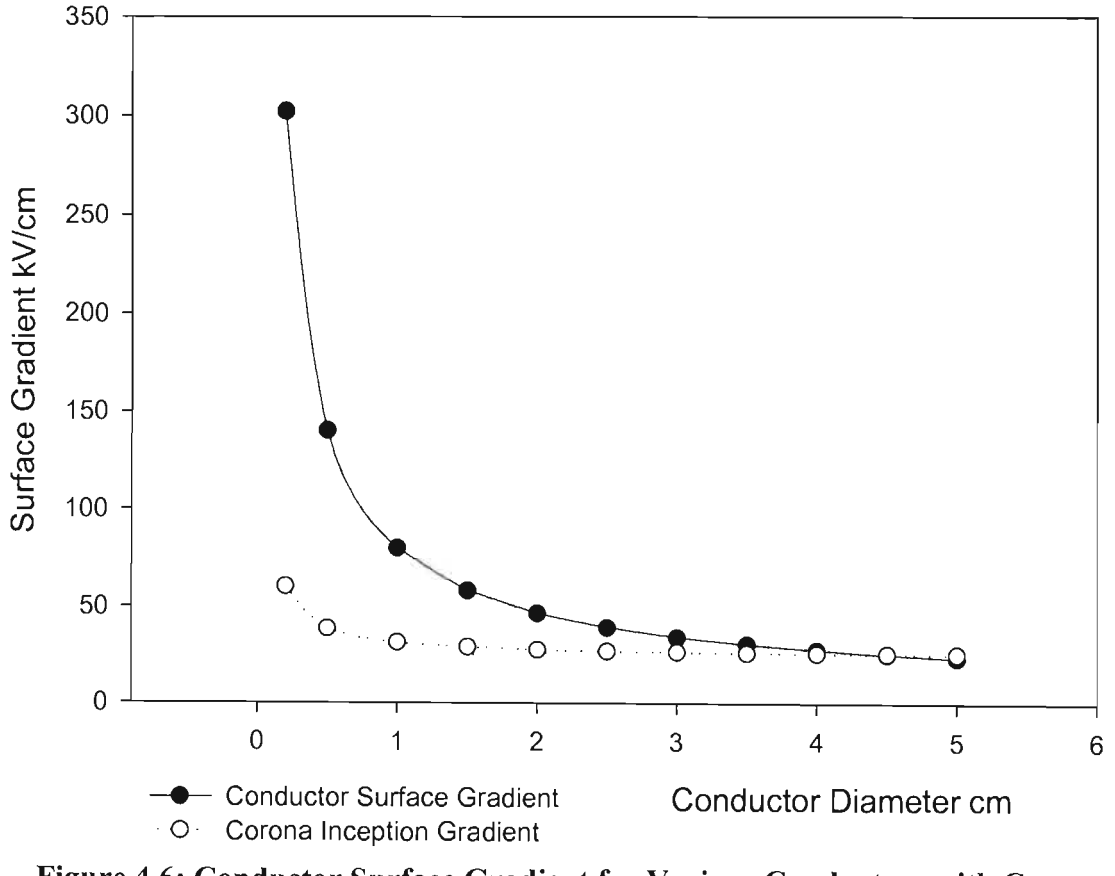

Figure 4.6: Conductor Surface Gradient for Various Conductors with Cage Diameter Fixed.

It would be possible to test conductors with larger diameters in the cage this would be achieved by increasing the supply voltage (which can go up to 500kV) until the conductor surface gradient exceeds the corona inception gradient for that particular conductor. All the simulations were based on a supply voltage of 200kV, this was done so in order to allow for any unanticipated difficulties with exceeding the corona onset voltage. If any of these occur, the voltage could be increased in order to put the conductor into corona.

Based on the simulation results, the diameter of the cage was decided upon. Next, the length of the cage had to be defined. From studying the Stellenbosch cage, it was deemed feasible to have a cage of similar length, which will be approximately 2m. Since the length of the cage has to be approximately 2 to 3 times the distance of the conductor to the cage [27]. This will eliminate any fringing effects at the ends of the cage. The mounting design of the cage follows the Stellenbosch design quite closely [26].

It has to be noted that the cage could also be fitted with a sprinkler system, this is so that the effects of rain on the conductor, both at positive and negative polarity can be tested and the results documented. The sprinkler system could, possibly be designed by other students doing corona work in the cage.

To ensure that the cage can be used for testing, through the entire spectrum of service conditions, which may occur on the line, the maximum surface gradient that the Cahora Bassa conductor may experience has to be known, this was earlier calculated to be 32.10 kV/cm. From the simulations presented above it has been shown that this surface gradient will be obtained within the cage without exceeding the DC source voltage of 200kV, thus ensuring that corona studies may be undertaken in such a cage. A detailed discussion on the design and construction of the cage and support structure can be found in Appendix A.

4.4 The Effect of Space Charge

Electric fields are vector quantities having magnitude and direction. The space charge density on the other hand is a scalar quantity having only a magnitude. Space charge density is essentially composed of two classes of charge carriers i.e.

- Small air ions and

- Charge aerosols

The two carriers are distinct due to their mobility and their nature.

4.4.1 Space Charge Behaviour

The behavioral pattern, of the Space charge phenomenon is easily visualized and can be described in qualitative terms. Near the conductor, small air ions, which are corona generated, are subject to a force caused by the constant polarity electric fields. These ions are also subject to convective forces by the wind as they move away from the line and the electric field due to the line decreases. If the conductor surface gradient increases, due either to increased voltage or a decrease in the radius of curvature of the conductor, the corona activity will obviously increase. This increased corona activity produces more small ions, which fill the region between the electrode and ground, which increases the electric field and small ion density [6, 696]. When the applied voltage is above the corona onset voltage, unipolar DC corona in air manifests itself in the space beyond the ionization layer, as a steady unidirectional flow of charged particles away from the coronating electrode. The flow of ions is steady and is determined by the magnitude and direction of the local electric field intensity vector $\vec{E}$. The conventional methods of describing DC ionized fields make use of several simplifying assumptions. They are as follows [5]:

- Ionic mobility's are constant (independent of electric field magnitude)
- Positive and negative ion mobility's are equal.
- The diffusion of ions is neglected
- The effect of wind, humidity and aerosols is neglected.

4.4.2 Bipolar and Unipolar Space Charge Effects

There is also a difference between the corona loss performance of unipolar and monopolar DC lines. On bipolar lines both the positive and negative polarity conductors, simultaneously present corona activity. Three space charge regions may be identified in such a case.

- A Positive unipolar region between the positive conductor and ground,
- A Negative unipolar region between the negative conductor and ground
- A Bipolar region between the two conductors.

In the bipolar regions, ions of both polarities mix which leads firstly to a reduction in the net space charge and secondly to a recombination and neutralization of the ions. This mixture of ions of opposite polarity reduces the effective space charge and results in a lower screening effect.

In the unipolar region, a screening effect is produced by the space charge present in the inter-electrode region. Lowering the electric field in the vicinity of the conductor and consequently reducing the intensity of ionization achieves this. This stabilizes the discharge activity and limits the corona current [10, 193].

Therefore, in bipolar cases, the corona current will be higher than in a corresponding unipolar case, since larger total amounts of positive and negative charges will have to be emitted to produce the same screening effect. Since corona loss is dependent upon the corona current, it leads to the conclusion that corona loss is higher in bipolar cases than in corresponding unipolar cases [4].

4.4.3 Calculation of the Space Charge Effect

From Gauss's Law, the divergence of the electric field intensity $\vec{E}$ is related to the charge density ρ by a constant. Also known as Poisson's equation.

$$\nabla \cdot \vec{E} = \frac{\rho}{\varepsilon_0} \qquad (4.9)$$

Where ε_0 is the permittivity of free space, a constant. The current density is given by the following equation.

$$\vec{j} = k\rho\vec{E} \qquad (4.10)$$

Where, k is the ionic mobility. The divergence of the current density is as follows:

$$\nabla \cdot \vec{j} = 0 \qquad (4.11)$$

Equations, 4.9, 4.10 and 4.11 describe the unipolar ionised field [3, 718-731].

Since the corona cage and conductor can be modelled as coaxial cylinders the problem can be reduced to a one-dimensional problem, due to the symmetry involved. I.e. the distributions of the potential φ, the electric field $\vec{E}$, and space charge ρ, are functions of the radial co-ordinate r, only. Figure 4.7 shows the corona cage configuration. (Not to scale)

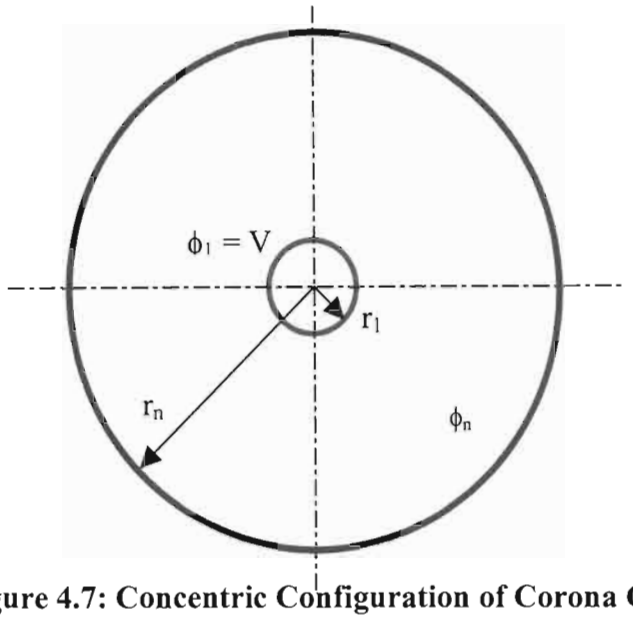

Figure 4.7: Concentric Configuration of Corona Cage

Where: ϕ_1 = the conductor voltage V.

r_1 = conductor radius.

ϕ_n = cage voltage = 0V.

r_n = cage radius.

In this geometry the exact solutions of the potential φ, the electric field $\vec{E}$, and space charge ρ, within the corona cage for the region R, (r_1<R<r_n), are known and are given in the closed form by the following formulae [15].

$$\varphi(r) = V - k_1 \cdot \left\{ f_1(r) - k_2 + k_3 \cdot \left[\ln\frac{r}{r_1} + \ln(k_3 + k_2) - \ln(k_3 + f_1(r)) \right] \right\} \qquad (4.12)$$

$$E(r) = \frac{k_1}{r} \cdot f_1(r) \qquad (4.13)$$

$$\rho(r) = \frac{\sqrt{r_1 \cdot E_0 \cdot \varepsilon_0 \cdot \rho_s}}{f_1(r)} \qquad (4.14)$$

Where: $k_1 = \sqrt{\dfrac{r_1 \cdot E_0 \cdot \rho_s}{\varepsilon_0}}$

$k_2 = \sqrt{\dfrac{r_1 \cdot E_0 \cdot \varepsilon_0}{\rho_s}}$

$k_3 = \sqrt{k_2^2 - r_1^2}$

$$f_1(r) = \sqrt{r^2 + k_2^2 - r_1^2}$$

$$\rho_s = \rho(r_1)$$

ρ_s can be determined implicitly by the transcendental equation:

$$V = k_1 \cdot \left\{ f_1(r_n) - k_2 + k_3 \cdot \left[\ln\frac{r_n}{r_1} + \ln(k_3 + k_2) - \ln(k_3 + f_1(r_n)) \right] \right\} \qquad (4.15)$$

Where: V is the applied voltage.

ε_0 is the permittivity of free space.

E_0 is the electric field at the surface of the coronating conductor, equal to the onset value in air, (this is found using Peeks formula).

Now for a simple example, lets use V = 200 kV, r_1 = 1.59 cm, r_n = 75 cm, E_0 = 28.25 kV/cm and $\varepsilon_0 = 8.85*10^{-12}$ F/m.

The value of k_1 was found to be 1044.595, k_2 = 43.00, k_3 = 42.97 and $\rho_s = 2.15*10^{-10}$.

These values are specific to the Cahora Bassa conductor, but can easily be changed to determine the k values for any type of conductor. The k's are found using an iterative process, which is based on an EXCEL© spreadsheet.

E_r which is the gradient in the presence of space charge can now be calculated and compared to E_{r0} that is the gradient in the absence of space charge.

As can be seen from figure 4.8, E_r, which is the voltage gradient within the cage taking the space charge into consideration, is drastically different to E_{r0} which is the gradient where the space charged is ignored. It shows that the space charge effect is such that it decreases the voltage gradient, for positive polarity in the vicinity of the conductor. The graph shows that the effect is more pronounced for larger diameter conductors.

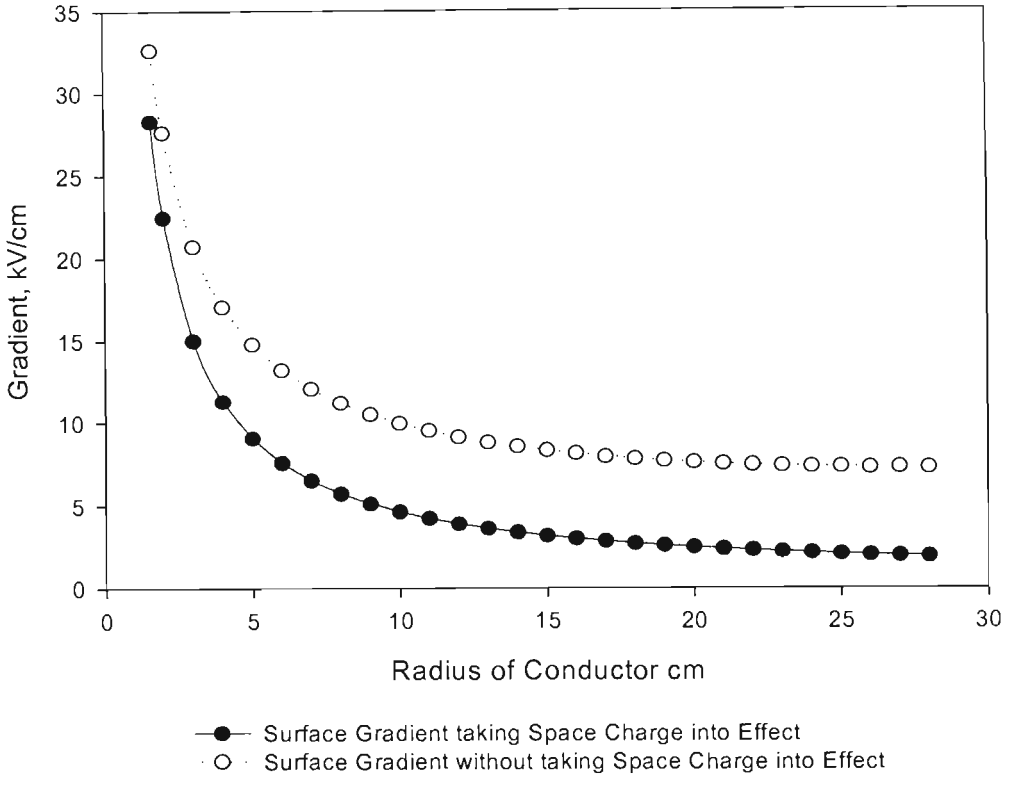

Figure 4.8: Electric Field Gradient in the Presence of Space Charge

4.5 SUMMARY

A laboratory corona cage is one tool for determining the corona performance of conductors. It was decided to design such a cage, which will be housed in the University of Durban-Westville's HVDC Laboratory.

A cage with a diameter of 1.5m was designed. This diameter would ensure that corona studies would, be able to be carried out without the fear of flashovers occurring.

The cage would consist of three sections. Two outer "guard" rings each 0.5m in length and a central measuring section, which is a 1m in length. A support structure was designed to accommodate the cage. The design of this, structure as well as the materials used is discussed in appendix A.

Basic calculations done, to determine the effect of the space charge phenomenon reinforces the result obtained from tests done around the world as well as results found in the HVDC reference book. The effect of the space charge phenomenon was quantified by the use of an example. It showed that in a corona cage configuration, the space charge actually decreased the surface gradient for the positive polarity.

CHAPTER 5

HVDC LABORATORY SET UP

The high voltage direct current laboratory at the University of Durban-Westville was established by the HVDC center of Excellence at the institution in 2001. Various stakeholders funded the project. It is situated on the main campus a few hundred meters away from the engineering block.

5.1 HVDC TEST KIT

The University of Durban-Westville has a High Voltage Direct Current (HVDC) Laboratory with a test kit which, is capable of delivering 500 kV Positive and 540 kV Negative, DC.

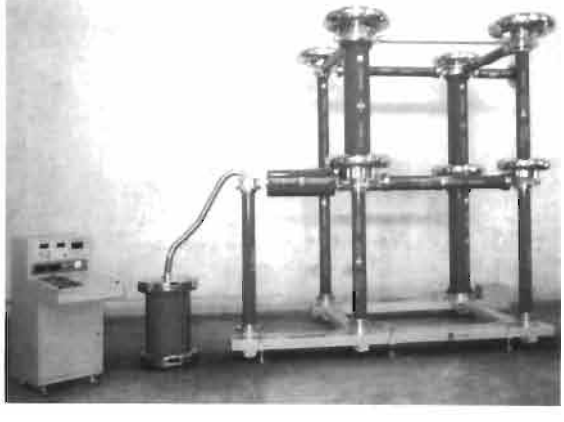

Figure 5.1: Assembled HVDC Test Kit [19]

The High Voltage DC test kit, basically consists of the following main components,

- High voltage test transformer
- Control panel
- Smoothing capacitor
- Silicone rectifier
- Isolating transformer

As well as other components such as a measuring resistor, insulating supports, corona shielding, aluminium electrodes, measuring devices and other assembly components. The isolating transformer is shown in figure 5.2.

Figure 5.2: Isolating Transformer

5.2 PRINCIPAL OF DC GENERATION

To generate direct voltages of small level (up to 50 kV), a simple half-wave rectifier circuit is adequate. For higher DC voltages a voltage doubler or cascade voltage doubler circuit (Voltage multiplier circuit) has to be used. Most HVDC tests require a moderate current, which is often less than 10 mA.

The test kit at the University of Durban Westville uses a half wave voltage doubler circuit and half wave voltage multiplier circuit, known as the Cockcroft-Walton Circuit [19] shown in figure 5.3.

In this circuit, rectifiers D1 and D3 will conduct and charge capacitors C1 and C3 in the negative half-cycle, while D2 and D4 will conduct and charge capacitors C2 and C4 in the positive half-cycle. The voltage across capacitors becomes $4V_{max}$ with respect to earth. The voltage across any individual capacitor or rectifier is only $2V_{max}$ at any time.

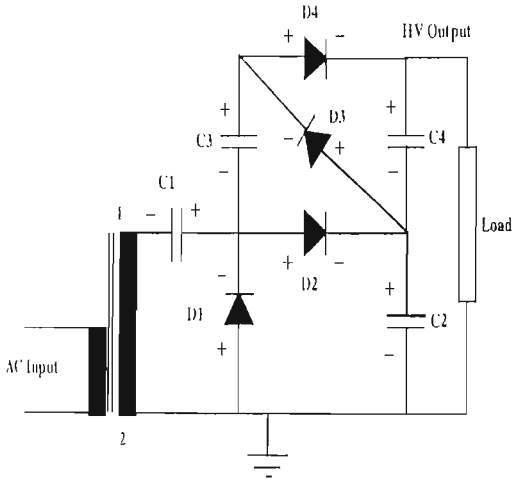

Figure 5.3: Cockcroft-Walton Circuit [19]

5.3 MEASUREMENT OF DC

Measurements will be carried out using high value resistors, thereby reducing the direct current to be measured. The current should be less than 1mA due to the limitations on the permissible loading of the source and also the thermal dissipation of the measuring resistor itself. The resistive divider used for measurement consists of two parts, one is the high voltage part which, is in the order of mega-ohms, and the other is the low voltage part which, is normally made in parallel arms to have different measuring ranges.

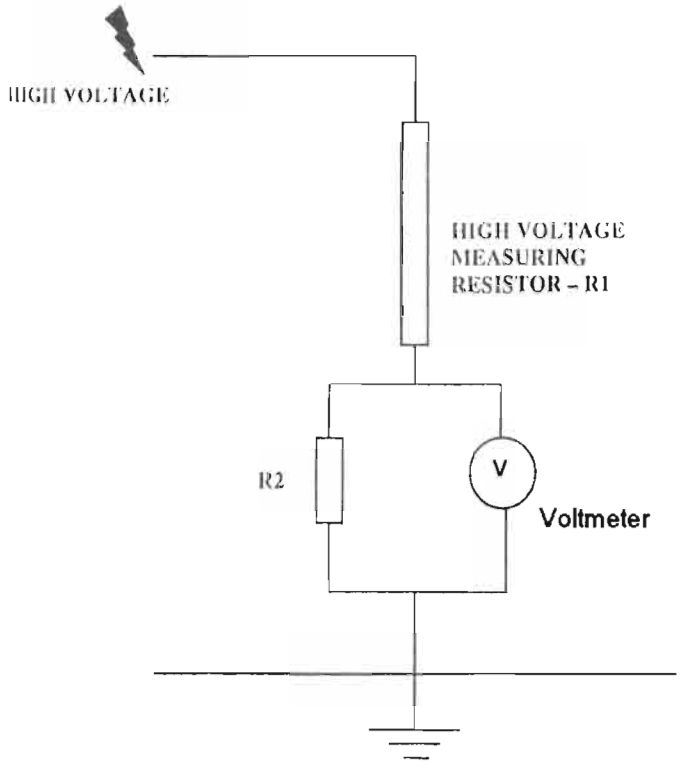

Figure 5.4: DC Measuring Circuit [19]

5.4 CLEARANCES REQUIRED

When setting up an HV laboratory up to 1 MV the following minimum clearances must be maintained:

For AC and DC	50cm for every 100kV
For Impulses	20cm for every 100kV

Due to the size of the test kit, some clearances within the laboratory do not comply with these minimum requirements, this problem is overcome by using fiber-glass insulation to cover the areas which fall within the danger zone.

5.5 EARTHING OF LABORATORY AND EQUIPMENT

The laboratory may only be entered once all the components that can assume high voltages in the contact zone are earthed.

Interlocking doors ensure that once the laboratory is entered, the supply to the test kit is immediately cut. Earthing is only allowed by a conductor that is earthed within the test area [19].

The earthing within the laboratory is done by means of earthing rods, as well as an automatic earthing switch. Earthing may only take place once the current source has been switched off, and may be removed only when there is no one present in the testing area or if the testing area is cleared once the earth has been removed.

All metallic parts of the setup which do not carry potential during normal testing has to be earthed reliably with at least 1.5 mm^2 copper conductor.

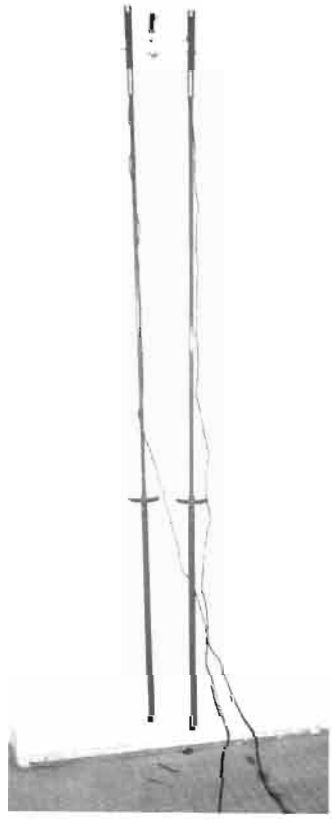

Figure 5.5: Earthing Rods

5.6 TEST SYSTEM SPECIFICATIONS

AC VOLTAGE	
Rated Voltage	100 kV (rms)
Rated Output (Continuous)	5 kVA – Continuous 7.5 kVA – Short time
Frequency	50 Hz
Short Circuit impedance Voltage	5% approximately with respect to rated continuous kVA and rated voltage.
DC VOLTAGE	
No Load Rated Output, Positive Polarity Negative Polarity	500 kV 540 kV
Rated Continuous Current	7.5 mA
Ripple Voltage	≤ 3% at rated current and voltage

Table 5.1: Test Kit Specifications [19].

5.7 ELECTRICAL BLOCK DIAGRAM OF THE LABORATORY TEST SET-UP

Below follows a block diagram of the laboratory set-up. As can be seen an isolating transformer is used for protection. The 220V AC supply is connected to the isolating transformer, which in turn is connected to the high voltage test transformer. The HV transformer is connected to the rectifier that outputs the DC voltage, This voltage is then applied to the corona cage which is connected to earth via a measuring impedance which is discussed in a later chapter.

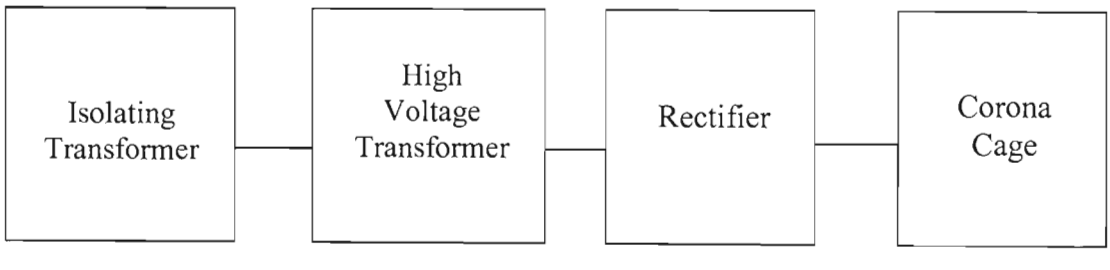

Figure 5.6: Laboratory Block Diagram

5.8 SUMMARY

The high voltage DC test kit at the University of Durban Westville is capable of delivering 540 kV Negative DC and 500 kV Positive DC. It utilises a Cockcroft – Walton rectifier circuit to generate DC from AC.

The clearances for AC and DC voltages are the same and is equal to 50 cm for every 100 kV. For impulse testing this requirement is reduced to 20 cm for every 100 kV. Certain parts of the laboratory which, did not comply with these requirements were modified in order to satisfy them.

The earthing system in the laboratory is very sound. Copper braids are used throughout the laboratory in order to ensure that all pieces of equipment which, are not live are earthed appropriately. All metallic parts of the test set-up which do not carry voltage during normal testing is earthed with at least 1.5 mm^2 copper conductor.

Safety in the laboratory is of the utmost importance. The laboratory may only be entered once all the components that can assume high voltages in the contact zone are earthed. Interlocking doors ensure that if the laboratory is accidentally entered while testing is taking place, the supply to the test kit will immediately be cut and earthing applied.

CHAPTER 6

TEST PROCEDURES AND EQUIPMENT

The tests, test procedures, aims of the tests as well as the equipment used during testing are discussed in this chapter.

6.1 TEST PROCEDURES

Three conductors were tested (1.00-cm diameter, 1.36-cm diameter, 1.76-cm diameter). These conductors were tested under the following conditions.

1. Strung up in the cage with no fan
2. Strung up in the cage with a fan blowing across (side fan) the cage
3. Strung up in the cage with a fan blowing "through" (front fan) the cage

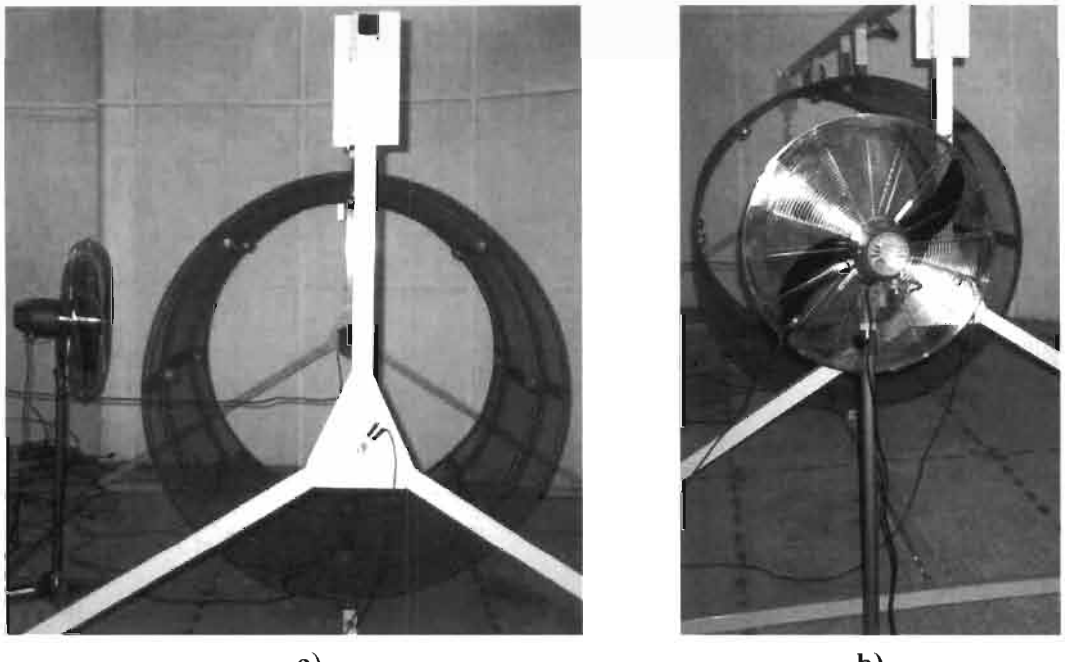

a) b)

Figure 6.1: a) Configuration of Fan Blowing from the Side, b) Configuration of Fan Blowing from the Front.

The coating was then applied to half of each conductor's length and the tests were then repeated, after waiting a day for the silicone to dry completely. Finally the entire length of the conductors, were painted and once again the tests were repeated, again after waiting a day for the silicone to dry. This procedure is shown in figure 6.2.

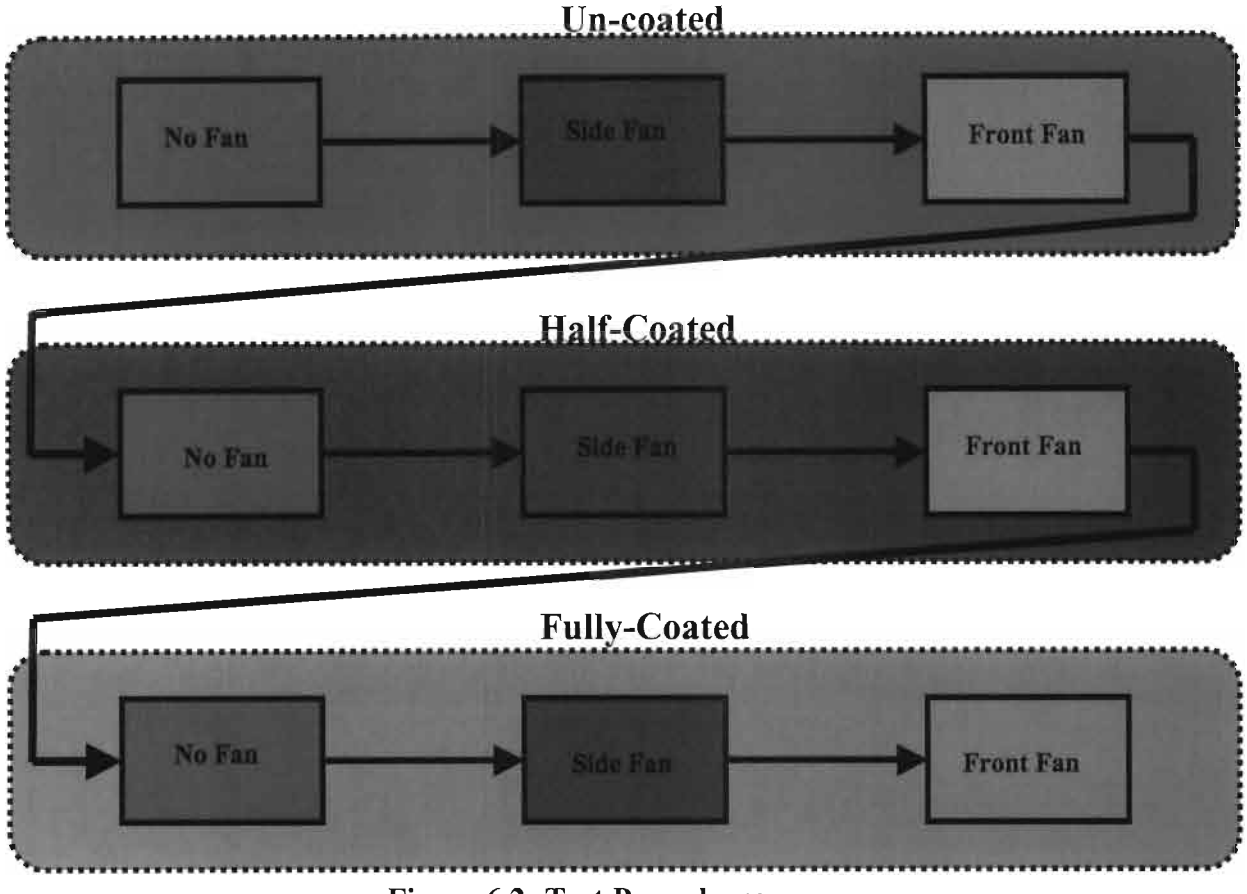

Figure 6.2: Test Procedures

6.2 Test Aims

The aims of the tests were to:

- Ascertain the effectiveness of the corona cage (Whether it could be used for corona studies).
- Determine the effect of wind on corona performance in a corona cage.
- Determine the effect of a silicone coating on the corona performance of conductors.

These aims were chosen in order to determine what can be done in order to mitigate corona activity on conductors under HVDC potential.

6.3 Measuring Equipment

In order to measure corona noise a series resistive element was required. The resistive element has a resistance, which is equal or very close to the impedance of the co-axial

cable, which connects it to the measuring scope, which is approximately 50 ohms. By using a parallel connection of resistors, of equal value, in a concentric ring the reactive component or inductance is reduced to negligible proportions. The resistor should be able to accommodate the corona loss current, which may flow through it. The parallel combination was used in order to to ensure that the cable impedance is matched so as to avoid reflections, which interfere with the measurements. The paralleling spreads out the current and enhances the shielding effect

The total resistance of the concentric shunt is given by the following formula:

$$R_{eq} = \frac{R}{n}$$

Where: R = resistance of one resistor

n = number of resistors

The resistors all have the same power carrying capacity. So the current carrying ability of each resistor can be calculated from the following:

$$I = \sqrt{\frac{P}{R}}$$

Where: P = power rating of resistor

R = resistance

Each resistor has a value of 56 ohms and a power rating of 5W. This means that the total current carrying capacity of the shunt resistor will be approximately 3A. This is much more than the expected corona loss current. Which, is expected to be at most in the hundreds of microamps range. Due to the nature of the progression of the project, corona noise measurements were not considered part of the scope. An ammeter was therefore used to measure the currents through a resistor to ground.

6.4 TESTS PERFORMED IN THE CAGE

After the cage was installed in the laboratory, tests were conducted, firstly to see that the cage worked and secondly to gain some valuable corona data on the corona performance of HVDC lines.

Figure 6.3 shows the completed cage, with a conductor strung, ready for testing.

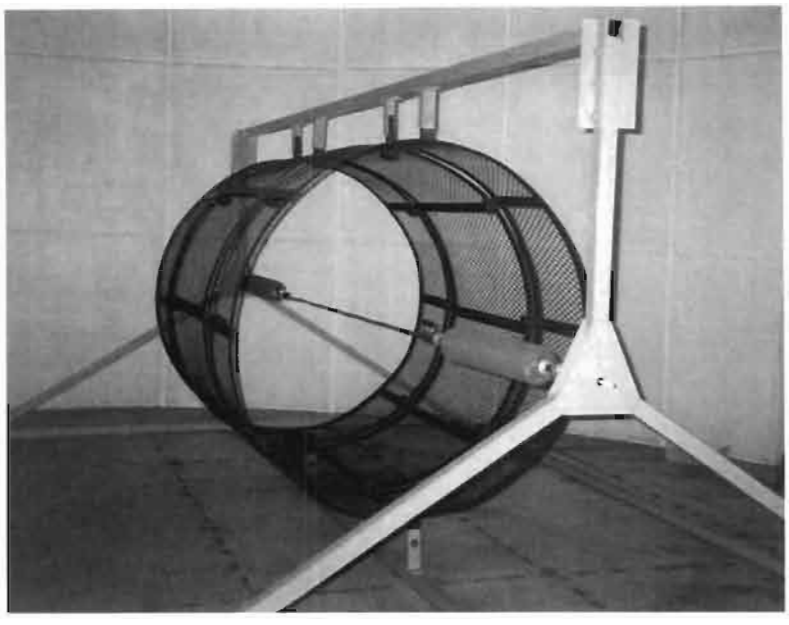

Figure 6.3: Completed Corona Cage

6.4.1 Initial Testing

The first tests to be conducted within the cage were to determine whether the cage would be able to be used for corona testing. As stated in chapter 4, for the largest conductor to be tested the cage diameter should be small enough to obtain corona at a sufficiently low voltage. At the same time the air gap clearance between the cage and the conductor should be large enough so that the breakdown voltage is higher than the onset voltage. A margin of at least 50% between these two voltages permits studies to be carried out at different conductor surface gradients above corona onset [4, 240].

The largest conductor available in the laboratory was a 1.76cm conductor, which happens to be the earthwire used on the Cahora Bassa line. The conductor was strung up and energised. Audible corona occurred at 60 kV, while visual corona started at 90 kV. This corresponds to electric field gradients of 15.34 kV/cm and 23.01 kV/cm respectively. Now taking corona inception to be when audible corona occurred, this would mean the inception voltage is 60 kV. This corresponds to a surface roughness factor of 0.4, this value is similar to values obtained from independent tests [21]. The voltage was increased and at 180 kV breakdown had not yet occurred. From this test it was obvious that the cage would satisfy the basic design criterion.

6.4.2 Corona Measurements

As mentioned in earlier chapters, the corona performance of a line is an important factor in its design. It is therefore clear that a better understanding of corona and its

associated effects, will help in the design and optimization of transmission lines. Corona tests and measurements are two ways of gaining this understanding of corona. The tests, which formed part of this thesis, were undertaken in an attempt to gain a better understanding of the corona phenomenon in a corona cage.

6.4.3 Conductors Used in the Tests

The conductors used in the tests were as follows:

- 1 cm diameter
- 1.36 cm diameter
- 1.76 cm diameter

Photographs of these conductors are shown below.

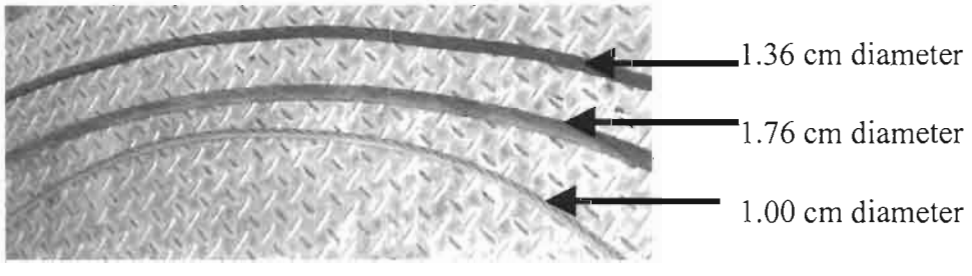

Figure 6.4: Conductors Used for Testing

6.4.4 Silicone Rubber (RTV) Coating

A silicone Room Temperature Vulcanised (RTV) coating "Insilcote HV 2000" was used on the conductors in order to determine the effect that it would have on the inception gradient as well as on the corona loss measurements. The coating was obtained from Mr. Roy Macey of Mace Technologies in Johannesburg.

This coating has been extensively used on insulators and bushings. The main reasons for its use are as follows:

- Excellent arc resistance
- Fast recovery of hydrophobicity after arcing
- Reduced contaminant collection
- Good adhesion to unprimed ceramic surfaces.

These factors influence the system as follows:

- Eliminates pollution flashover
- Reduces maintenance costs
- Improves system reliability.

A description of the physical properties of "Insilcote HV 2000" is shown below [18].

As supplied:

Appearance	Sky blue liquid
Percentage Solids by weight	55%
Specific gravity at 25 deg C	1.2

Table 6.1: Physical Properties of Silicone Coating as Supplied

Figure 6.5: Insilcote and Catalyst

As cured:

Specific gravity	1.43
Dielectric strength	55 kV/mm
Dielectric constant at 50 Hz	3.0
Surface resistivity	$> 1*10^{12}$ ohms
Volume resistivity	$> 2*10^{13}$ ohms
Loss tangent at 50Hz	0.017
Water droplet contact angle (0.1 cc distilled water droplet)	100 degrees

Table 6.2: Physical Properties of Silicone Coating after curing

6.4.5 Fan for the Dispersal of the Space Charge

A fan was used in order to disperse the space charge and to measure the effect that the space charge will have on the corona inception gradient as well as on the corona loss levels. Readings were taken with the fan blowing air through the cage, and without the fan blowing. An industrial pedestal fan was purchased from Luft Industries in Durban. This fan was used to blow air across and through the corona cage in an effort

to quantify the space charge effect that may exist within the cage. The technical specifications and diagram of the fan follows [16].

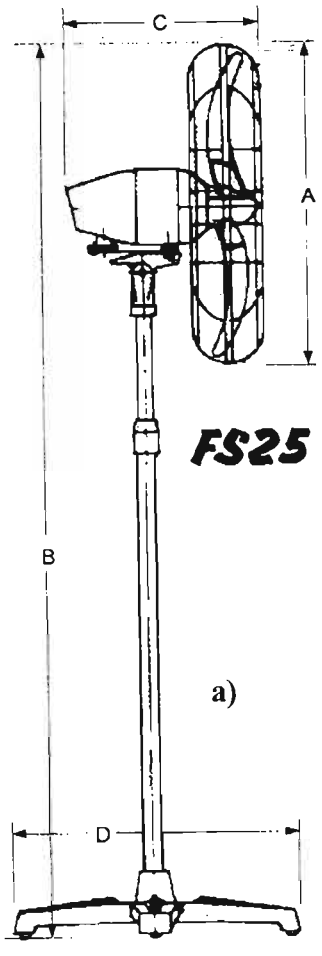

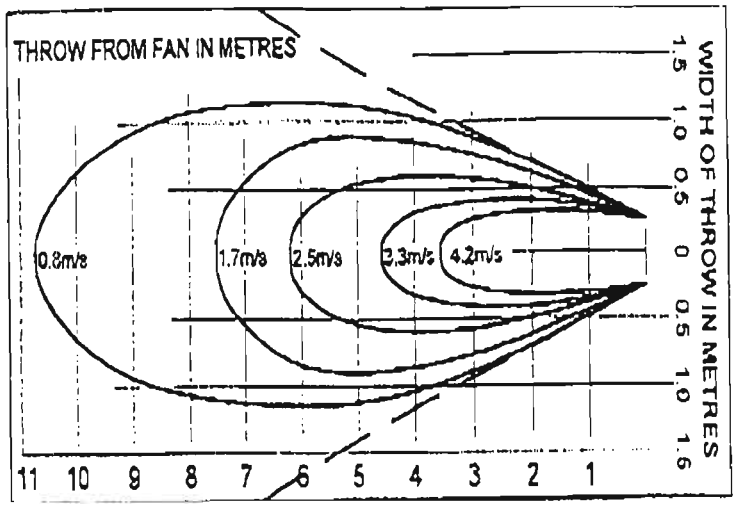

Dimension	A	B	C	D
Length mm	690	1930	360	615

Figure 6.6: a) Diagram of Fan used, b) Fan Speeds at Various Distances.

Speed setting	1	2	3
Fan speed rpm	1400	1250	1150
Volume m^3/s	2.95	2.67	2.45
Noise dBA	56	49	46
Power Watts	200	140	120
Power factor	0.83	0.95	0.92

Table 6.3: Technical Specifications of the Fan [16]

Figure 6.7: Photograph of Fan

6.4.6 Ammeter Used for Measurements

The ammeter that was a ROBIN OM500T, 30 000 Ohm/Volt Taut Band Multimeter.

Ammeter Specifications

Table 6.4 gives the ammeter specification [24].

Range	DC Voltage	*0 - 0.25 – 1 - 2.5 – 10 - 50 – 250 - 1000V*
	AC Voltage	*0 - 0.25 – 10 – 25 – 100 – 250 - 1000V*
	DC Current	*0 - 50μ - 5m - 50m - 500m - 12A*
	AC Current	*1 - 12A*
	Resistance	*0 - 5K - 50K - 500K - 5M*
	dB	*-20 ~ +10dB ~ +64dB at AC Volt range.*
	Continuity	*Continuity test by buzzer sound.*
	Off	*Meter protection during transit.*
Accuracy	DC Voltage	*± 3% of Full Scale Value*
	AC Voltage	*± 4% of Full Scale Value*
	DC Current	*± 3% of Full Scale Value*
	AC Current	*± 4% of Full Scale Value*
	Resistance	*± 3% of Scale arc*
Sensitivity	DC Voltage	*30 KΩ/V*
	AC Voltage	*10 KΩ/V*

Table 6.4: Ammeter Specifications [24].

6.5 SUMMARY

Initial testing of the cage proved successful. The largest conductor in the laboratory was a 1.76 cm diameter conductor and this conductor when tested in the cage showed that the 50% criterion between onset voltage and breakdown voltage was adhered to.

Three conductors were available for testing, they were all stranded conductors with the following diameters, 1.00 cm, 1.36 cm, 1.76 cm.

The silicone rubber used in the testing was obtained from Mace Technologies in Midrand, Johannesburg. The silicone has the following properties

- Excellent arc resistance
- Fast recovery of hydrophobicity after arcing
- Reduced contaminant collection
- Good adhesion to unprimed ceramic surfaces.

A large fan was purchased. This was done so that the effects of wind on the corona phenomenon may be studied in the cage.

CHAPTER 7

TEST RESULTS

In this chapter the test results are presented and analyzed. These results mainly deal with the results of tests done to determine the effect of the silicone coating on the corona performance of several conductors.

7.1 TEST RESULTS

In this section, all results of tests done with no fan present will be represented graphically in red, while the results of tests done with the fan blowing through the side of the cage will be in blue and the results obtained with the fan blowing through the front of the cage is shown in green.

7.1.1 Effect of Wind on Uncoated Conductors

The testing of all the conductors was done under the following conditions:

- Laboratory air-conditioning off
- "Clean" surface condition

Point one above is important as some fluctuations in measurements were noticed when the laboratory air-conditioning was on and when it was off. These first tests dealt with the effect of wind on the corona currents generated. The conductors were strung up and tested without any silicone coating. Corona current was measured without any simulated wind, then with a side wind and finally with a front wind. The results for the three conductors are now shown.

7.1.1.1 Results of 1.00-centimeter diameter conductor

The results of this set of tests seem to indicate that corona current is generally not increased for the 1.00-cm diameter conductor, with wind blowing over it. Wind blowing from the side of the cage has a greater impact on current increase than wind blowing through the front of the cage. Wind blowing from the front of the cage actually seems to decrease the measured corona current. Based on these results it is still not certain whether the effect of wind on this conductor in a small corona cage is significant.

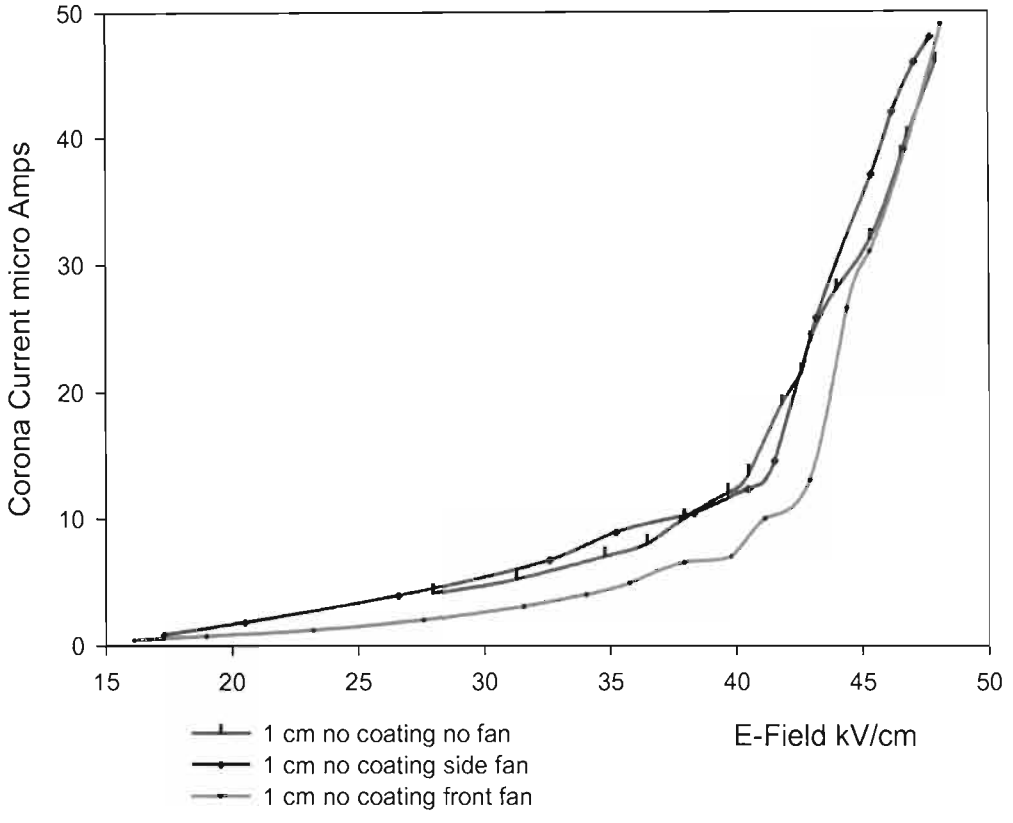

Figure 7.1: Effect of Wind on an Un-coated 1.00-cm Conductor

7.1.1.2 Results of 1.36-centimeter Diameter Conductor

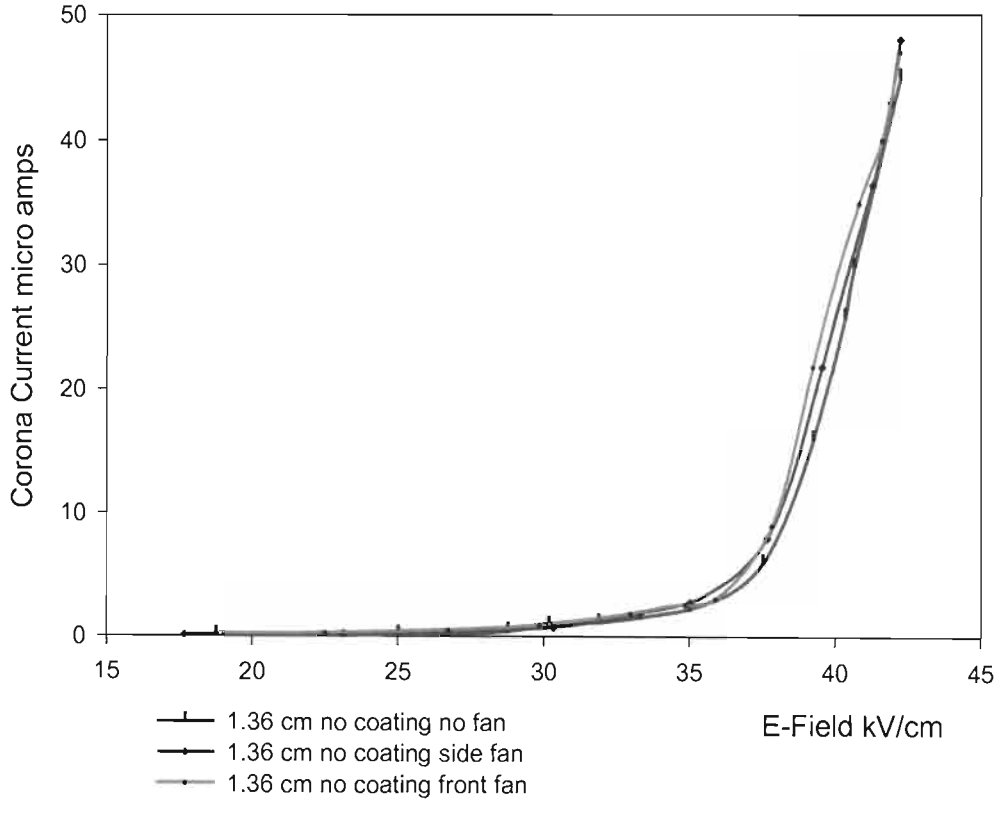

Figure 7.2: Effect of Wind on an Un-coated 1.36-cm Conductor.

The results shown in figure 7.2 indicate that the effect of wind is not a major contributor to corona current increase. Based on these results it is also not clear what effect wind has on a stranded, clean un-coated conductor. Generally it seems as though the corona current measured without the fan blowing from the front or the side is lower, but only marginally. This result is not conclusive on its own.

7.1.1.3 Results of 1.76-centimeter Diameter Conductor

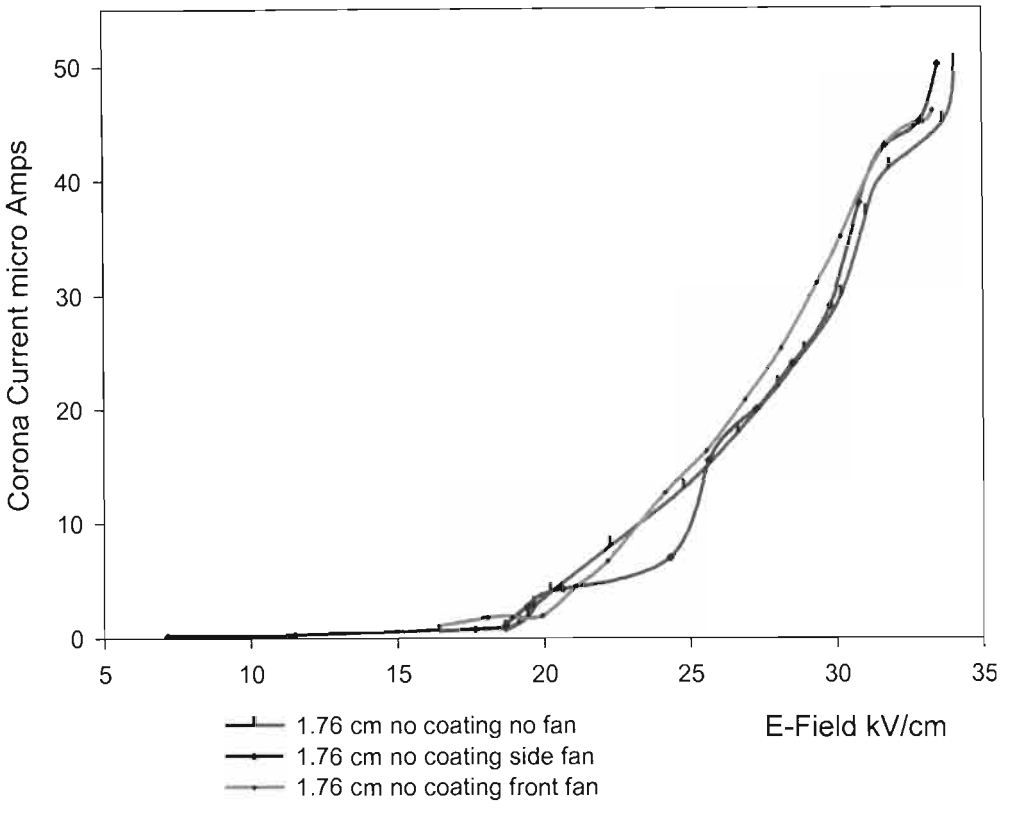

Figure 7.3: Effect of Wind on an Un-coated 1.76-cm Conductor.

Figure 7.3, is also not conclusive with regards to the effect of wind on the corona current generated. From the results obtained it seems as though the effects of wind in a corona cage on a clean, stranded, un-coated conductor are minimal. For conductor surface gradients in excess of 25kV/cm, the corona currents generated with the fan blowing is once again marginally higher than those recorded without the fan blowing.

7.1.1.4 Discussion of the Effects of Wind on Un-coated Conductors in the Corona Cage

Figures 7.1, 7.2 and 7.3 indicate that the effect of wind on a clean, stranded, uncoated conductor in a corona cage is minimal. These results were quite surprising since it was expected that the effect of wind blowing over the conductor would have had a greater

effect on the corona current, than what was measured. However, previous work done by Khalifa and Morris [1] showed that wind had little effect on corona losses on monopolar lines in a one conductor to ground plane, configuration, which is basically the similar to the cage set-up. Further testing is required with a more powerful fan. It is also recommended that similar tests be performed with the surface condition of the conductors being changed, i.e. decreasing the roughness factor.

7.1.2 Effect of Wind on Half Coated Conductors

The conditions under which these conductors were tested were the same as the conditions described in section 7.1.1 These tests were carried out a day after the tests discussed in section 7.1.1 The results of these tests are given below.

Figure 7.4: Half-coated conductors'

7.1.2.1 Results of 1.00-centimeter Diameter Conductor

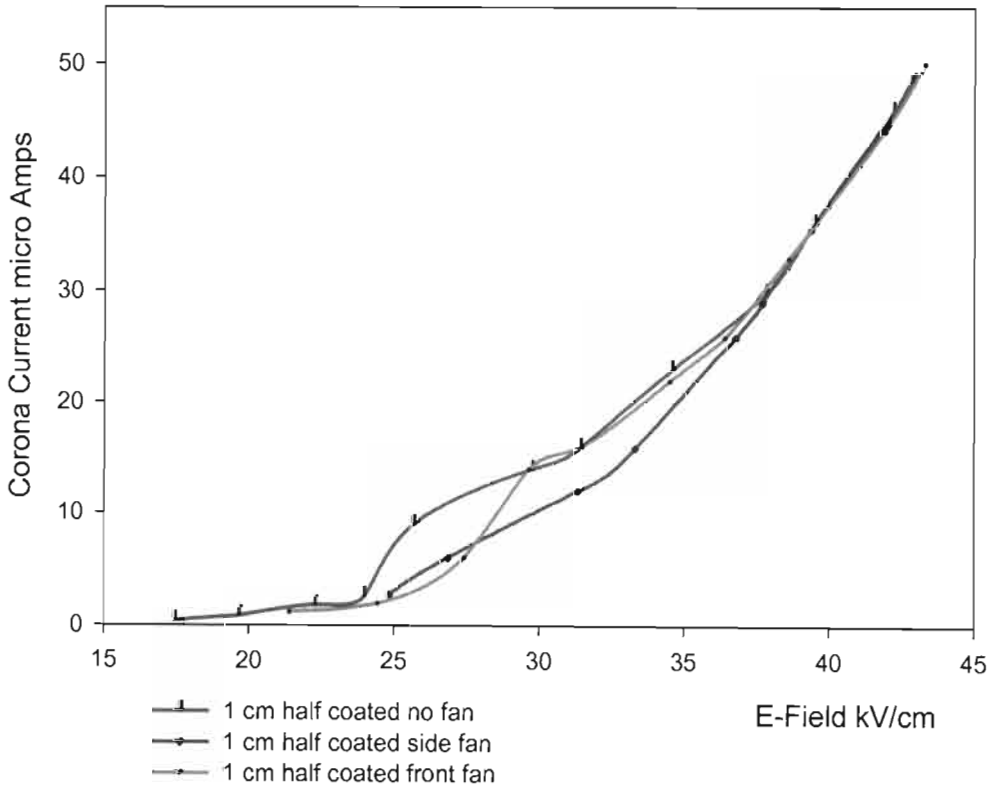

Figure 7.5: Effect of Wind on a Half Coated 1.00 cm Diameter Conductor

These results shown in figure 7.5, once again seems to indicate that the effect of wind on this type of conductor in a cage is minimal, not withstanding the fact that the conductor is now half-coated with silicone. In fact, for a certain interval of electric field strength, the corona current due to the fan not being present is actually higher than when the fan is blowing from the front or from the side.

7.1.2.2 Results of 1.36-centimeter Diameter Conductor

The results shown in figure 7.6 are interesting due to the fact that the corona current produced with the fan blowing from the front of the cage is higher than when it blows from the side or when it is not blowing at all. Similarly the corona current produced when the fan is blowing from the side position is generally higher than the current produced when the fan is not blowing at all. This result would seem to indicate that the effect of wind on this specific conductor is such that it increases the corona current produced. The fan blowing from the front has a greater impact of corona current increase than the fan blowing from the side, which in turn produces more corona current than when it is not blowing at all.

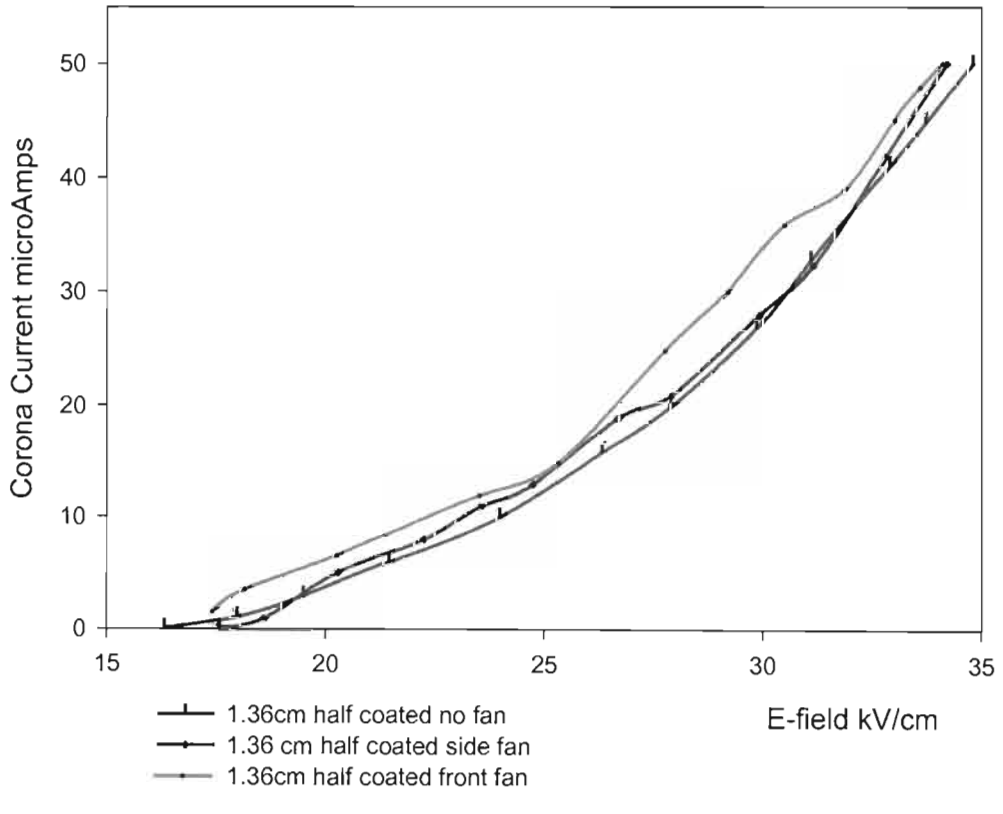

Figure 7.6: Effect of Wind on a Half Coated 1.36 cm Diameter Conductor

7.1.2.3 Results of 1.76-centimeter Diameter Conductor

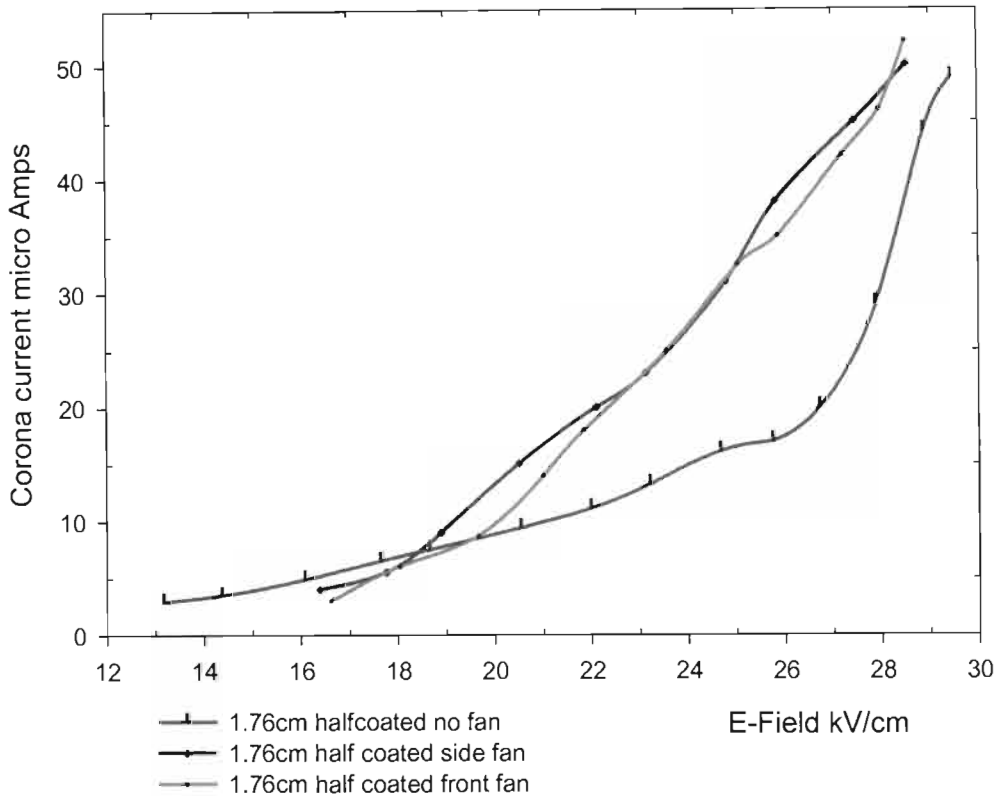

Figure 7.7: Effect of Wind on a Half Coated 1.76 cm Diameter Conductor

The results in figure 7.7 are similar to the results shown in figure 7.3. However this time the difference is more marked. Corona currents produced while the fan was blowing are generally the same whether the fan was placed in front of the cage or at the side of the cage, while corona currents measured without the fan are generally lower. This would seem to indicate that wind blowing over this conductor has more of an effect when it is half coated than when it is not coated at all.

7.1.2.4 Discussion of the Effects of Wind on Half Coated Conductors in the Corona Cage

The results of the effects of wind on half silicone-coated conductors differs markedly from the results obtained in the precious section. One of the main differences is that for similar electric field levels the corona current measured for the half-coated conductors are higher than that measured for the un-coated conductors. For the 1.00-cm diameter conductor the results are similar to the results for all the conductors in the preceding section, however for the larger conductors we notice a difference.

For the 1.36-cm diameter conductor, the corona currents produced when the fan blew from the front of the cage is higher than when it blew from the side or when it was

switched off. The lowest average corona currents were measured when the fan was off and the highest when the fan was blowing from the front. This indicates that wind blowing over this specific conductor when it is half coated with silicone, increases the corona current produced.

The 1.76-cm conductor is very different to the previous two conductors tested. The results obtained for the corona current when the fan was blowing from the side and from the front are almost identical, while the current measured when the fan was switched off is much less.

The results from the three conductors indicate that the effect of wind on the half silicone-coated conductors increases as the conductor diameter increases. There is also not much of a difference in the effect produced by wind from the side or the front of the cage.

7.1.3 The Effect of Wind on Fully Coated Conductors

Once again the test conditions for testing fully coated conductors follows the procedures described in chapter 6. The conditions under which testing took place are also the same as in sections 7.1.1 and 7.1.2. These tests took place a day after the tests described in section 7.1.2 and two days after those described in section 7.1.1.

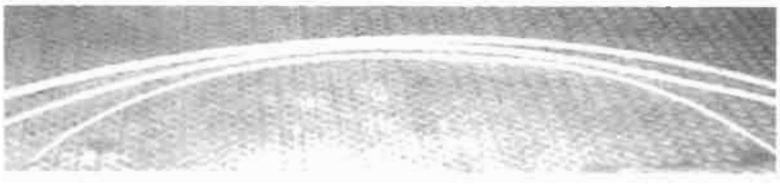

Figure 7.8: Fully coated conductors'

7.1.3.1 Results of 1.00-centimeter Diameter Conductor

The results shown in figure 7.9 below are similar to the results obtained in figure 7.5 where we had a half silicone-coated conductor. Generally the effect of wind seems not to play a major role in the corona current produced by this specific conductor even with it being fully silicone-coated. It would be safe to say that this conductors' performance is not affected by wind to such an extent where the corona current produced rises markedly.

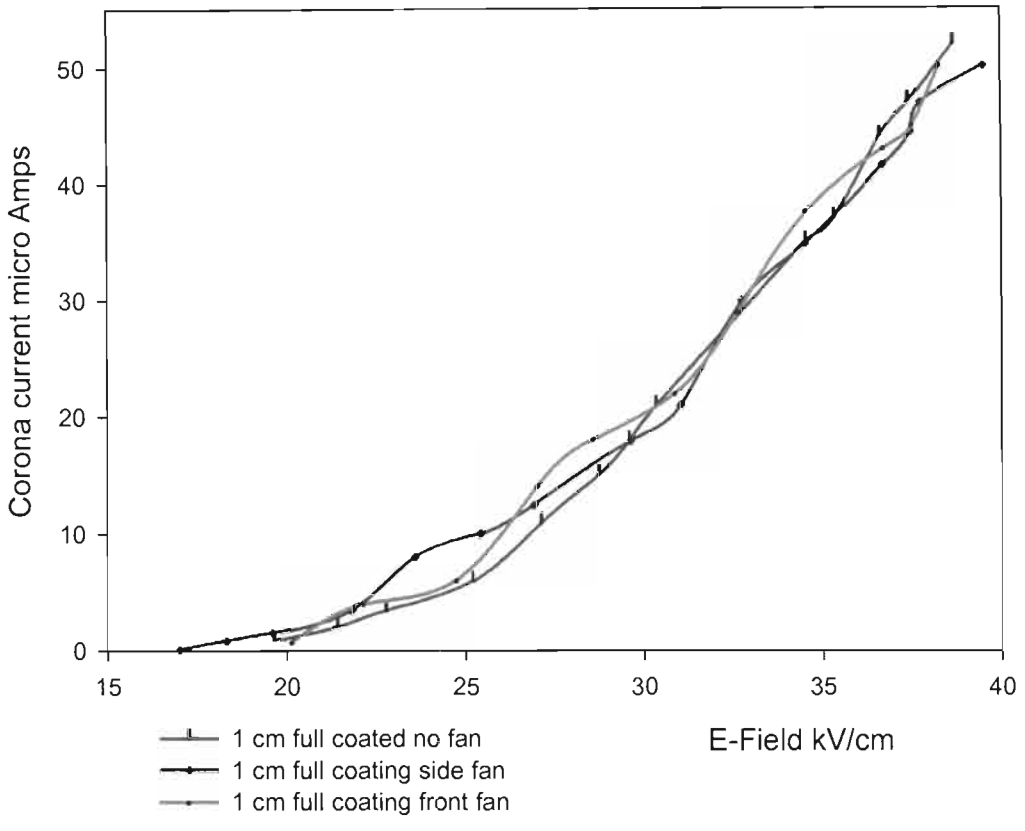

Figure 7.9: Effect of Wind on a Fully Coated 1.00-cm Diameter Conductor

7.1.3.2 Results of 1.36-centimeter Diameter Conductor

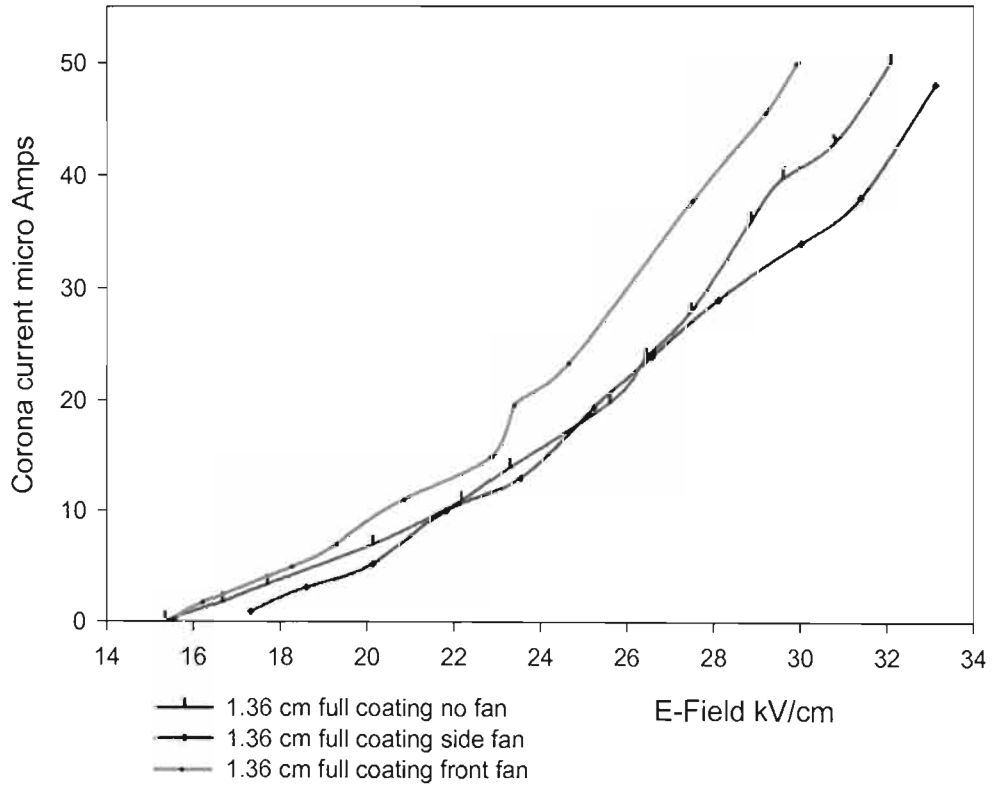

Figure 7.10: Effect of Wind on a Fully Coated 1.36-cm Diameter Conductor

The results obtained for the fully coated 1.36-cm fully silicone-coated conductor is very similar to the results obtained for the half silicone-coated 1.36-cm conductor. The main difference however is the fact that the corona current has been increased. Under the half silicone-coated condition a surface gradient of 25 kV/cm produced currents ranging from 12 to 14 μA. Under the fully silicone-coated condition 25 kV/cm corresponds to currents of between 18 and 25 μA. This will be further discussed in section 7.2.

7.1.3.3 Results of 1.76-centimeter Diameter Conductor

As with the results shown in figure 7.10, the results shown in figure 7.11 are similar to the results for the conductor when it is half coated, as shown in figure 7.7. Once again the main difference is the increase in corona current measured from the half coated to the fully coated version. For example at 20 kV/cm the half silicone-coated conductor gives values of between 8 and 13 μA. On the other hand the fully silicone-coated conductor gives values of between 12 and 18 μA.

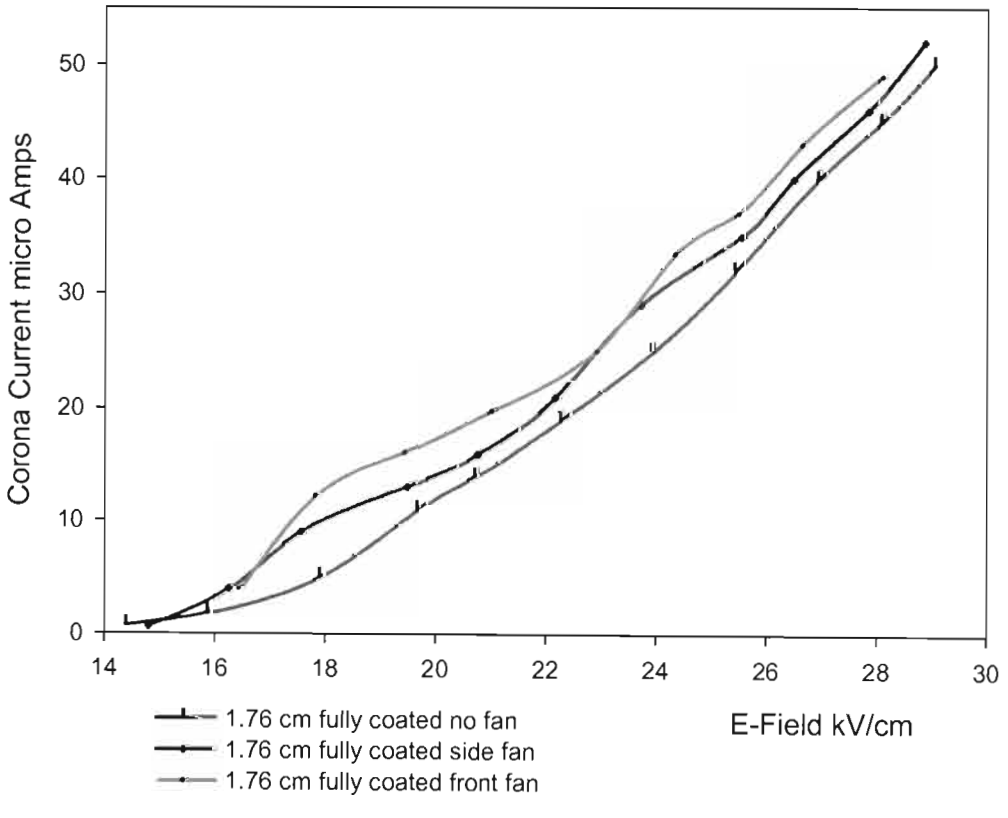

Figure 7.11: Effect of Wind on a Fully Coated 1.76-cm Diameter Conductor

7.1.3.4 Discussion of the Effects of Wind on Fully Coated Conductors in the Corona Cage

These results tend to indicate that the effect of wind is more pronounced on conductors that are fully silicone-coated.

For the 1.00-cm conductor, the results seem to indicate that although the conductor is fully coated, there is not much of a difference in corona current when the fan is positioned from the side, from the front or not on at all.

The 1.36-cm conductor has a major difference between corona loss when the fan is off and when it is on. The lowest currents were measured when the fan was off and the highest when the fan was in front of the cage.

The results for the 1.76-cm conductor are similar to those of the 1.36-cm conductor except the differences between the currents measured with the fan from the side and from the front are not as big as for the 1.36-cm conductor.

7.2 Further Analysis of Test Results

In this section, all results of tests done with no coating present on the conductor will be represented graphically in red, while the results of tests done with the conductor half silicone-coated will be in blue and the results obtained with the conductor fully silicone-coated is shown in green.

These graphs were produced after analysis of the results obtained from the first set of tests performed in the cage. This was done in an effort to determine the effect of the coating on the corona losses incurred by the conductors.

7.2.1 Effect of Coating with No Fan Present

The data from the tests performed without any wind was used to draw these graphs. The results used in the graphs, obtained for un-coated conductors were obtained a day before the results for the half silicone-coated conductors which was in turn obtained a day before the results for the fully silicone-coated conductors.

7.2.1.1 Results of 1.00-centimeter Diameter Conductor

Figure 7.12 indicates that the corona current is dramatically increased when the conductor is coated with silicone. The fully silicone-coated conductor has the highest measured current of the three. With the uncoated conductor having the lowest measured current. At a surface gradient of 30 kV/cm the uncoated conductor produces

a current of about 5 μA, while the half-coated conductor produces a corona current of 14 μA and the fully coated conductor produces a current of about 20 μA.

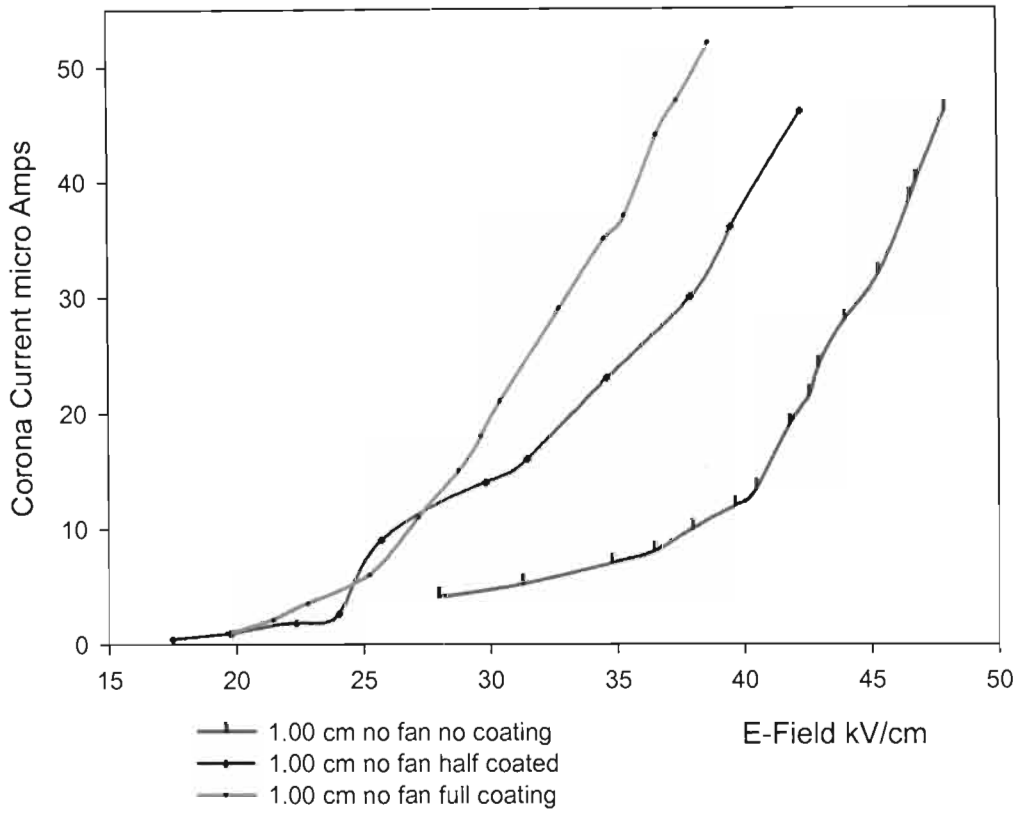

Figure 7.12: Effect of the Coating on a Wind Free 1.00-cm Diameter Conductor

7.2.1.2 Results of 1.36-centimeter Diameter Conductor

These results are similar to the results obtained for the 1.00-cm conductor. At 30 kV/cm, the un-coated conductor produces a current of about 1 μA, while the half-coated conductor, produces a current of 28 μA and the fully coated conductor, produces a current of 41 μA. The results of the un-coated conductor is not accurately with respect to the results obtained for the half coated and fully coated conductors, as the corona current was measured for the 1.00-cm conductor, by increasing the voltage from zero while the other measurements were made by decreasing the voltage from the maximum possible, for the specific conductor in the cage and the scale on the ammeter.

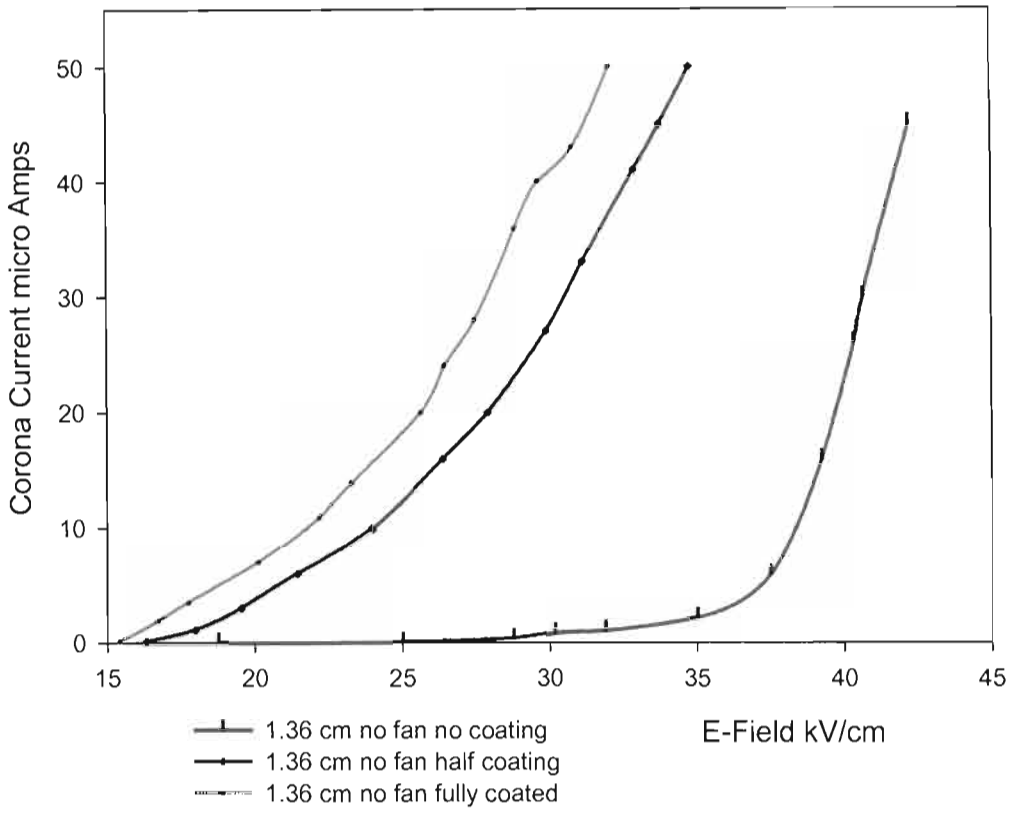

Figure 7.13: Effect of the Coating on a Wind Free 1.36-cm Diameter Conductor

7.2.1.3 Results of 1.76-centimeter Diameter Conductor

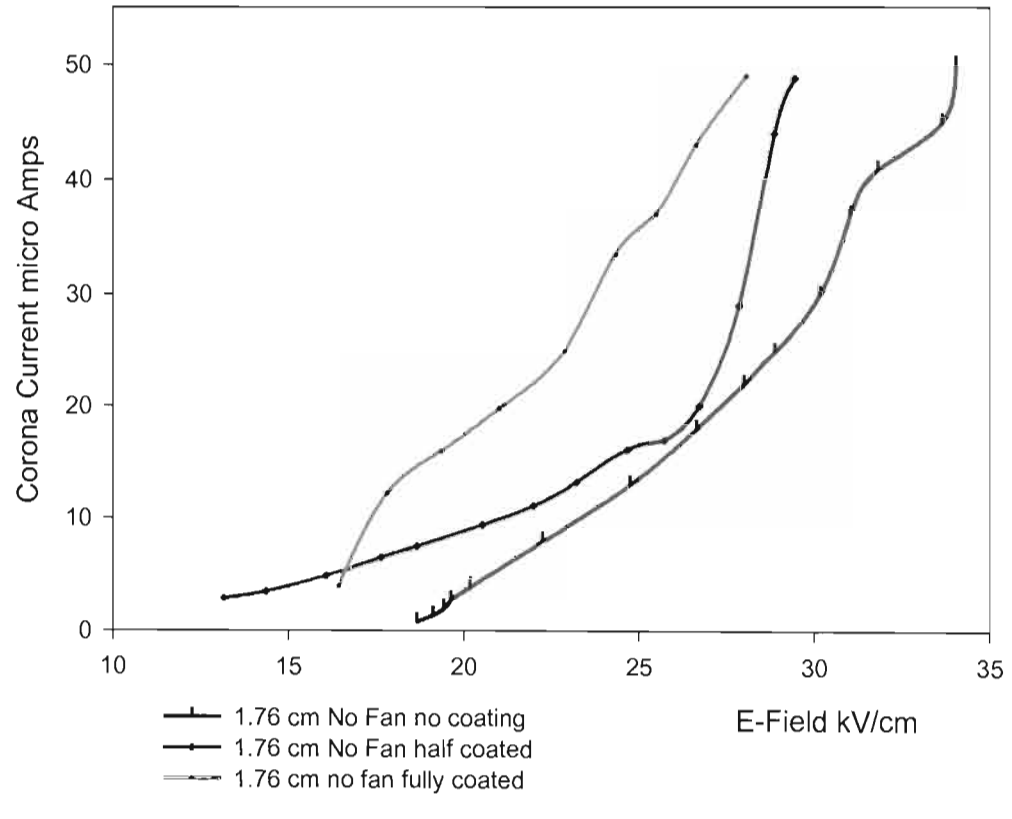

Figure 7.14: Effect of the Coating on a Wind Free 1.76-cm Diameter Conductor

Once again these results are similar to the results obtained for the 1.00-cm conductor as well as those obtained for the 1.36-cm conductor. This time when the conductors experienced a surface gradient of 30 kV/cm, the half coated conductor produced a corona current of about 30 μA, while the half-coated conductor produced a current of over 50 μA and the fully-coated conductor produced a current which was above the half-coated conductor current. The current could not be measured by the ammeter as it could only measure up to 50 μA. The assumption that was made that the fully coated conductor would produce a higher corona current than the half coated conductor is valid since this was the trend shown by the previous two examples.

7.2.1.4 Discussion of the Coating Effects with No Fan Present

The results that were shown in the three graphs above are quite surprising. It was expected that the application of the silicone coating would decrease the corona currents measured since it would decrease the surface gradient experienced on the conductors' surface. See appendix D.

7.2.2 Effect of Coating with a Side Fan Present

As was stated before these results were obtained from the tests done previously, the data was manipulated and represented graphically. The results below show the effects of the silicone coating on the conductors when the fan was blowing from the side position.

7.2.2.1 Results of 1.00-centimeter Diameter Conductor

The results of the 1.00 cm diameter conductor with the fan blowing from the side, are shown in figure 7.15.

These results are similar to those obtained when the fan was off, however there does not seem to be major difference for the corona currents measured for the conductor, when the fan is blowing from the side or when it was not blowing at all.

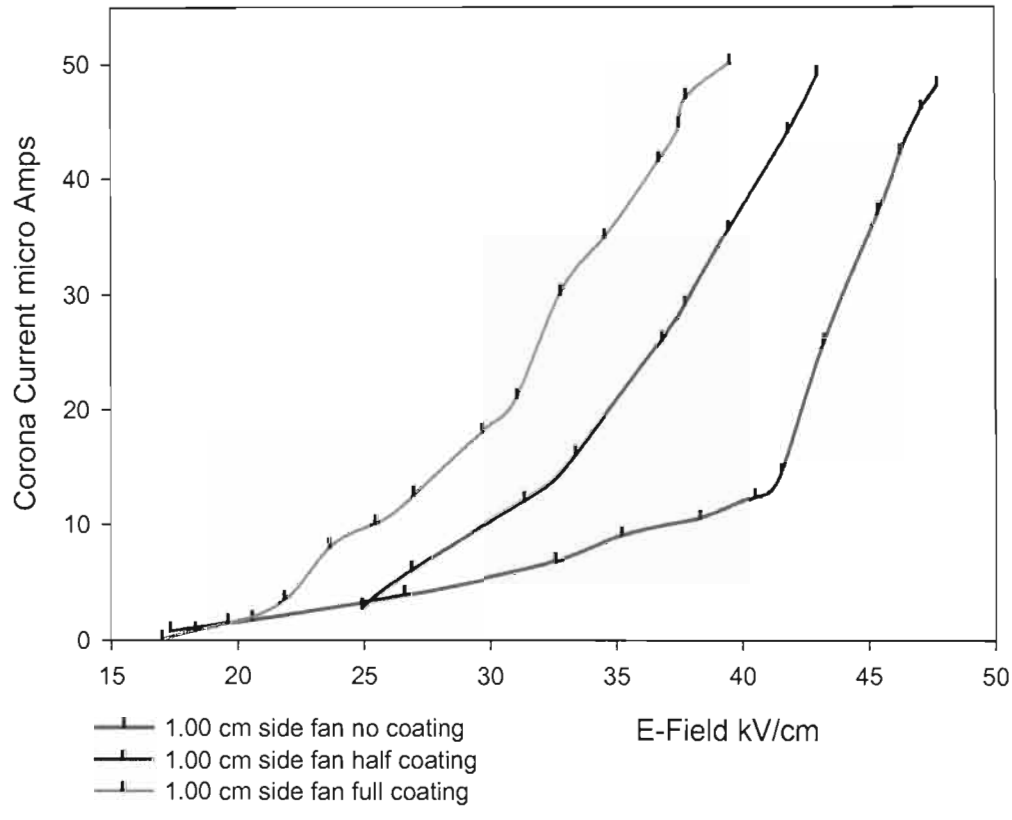

Figure 7.15: Effect of the Coating on Side Wind Blown 1.00-cm Diameter Conductor

7.2.2.2 Results of 1.36-centimeter Diameter Conductor

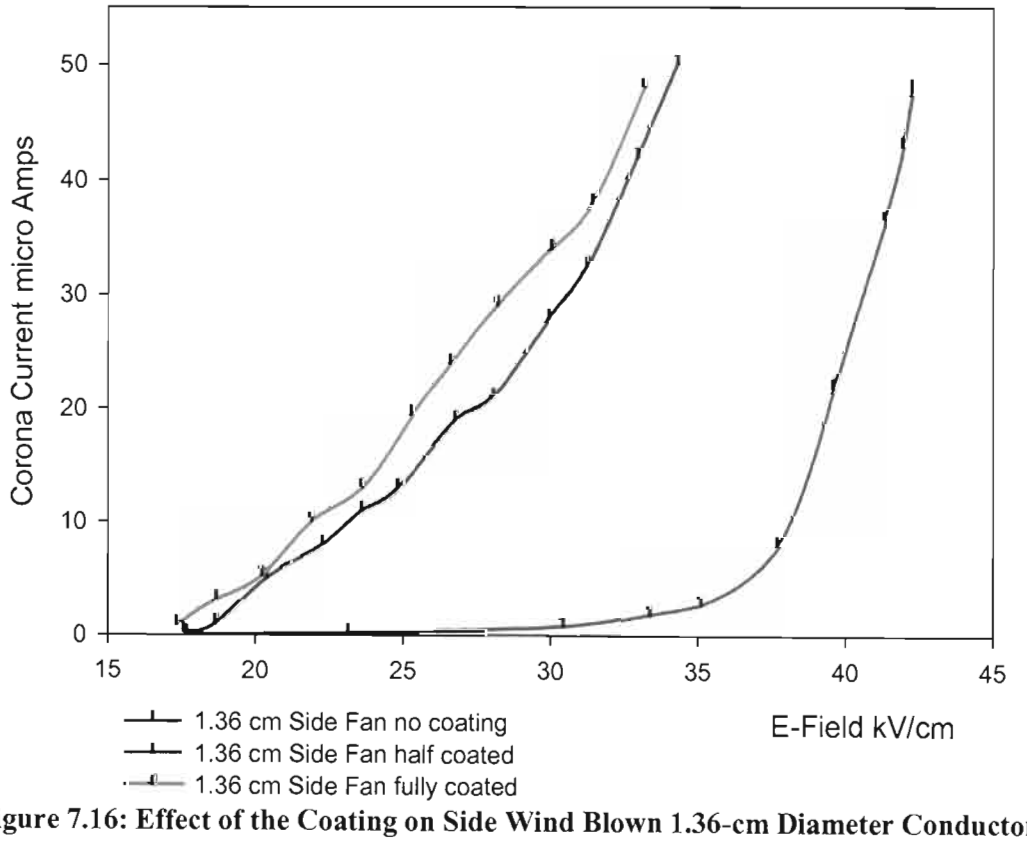

Figure 7.16: Effect of the Coating on Side Wind Blown 1.36-cm Diameter Conductor

The results are shown in figure 7.16. Once again these results are similar to those obtained when the fan was not present. As is the case with the previous graphs, the coated conductor has the highest measured corona current, followed by the half-coated conductor.

7.2.2.3 Results of 1.76-centimeter Diameter Conductor

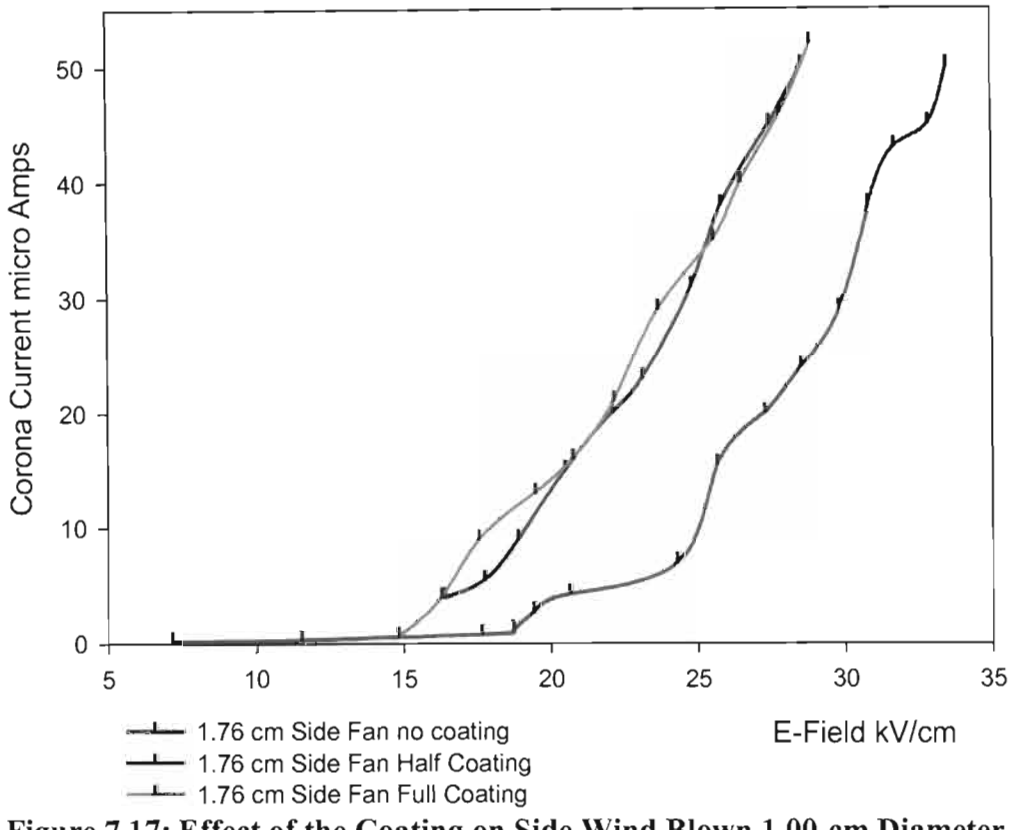

Figure 7.17: Effect of the Coating on Side Wind Blown 1.00-cm Diameter Conductor

Again we see that the results are similar to the results obtained for the same conductor without the fan present. We notice that this time the highest currents are recorded for the fully coated conductor as well as for the half-coated conductor while the lowest currents are measured for the un-coated conductors.

7.2.2.4 Discussion of the Coating Effects with a Side Fan Blowing

As with the results obtained for the effects of the coating with no fan present, we notice that the coating increases the corona currents measured. Once again the larger diameter conductors produce higher corona currents at the same applied field when compared to the smaller diameter conductor. This is due to the higher applied voltage

required to obtain the same electric field strength on a large conductor in comparison to the voltage required to obtain that specific field strength on a smaller conductor.

7.2.3 Effect of Coating with a Front Fan Present

7.2.3.1 Results of 1.00-centimeter Diameter Conductor

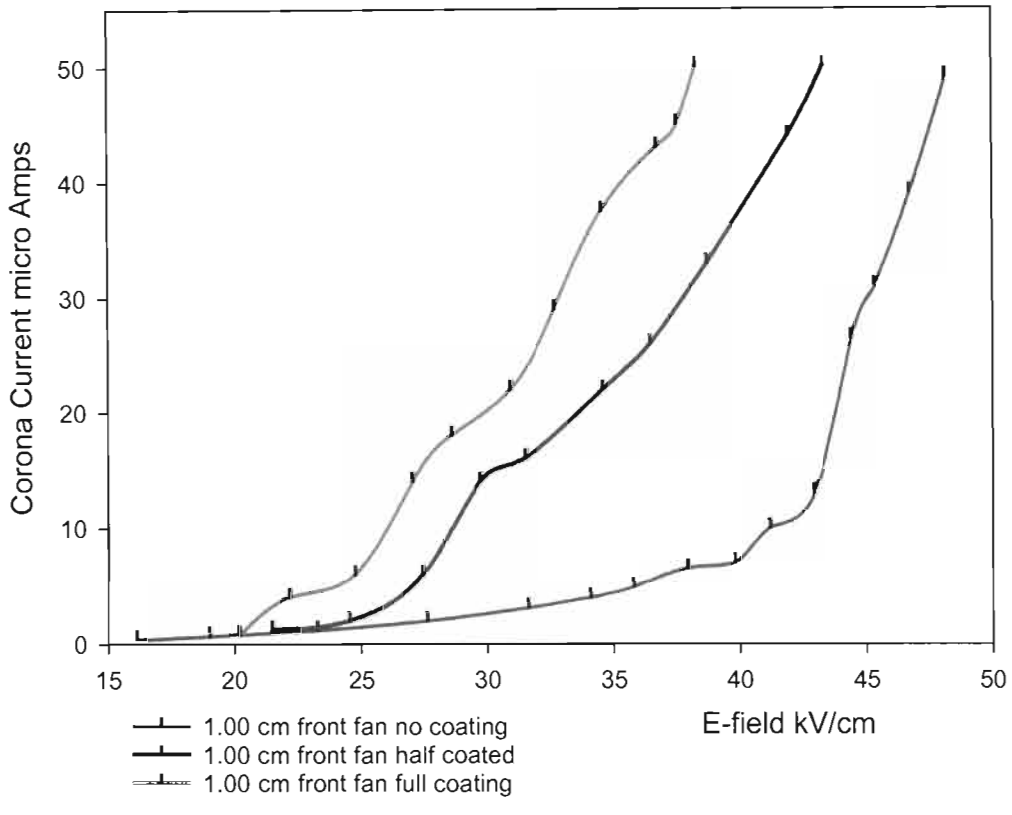

Figure 7.18: Effect of the Coating on a Front Wind Blown 1.00-cm Diameter Conductor

As can be seen from the figure above these results are once again similar to the previous results obtained for this specific conductor. Since the effect of wind was minimal on this specific conductor the results being similar are what was expected.

7.2.3.2 Results of 1.36-centimeter Diameter Conductor

Again the results are similar to previous results taken. Once again the fully coated conductor has the highest corona currents measured with the half-coated conductor having the second highest measured corona current. This result follows the trend of the 1.00 cm diameter conductor. This was expected since it was earlier shown that the effect of wind on the conductors was minimal.

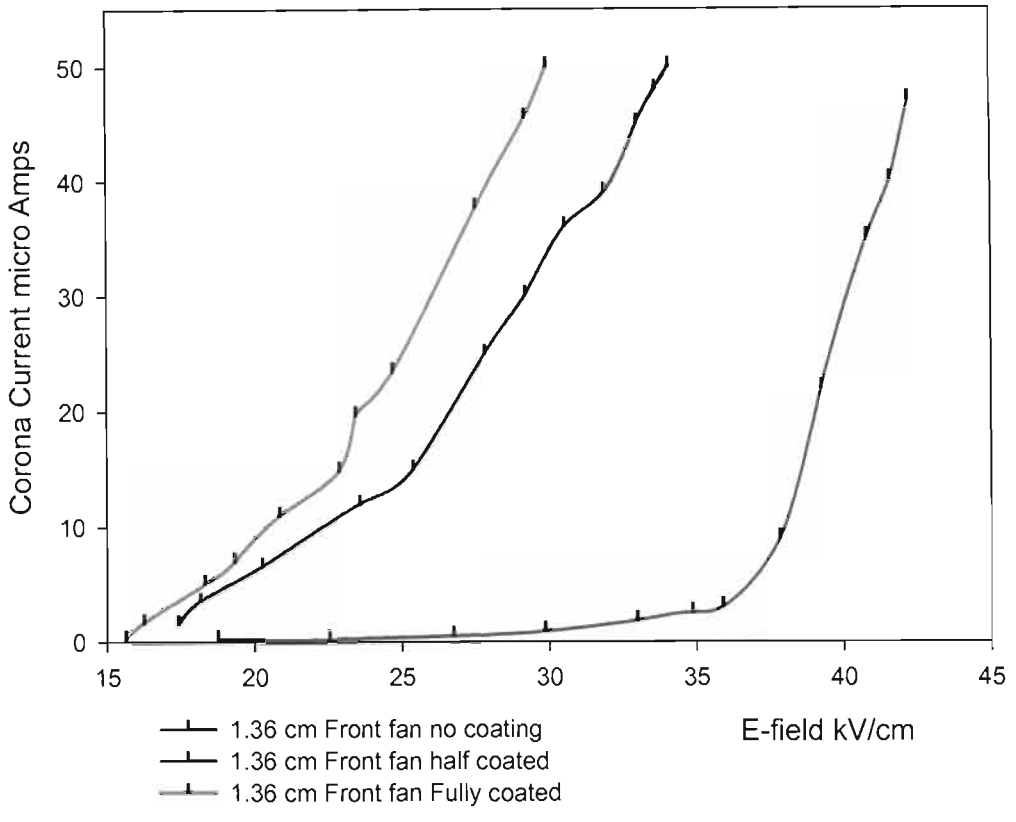

Figure 7.19: Effect of the Coating on a Front Wind Blown 1.36-cm Diameter Conductor

7.2.3.3 Results of 1.76-centimeter Diameter Conductor

Finally we see that the results obtained for this conductor once again follows the trend set out by the other two conductors to be tested. This is shown in figure 7.20. However this time the differences in the corona currents measured from when the fan was blowing to when it was off is not as marked as in previous cases. Also the results for the half coated conductor and for the fully coated conductor are closer together. This could imply that the effect of the coating is not that much between a fully coated conductor and a half coated conductor for this specific conductor.

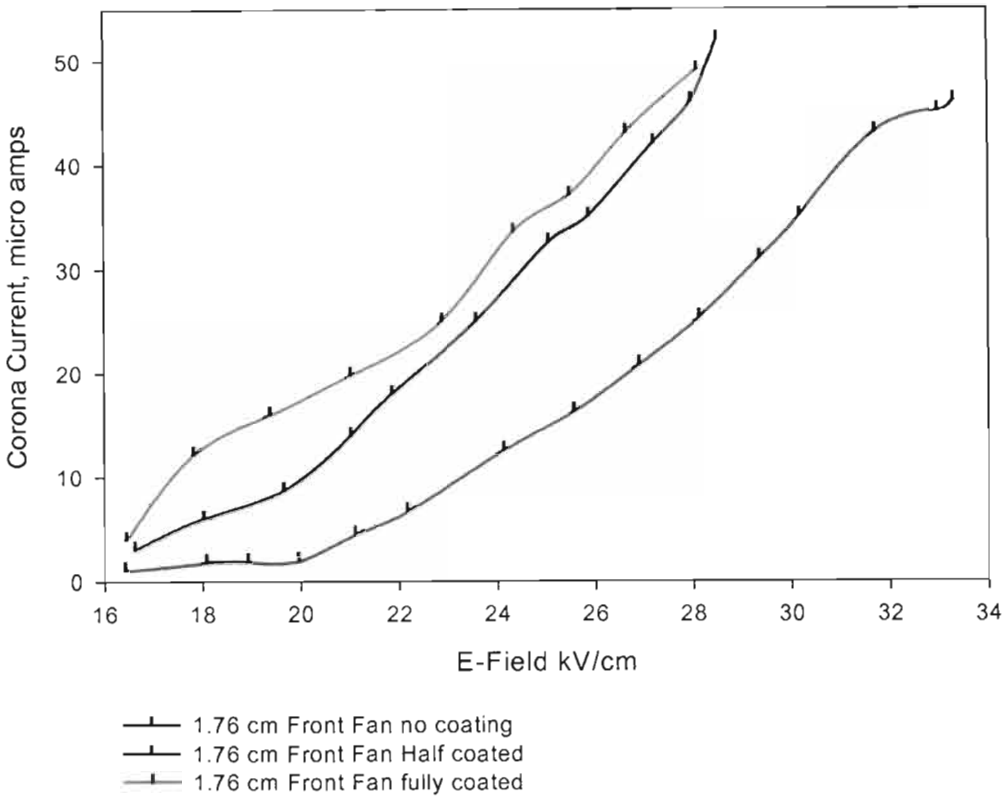

Figure 7.20: Effect of the Coating on a Front Wind Blown 1.76-cm Diameter conductor

7.2.3.4 Discussion of the Coating Effects with a Front Fan Blowing

As with the results obtained when the fan was off and when the fan was positioned to the side of the cage, the coating increases the corona current measured when the fan blows from the front of the cage. These results are similar to the results obtained for the other two conditions.

7.3 Analysis of the Effect of the Silicone Coating

The effect of the silicone coating on corona currents and corona losses measured was unexpected. It was hypothesized that the use of the silicone coating would decrease the corona currents measured and therefore decrease corona losses incurred. This, however, was not the case.

In an attempt to explain this phenomenon of increased corona activity when the coating was applied, a time domain analysis of the current pulses was done. This analysis was carried out using a 1.36 cm diameter conductor, initially the conductor

was tested without a coating present, then with half of it coated and finally it was tested after being fully coated. Thereafter the coating was stripped off the conductor and the tests repeated after the conductor was sanded down with sandpaper.

7.3.1 Analysis of the Uncoated conductor

As can be seen in figure 7.21, the voltage pulses are fairly wide spread from each other. The current pulses are in phase with the voltage pulses and flow through a fifty ohm resistor. The 0.5 V/division of the voltage pulses thus corresponds to a 10 mA/division for the current pulses. From this point forward the voltage per division will be divided by the resistor value to get the current value per division. The supply voltage was 112.5 kV, which corresponds to a surface gradient of 35.18 kV/cm.

Figure 7.21: Time domain analysis of Uncoated conductor corona current pulses

7.3.2 Analysis of the Half coated conductor

The results for the half coated conductor is shown in figure 7.22 as can be seen, the current pulses are much more frequent than for the uncoated conductor. This could be ascribed to the fact that the capacitance of the cage to conductor configuration has been changed with the introduction of the silicone coating. This will be discussed later in this chapter. The applied voltage was once again 112.5 kV, which corresponded to a surface gradient of 35.18 kV/cm.

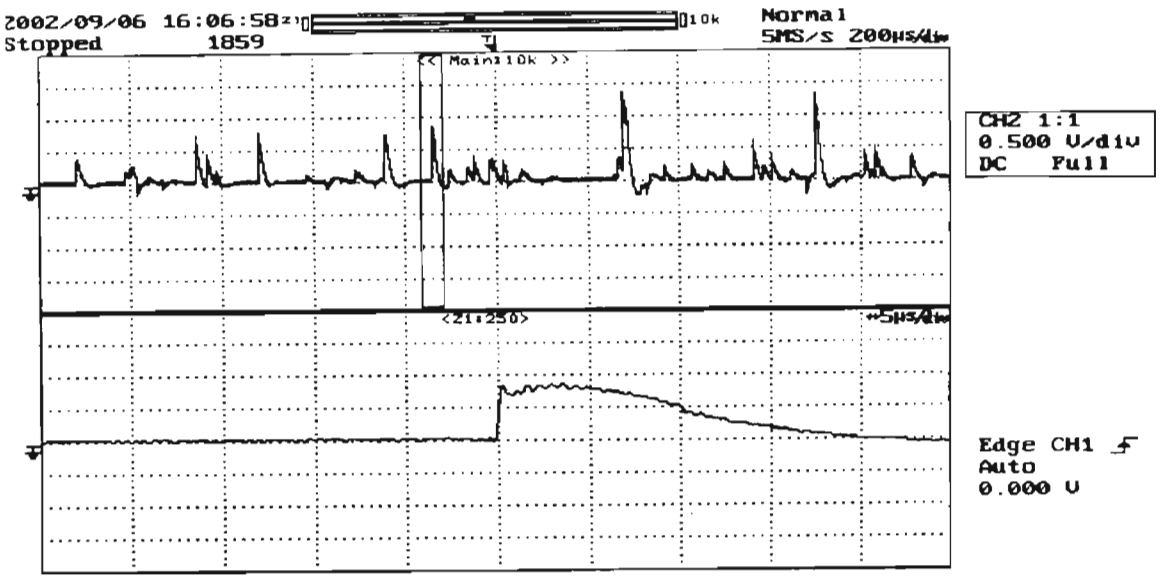

Figure 7.22: Time domain analysis of Half coated conductor corona current pulses

7.3.3 Analysis of the Fully coated conductor

The trend displayed in figure 7.22 is repeated in figure 7.23. A note should be made that in this figure the current division is 20 mA/division. Once again the current pulses have increased in frequency. As before this can be ascribed to the increase in the capacitance of the cage to conductor configuration. This time the applied voltage was 116.8 kV this corresponds to a surface gradient of 36.52 kV/cm.

Figure 7.23: Time domain analysis of Fully coated conductor corona current pulses

7.3.4 Analysis of the Sanded conductor

Figure 7.24 shows the results of the time domain analysis of the corona current pulses of the sanded 1.36 cm diameter conductor. As can be seen the pulses do not occur very frequently. This is attributed to the fact that the conductor has had all its rough edges and little strands sanded fine. Therefore there are not that many point sources where the electric field is intensified. Consequently the corona pulses are fewer and the corona currents measured are much lower. The applied voltage was 114.6 kV and this corresponds to a surface gradient of 35.83 kV/cm. The current division is once again 20 mA/division. What is noticeably different here is that the pulses have a higher amplitude than for the other three surface conditions.

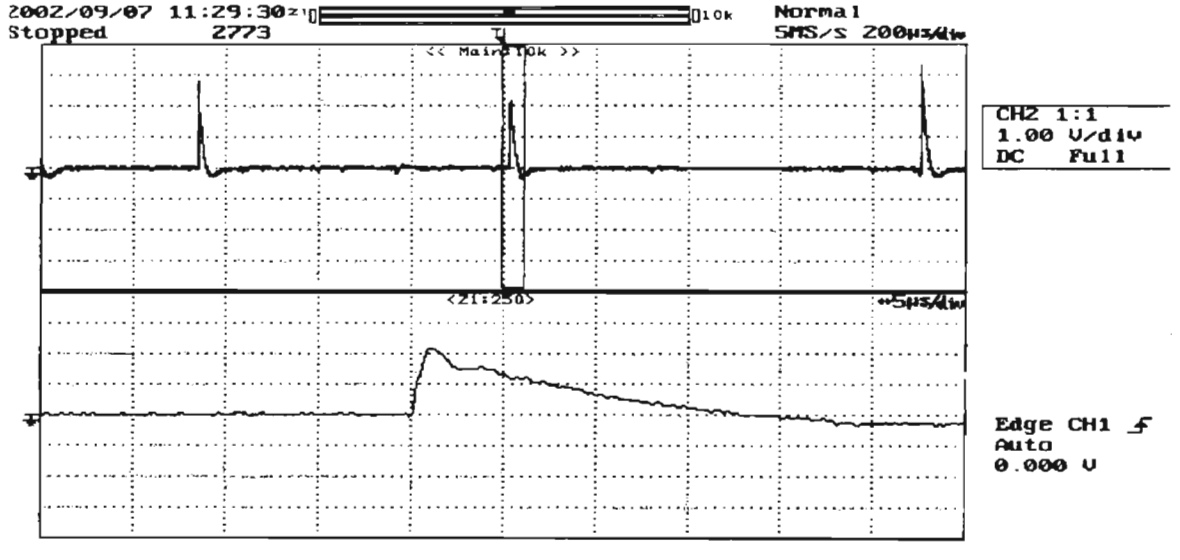

Figure 7.24: Time domain analysis of the sanded conductor corona current pulses

7.3.5 Discussion of the corona currents due to varying surface conditions

The increased corona current measured with the coating applied to the conductor was quite surprising and unexpected. This occurrence could be attributed to three factors.

- An increase in the capacitance of the conductor to cage configuration.
- Air bubbles in the coating could cause partial discharges to occur.
- The boundary effect brought into account due to the permitivity of the silicone coating.

The increase in capacitance

We know that $i = {dq}/{dt}$, this implies that $q = \int i.dt$. This says that if we have an increase in current as shown in the time domain analysis we will have a corresponding

increase in the charge q. Now as was shown for the same applied voltage, the currents measured with the coating applied was higher than those measured without `the coating. The formula, which relates the charge to the applied voltage, is as follows: $q = CV$. Where C is the capacitance. Now if the voltage remains constant and the charge measured increases this implies that the capacitance has increased, as shown in the following formula, $C = \frac{q}{V}$. Capacitance is defined as the ratio of the charge on one of its conductors to the potential difference between the conductors. A capacitor is defined as an electrical device, which consists of two conductors separated by a dielectric medium and is used for storing electrostatic energy [28]. The definition of a capacitor gives an indication of what could be increasing the capacitance of the cage to conductor configuration. The relative dielectric strength of air is taken as 1. The dielectric strength of the coating is 2.4 [18] relative to air. All calculations will employ the use of the relative dielectric strengths of the materials.

For the conductor to cage configuration shown in figure 7.25 the capacitance in Farads/meter is given by the following formula: $C = \frac{2\pi\varepsilon_2}{\ln\left(\frac{c}{a}\right)}$, where ϵ_2 = relative dielectric strength of air, c = radius of the cage, a = radius of the conductor.

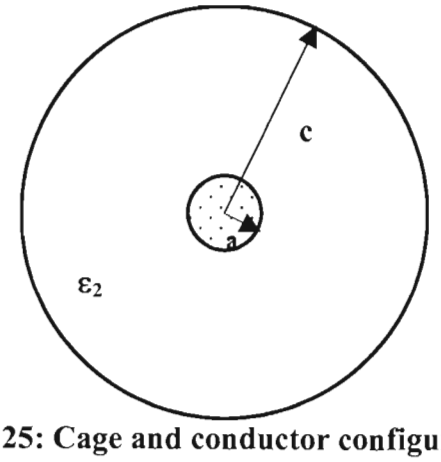

Figure 7.25: Cage and conductor configuration

The electric circuit diagram of figure 7.25 is as follows:

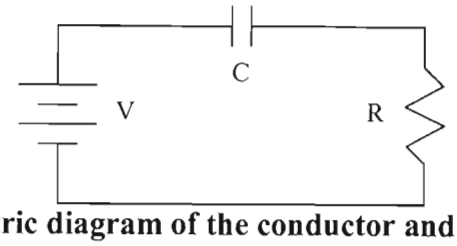

Figure 7.26: Electric diagram of the conductor and cage configuration

Where, V is the applied voltage, C is the capacitance of the conductor to cage configuration and R is the measuring resistance.

Now with a coating applied to the conductor the configuration changes as follows:

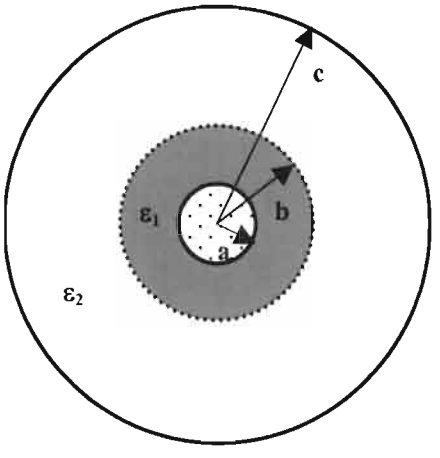

Figure 7.27: Corona cage with a coated conductor

As shown in figure 7.27 the coating has changed the conductor to cage configuration. There will now be an extra capacitance between the conductor and the coating. The capacitance in Farads/meter is as follows, $C_1 = \frac{2\pi\varepsilon_1}{\ln\left(\frac{b}{a}\right)}$, here ϵ_1 is the relative dielectric strength of the coating, b = radius of the coating and a = radius of the conductor. Furthermore the capacitance in Farads/meter of the cage to coating will now be as follows, $C_2 = \frac{2\pi\varepsilon_2}{\ln\left(\frac{c}{b}\right)}$, where ϵ_2 is the relative dielectric strength of air, c = radius of the cage and b = radius of the coating.

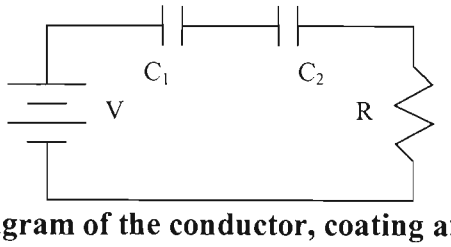

Figure 7.28: Electric diagram of the conductor, coating and cage configuration

In the figure above, V = applied voltage, C_1 = capacitance between the conductor and the coating, C_2 = the capacitance between the cage and the conductor and R = measuring resistance.

Without the coating the capacitance of the conductor to cage configuration for a 1.36 cm diameter conductor is

$$C = \frac{2\pi.1}{\ln\left(\frac{75}{0.68}\right)} \text{F/m} = 1.33595 \text{ F/m.}$$

Now with the coating having a thickness of 0.75 mm the capacitance of the coating and conductor configuration is as follows,

$$C_1 = \frac{2\pi.(2.4)}{\ln\left(\frac{0.6815}{0.68}\right)} \text{F/m} = 6.844*10^3 \text{ F/m.}$$

This implies that the charge which gets produced between the coating and the conductor is much higher than what gets produced in air, since the capacitance in the coating is much higher than the capacitance of free air.

The coating to cage capacitance is as follows,

$$C_2 = \frac{2\pi.1}{\ln\left(\frac{75}{0.6815}\right)} \text{F/m} = 1.33658\text{F/m.}$$

Once again we see that the capacitance of the coated conductor to cage configuration is higher than that of the uncoated conductor to the cage. So more charge will get produced in this region than what will be produced in air if there was no coating on the conductor.

Both the coating to conductor region as well as the cage to coating region now has a higher capacitance value than the single cage to conductor region. This implies that together both regions will produce more charge than what was produced by the single region. Consequently, more current will be produced.

We can now calculate the total capacitance of the two regions. From figure 7.28 we see that C_1 and C_2 are in series therefore we add them as follows,

$$C_t = \frac{1}{\sum_1^2 \frac{1}{C_n}} = \frac{1}{\frac{1}{6.844*10^3} + \frac{1}{1.33658}} = 1.33632 \text{ F/m.}$$

This value is 370 μF/m higher than what was calculated for the single region capacitance (i.e., the capacitance of the uncoated conductor to the cage).

Increase in current due to partial discharges

The increased current could also be attributed to microscopic air particles, which could have existed in the silicone rubber coating. This can be modeled using a field simulation software package [23].

The figure below shows that these microscopic air particles would cause local electric field intensification within the coating. Once again QUICKFIELD was used for the field modeling.

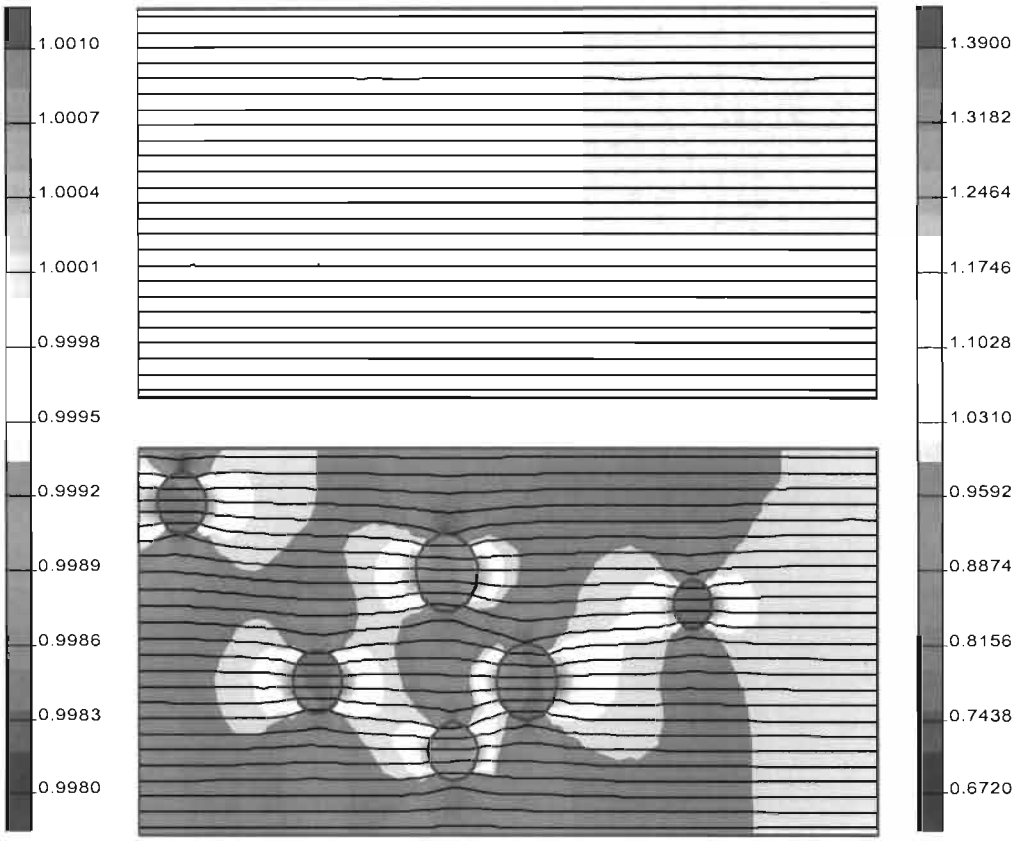

Figure 7.29: Uniform and non – uniform field distribution

The first block above corresponds to a cross sectional area of the silicone rubber used on the conductors. The legend on the left is associated with this block. As can be seen this simulation was carried out without any air particles present in the coating. The uniform field obtained due to this is as expected, uniform. The field has a value of about $1.0 * 10^7$ V/m.

The second block represents the coating with air particles present. The area inside these particles has a relative permittivity of 1, while the rest of the area in the block has permittivity of 2.4. As a result of these air particle, we can see an intensification of the electric field within the silicone. The eletric field is now non-uniform. With the field strength across the air particles being the highest. This field strength can be quantified by using the right hand side legend. The peak value of the field is $1.39 * 10^7$ V/m. This is 39% higher than the value of the field measured without air particles present. If this field value is high enough, we may have partial discharges occuring across the air particles.

Increase in E-Field in air due to boundary effects

From electromagnetic field theory we know that the normal component of electric flux density across a charge – free boundary, must be continous. This implies that the normal component of the flux density at the surface of the coating has to be equal to the normal component of the flux density of the air adjacent to the coating. This leads to the following equation:

$$D_{r1} = D_{r2}$$

Where: D_{r1} = flux density in region 1 (the coating) at radius r.

D_{r2} = flux density in region 2 (air) at radius r.

Since $D = \varepsilon E$, this implies that:

$$\varepsilon_1 E_1 = \varepsilon_2 E_2$$

at the boundary r. Where: ε_1 and ε_2 are the permitivities of the coating and air respectively.

E_1 and E_2 are the electric field gradients in the coating and air respectively.

The coating has a permitivity 2.4 times that of air. This means that the electric field gradient in the air is 2.4 times that of the electric field in the coating. Dependant upon the volt drop across the silicone coating, this could mean that the electric field gradient in air is higher with the coating present than if it were not present. A more thorough discussion of this is shown in Appendix D.

7.4 POWER LOSSES INCURRED

From the previous discussions it is clear that the larger the conductor diameter, the larger the corona currents measured will be at the same gradient and the same surface conditions. For example, at 20 kV/cm, the 1.76 cm diameter uncoated conductor will have the largest corona current measured, followed by the 1.36 cm diameter uncoated conductor with the 1.00 cm diameter uncoated conductor having the lowest currents measured, the same can be said about the half coated and fully coated conductors. This in turn means that the larger the diameter of the conductor the larger the corona losses incurred at the same gradient, since P = IV, and for the larger diameter conductor a larger V is required to obtain the same gradient when compared to a smaller diameter conductor. Since the Cahora Bassa line utilizes a larger diameter conductor for power transmission we can say that the power losses incurred by the line with a coating present will be higher than the losses incurred by the largest diameter conductor, which we tested, which was 1.76 cm in diameter.

Using the results obtained for the 1.76 cm wind free conductor tests we can get an idea of the power losses which will be incurred by using the coating on the Cahora Bassa line. In order to make a comparison between the conductor being uncoated, fully coated and half coated lets say that the Cahora Bassa line operates at about 19 or 20 kV/cm. The power losses measured in the laboratory cage was for a 1.0 m long conductor. So for the Cahora Bassa line which is 1400 km long the power loss, up to 20 kV/cm for the quad conductor bundle will be greater than the following figures due to the conductor used being larger than the one tested. The comparitive levels are shown in table 7.1 below. In the table below a * represents data that was either to small or to large to be measured by the instruments available in the laboratory.

E-Field	Power Loss in W		
kV/cm	No Coating	Half Coated	Fully Coated
15	*	1314	*
16	*	1578	*
17	*	1862	2979
18	0.0000	2760	4928
19	416.8	3330	6452
20	1753	3943	7448

Table 7.1: Expected Power Losses Incurred by a 1400 km long, 1.76 cm diameter, Quad conductor bundle.

At 19 kV/cm the losses incurred by the coated conductor is more than 15 times higher than for the uncoated conductor. At 20 kV/cm the losses incurred by the fully coated conductor is 4.2 times greater than for the uncoated conductor. So for the Cahora Bassa line these losses will be even greater.

7.5 SUMMARY

When the conductors were un-coated, the effects of wind blowing over them were minimal. This is verified by the tests done by Khalifa and Morris [1]. Once the conductors were half-coated, differences in corona currents measured were noted when the fan was blowing and when it was off. Generally the corona currents measured for the half-coated conductors were higher than the corona currents measured for the same un-coated conductors at the same surface gradient. The fan seemed to play more of a role the larger the conductor diameter became. This means that the fan had the least effect on the 1.00-cm diameter half-coated conductor, it had more of an effect on 1.36-cm diameter half-coated conductor and it had the most effect on the 1.76-cm diameter half-coated conductor. The fan blowing from the front produced the highest corona currents measured while the fan blowing from the side produced the next highest currents measured.

Results obtained for the fully coated conductors were very similar to the results obtained for the half-coated conductors. The only difference being that the corona currents measured for the various conductors were higher, at the same surface gradient than those measured when they were half-coated. Once again the fan played a role for the larger diameter conductors while the effects it had on the 1.00-cm diameter conductor were negligible. The effect of the fan blowing from the front of the cage resulted in the highest corona currents being measured, while the fan blowing from the side produced the second highest corona currents measured.

When the data was manipulated to determine the effect of the coating on the corona current, a trend emerged. This was that the highest corona currents were measured on the conductors that were fully coated. The next highest currents were measured for the conductors that were half-coated, while the lowest currents were measured for the un-coated conductors. This indicates that the effect of the silicone coating was that it increased the corona current measured from the conductors tested.

This increase in corona currents measured is attributed to the following:

- An increase in the cage to conductor configuration due to the coating and
- Partial discharges taking place within the silicone coating due to air particles in the coating.
- The boundary value effect brought about by the coatings permitivity.

The effect that this increased corona currents had on corona losses was marked. If the coating were to be used on the Cahora Bassa line, corona losses would be at least four times greater than what is currently experienced on the line.

With this in mind it is not recommended that this specific coating be used on transmission lines to mitigate the effects of corona until further tests and studies are conducted. It is further recommended that similar tests be conducted, however this time a more sensitive ammeter should be used so that corona currents, which correspond to surface gradients of 15 kV/cm and below, may be measured.

CHAPTER 8

CONCLUSIONS

8.1 CONCLUSIONS

- Laboratory cages are useful tools in determining the AC and DC corona performance of particular conductors. It has been shown that in a corona cage, it is quite simple to generate the surface gradients on conductors that are required to ensure corona activity.

- A large enough margin exists between corona onset voltage and breakdown voltage for the corona cage designed and constructed at the University of Durban-Westville for it to be used for testing of corona phenomenon on conductors. This was demonstrated by the 50% voltage criterion test. The largest conductor to be tested within the cage was strung up and the corona inception voltage was measured and recorded. The voltage was then increased until flashover occurred. No flashover occurred even though the voltage was increased to more than twice the inception voltage.

- The effect of wind on corona current on clean stranded conductors in the cage is minimal. The results of the tests, which determined the effects of wind on the conductor within a corona cage, have, been documented in this thesis. It is backed up by the results obtained by Khalifa and Morris in their tests.

- The effect of the silicone coating is such that it increases the corona currents measured in the presence and in the absence of wind. I.e. once the conductors were coated they produced larger corona currents than when they were un-coated. This occurred under all types of wind conditions.

- The effect of wind is increased for larger conductors that are coated compared to smaller diameter conductors that are also coated. I.e. The larger the conductor the larger the effect of wind on it once it has been coated with silicone.

- Further tests need to be undertaken to further measure the effects of the silicone coating at lower surface gradients than at those that were used for the tests

documented in this thesis. It is therefore recommended that a more sensitive ammeter be used in such tests.

- The coating will increase the corona losses incurred on the Cahora Bassa line and therefore it is not recommended that it be used on the line.
- The coating increases the corona currents in one of three ways:
  - Firstly it increases the capacitance in the cage.
  - Secondly if the coating has air particles trapped in it, they will lead to partial discharges taking place.
  - Finally due to the boundary conditions of electromagnetic field theory, the electric field on the surface of the coating may be several times higher than the field without the coating present. This leads to higher corona activity.

8.2 Further Work

Further work in the cage is recommended under the following:

- A study of the effects of conductor surface condition on corona currents (this will be a spin off of this project).
- Measurement of the radio frequency excitation functions of a range of conductors, the results of which should be compared to international work done.
- A study of the radio noise generated by the RTV coating.
- A study of radio noise generated by fire under HVDC potential. The corona cage can be used to measure these quantities in the presence of fire.

REFERENCES

1. M.M Khalifa, R.M. Morris. **A Laboratory Study of the Effects of Wind on DC Corona.** IEEE Transactions on Power Apparatus and Systems, VOL. PAS-80, No. 3. March 1967, pg 290 – 298.

2. AH Morton. **Advanced Electrical Engineering.** Pitman Publishing Limited, London 1977.

3. PS Maruvada, W Janischewskyj. **Analysis of Corona Losses on DC-Transmission Lines: I – Unipolar Lines.** IEEE Transactions on Power Apparatus and Systems, VOL Pas-88, No. 5, May 1969, p.p. 718-731.

4. PS Maruvada. **Corona Performance of High-Voltage Transmission Lines.** Research Studies Press LTD, 2000.

5. PS Maruvada. **Corona-Generated Space Charge Environment in The Vicinity of HVDC Transmission Lines.** IEEE Transactions on Electrical Insulation, VOL. EI-17 No. 2, April 1982, p.p. 125–130.

6. GB Johnson. **Degree of Corona Saturation for HVDC Transmission Lines.** IEEE Transactions on Power Delivery, VOL 5 No. 2, April 1990, p.p. 695-707.

7. VL Chartier. **Determination of Corona Generation Functions.** Understanding Power Line Electromagnetic Fields and Corona. Washington State University, 1993.

8. LM Geldenhuis. **Die Korona Verskynsel Op Hoogspanning Gelykstroom Transmissie Lyne.** Thesis submitted in partial fulfillment of the degree of Baccaleureus Ingenieurswese at the University of Stellenbosch. November 1996.

9. NN Rao. **Elements of Engineering Electromagnetics.** Prentice Hall, New Jersey, Fourth Edition 1994.

10. **EPRI, HVDC Transmission Line Reference Book.** Paolo Alta 1993.

11. **EPRI, Transmission Line Reference Book 345kV and Above.** Second Edition. Paolo Alta, 1982.

12. **EPRI, HVDC Reference Book, The Dalles Project.** Paolo Alta 1975.

13. K.R. Hubbard. **Evaluation of Electrical and Magnetic fields of the Cahora Bassa HVDC Transmission Line.** Eskom Technology Group, Research report, 1999.

14. S Ramo, JR. Whinnery, T Van Duzer. **Fields and Waves in Communication Electronics, Third Edition.** John Wiley, 1994.

15. W Janischewskyj, G Gela. **Finite Element Solution for Electric Fields of Coronating DC Transmission Lines**. IEEE Transactions on Power Apparatus and Systems, VOL PAS-98, No. 3, May/June 1979.

16. **Firmstar air circulators, Series "FS/FW". Information sheet.** LUFT Industries, NATAL (PTY) LTD. Website: www.luft.co.za

17. JP Holtzhausen et al. **High Voltage Engineering.** JP Holtzhausen et al, University of Stellenbosch, May 2000.

18. **Insilcote HV 2000" High Voltage Insulator Coating.** Information Brochure. A joint development by: Electric power research group, University of the Witwatersrand and Mace Electrical Technologies.

19. MWB (India) LTD. **Instruction Manual, 500kV – DC Test Set.**

20. **Magnetic Fields Exploration of the earth's magnetosphere.** http://www-istp.gsfc.nasa.gov/Education/wmfield.html.

21. Personal Discussions. AC Britten 2002.

22. AC Britten. **Postgraduate HVDC Lecture Notes**. University of Durban – Westville, July 2000.

23. **Quickfield, professional version instruction manual.**

24. **ROBIN OM 500T 30 000 Ohms/Volt Multitester, Instruction Manual.** Robin Electronics Limited. Precision Centre, Dwight Road, Watford, Herts, WD 1 8SS.

25. **Tablecurve® 2D Instruction Manual.** SPSS Science Inc. 233 S. Wacker Drive, 11th Floor, Chicago, IL 60606-6307, USA. Website: www.spssscience.com

26. AC Tomkins. **The Design, Construction and Testing of a Corona Cage.** Thesis submitted in partial fulfillment of the degree of Bachelor of Science in Engineering at the University of Cape Town, November 1986.

27. MG Comber, LE Zaffanella. **The use of Single Phase Test Lines and Cages to Evaluate the Corona Effects of EHV and UHV Transmission Lines.** IEEE Transactions on Power Apparatus and Systems, VOL PAS - 93, Jan/Feb 1974, p.p. 81-90.

28. CL. Wadhwa. **Electric Power Systems. Third Edition.** New Age International (P) Limited, Publishers. 2001.

29. EH Gehrig, AC Peterson, CF Clark, TC Rednour. **Bonneville Power Administration's 1100 – kV Direct Current Test Project: II – Radio Interference and Corona Loss.** IEEE Transactions on Power Apparatus and Systems, Vol. PAS – 86, No 3 March 1967.

30. PS Maruvada, RD Dallaire, OC Norris-Elye, JS Goodman. **Environmental effects of the Nelson River HVDC transmission lines – RI, AN, Electric Field, Induced Voltage, and Ion Current distribution tests.** IEEE Transactions on Power Apparatus and Systems, Vol. PAS – 101, No 4 April 1982.

Bibliography

31. U.S Department of Commerce. **Measurement of Ion Current Density at Ground Level in the Vicinity of High voltage DC Transmission Lines.** December 1981.

32. PS Maruvada, W Janischewskyj. **Analysis of Corona Losses on DC-Transmission Lines: II – Bipolar Lines.** IEEE Transactions on Power Apparatus and Systems, VOL Pas-88, No. 10, October 1969, p.p. 1476-1491.

33. RM Morris, AR Morse, JP Griffin, OC Norris-Elye, CV Thio, JS Goodman. **The Corona and Radio Interference Performance of the Nelson River HVDC Transmission Lines.** IEEE Transactions on Power Apparatus. Vol. PAS – 98, No. 6 Nov/Dec 1979.

34. RD Dallaire, PS Maruvada. **Corona Performance of a ± 450 kV Bipolar DC Transmission Line configuration.** IEEE transactions on Power Delivery, Vol PWRD – 2, No. 2, April 1987.

35. RM Morris, PS Maruvada. **Conductor Surface Voltage Gradients on Bipolar HVDC Transmission Lines.** IEEE Transactions on Pwer Apparatus and Systems. Vol. PAS – 95, No. 6, Nov/Dec 1976.

36. GL Reiner, EH Gehrig. **Celilo – Sylmar ± 400 kV Line RI Correlation with Short Test Line.** IEEE Transactions on Power Apparatus and Systems, Vol. PAS – 96, No. 3, May/June 1977.

37. MG Comber, GB Johnson. **HVDC Field and Ion Effects Research at Project UHV: Results of the Electric Field and Ion Current Measurements.** IEEE Transactions on Power Apparatus and Systems, Vol. PAS – 101, No. 7, July 1982.

38. DH Nguyen, PS Maruvada. **An Exposure Chamber for Studies on Human Perception of DC Electric Fields and Ions.** IEEE Transactions on Power Delivery, Vol. (, No. 4, October 1994.

39. PS Maruvada, RD Dallaire, R Pedneault. **Development of Field – Mill Instruments for Ground – Level and Above – Ground Electric Field Measurement under HVDC Transmission Lines.** IEEE Transactions on Power Apparatus and Systems, Vol. PAS – 102, No. 3, March 1983.

40. MG Comber, R Kotter, R McKnight. **Experimental Evaluation of Instruments for Measuring DC Transmission Line Electric Fields and Ion Currents.** IEEE Transactions on Power Apparatus and Systems, Vol. PAS – 102, No. 11, November 1983.

41. Y Sunaga, Y Sawada. **Method of Calculating Ionized Field of HVDC Transmission Lines and Analysis of Space Charge Effects on RI.** IEEE Transactions on Power Apparatus and Systems, Vol. PAS – 99, No. 2, March/April 1980.

42. K Adamiak. **Adaptive Approach to Finite Element Modelling of Corona Fields.** IEEE Transactions on Industry Applications, Vol. 30, No. 2, March/April 1994.

43. MG Poland, MW Belsher, AA Osipovich. **Bonneville Power Administration's 1100 – kV Direct Current Test Project: I – Measurement and Instrumentation.** IEEE Transactions on Power Apparatus and Systems, Vol. PAS – 86, No. 3, March 1967.

44. L Paris, M Sforzini. **RI Problems in HV – Line Design.** IEEE Transactions on Power Apparatus and Systems, Vol. PAS – 87, No. 4, April 1968.

45. Y Sawada, T Sasano, Y Sunaga, T Tsuzura. **The Radio Interference Characteristics of Four and Three – Conductor Bundles of HVDC Line: Shiobara 600 – kV Laboratory.** IEEE Transactions on Power Apparatus and Systems, Vol. PAS – 96, No. 6, November/December 1977.

46. W Janischewskyj, A Arainy. **Corona Characteristics of Simulated Rain.** IEEE Transactions on Power Apparatus and Systems, Vol. PAS – 100, No. 2, February 1981.

47. BM Bailey. **Progress Report on the BPA HV DC Test Line Radio Noise and Corona Loss.** IEEE Transactions on Power Apparatus and Systems, Vol. PAS – 86, No. 10, October 1987.

48. GJ Van Uytven, AW Hannah, I Reinart, LJ Cole. **Design of the Proposed ± 400 kV DC Gull Island Transmission Lines.** IEEE Transactions on Power Apparatus and Systems, Vol. PAS – 97, No. 2, March/April 1978.

APPENDIX A

DESIGN DIAGRAMS AND PHOTOGRAPHS

Below follows the final design diagrams of the corona cage.

Diagrammatic Representations of the Corona Cage

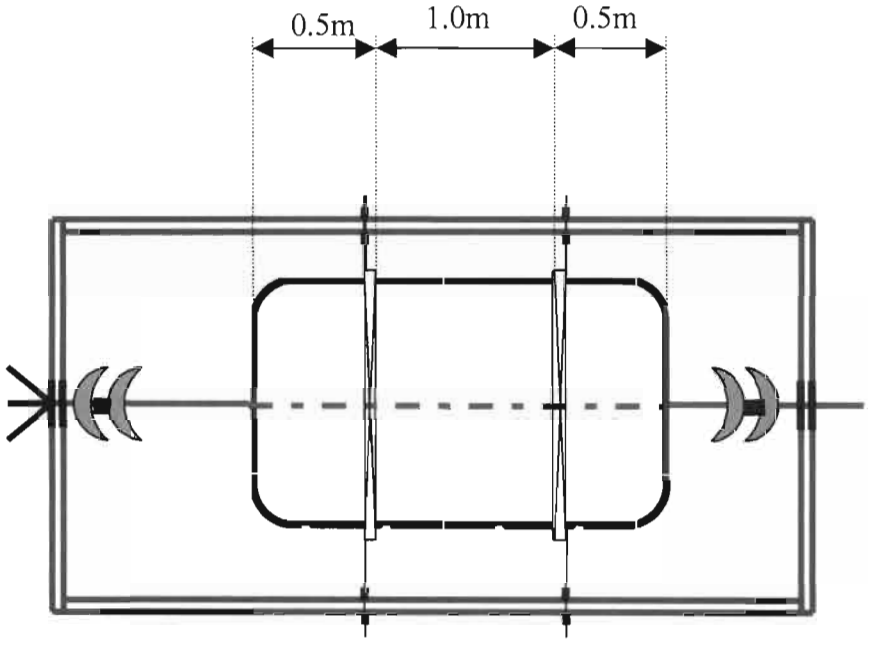

Figure A.1: Side View of the Corona Cage

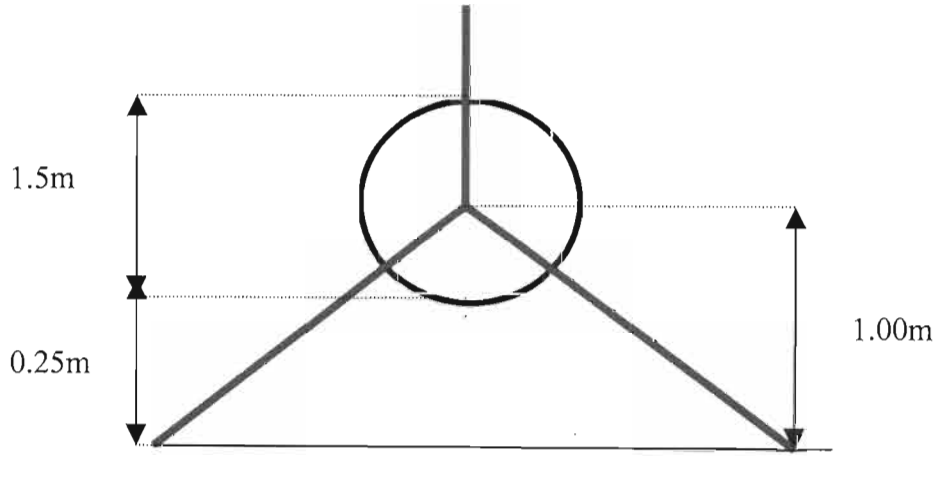

Figure A.2: Front View of the Corona Cage

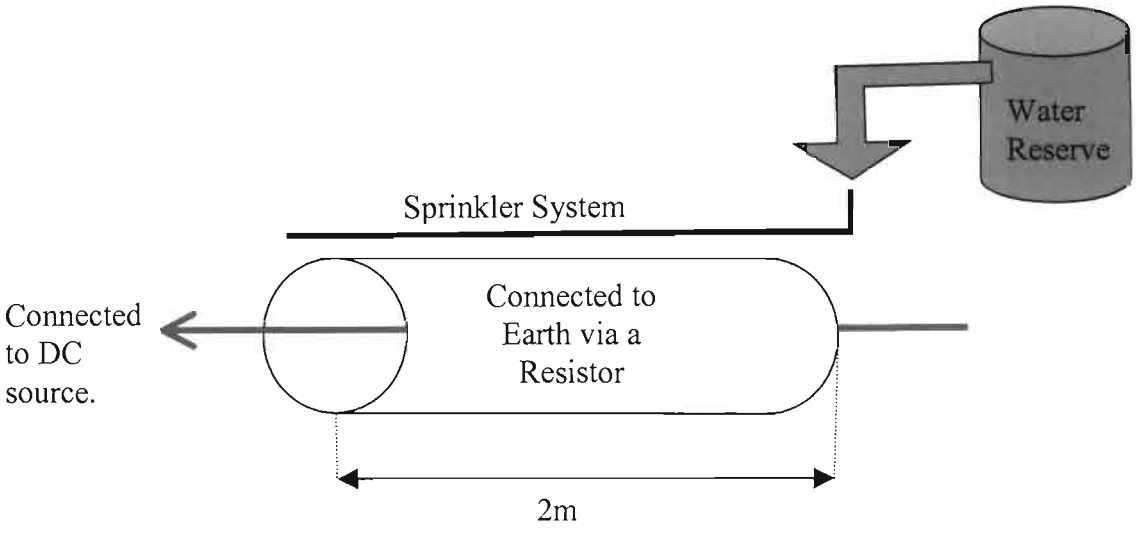

Figure A.3: Schematic of the Corona Cage, Showing Sprinkler System and Earthing Connection

Once these diagrams were finalized they were handed to the technical support team at the university who then built the cage, using the following materials:

THE MATERIALS USED IN THE CONSTRUCTION OF THE CAGE:

Support Structure

The support structure with a length of 5 m, a width of 3 m and a height of 2 m used 50 by 50-mm square steel tubing. The total tubing required for the support structure was calculated to be 30m, however 36m of this tubing was purchased in order to cover any contingency that may have arisen during the construction work.

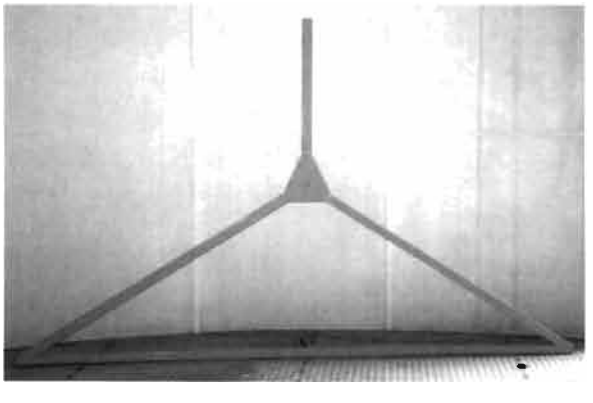

Figure A.4: A-frame Section of Support Structure.

The a-frame end fitting of the support structure is shown in figure A.4. Two of these a-frames were used, one on either end of the structure. Square tubing was used one the bottom points of the a-frame to connect them together. Angle iron and square tubing

was used on the top point of the a-frame. The angle iron was used for supporting the weight of the cage.

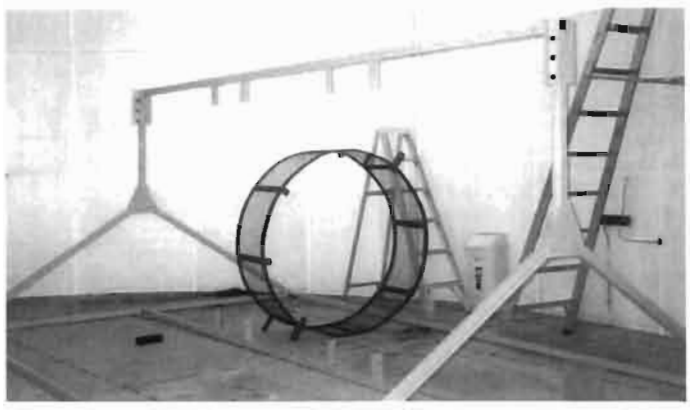

Figure A.5: Completed Support Structure

Figure A.5 above shows the completed support structure. The entire support structure can be easily dismantled and transported to another location.

Cage Rings

The cage was built out of steel mesh. With eight, 3mm flat bar struts for support on the length of each ring. The total length of steel mesh required for the cage was 2m. However 2.5 meters was bought in case of contingencies. The width of mesh required was calculated using the following formula.

$$w = 2 \cdot \pi \cdot r \qquad \text{(A.1)}$$

Where: w = width

r = cage radius

Since r = 75cm, w = 471cm. The total steel mesh which was ordered was 5 by 2.5-m. This equals 12.5 m^2. Also, 16m of flat bar was required. 20m was bought once again for contingency purposes.

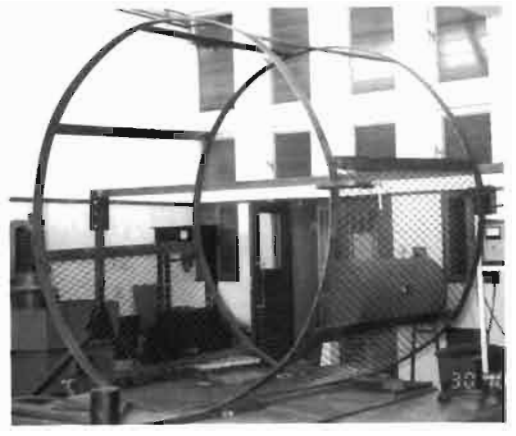

Figure A.6: Mesh being Attached to Center ring

Figure A.7: Completed Outer Ring

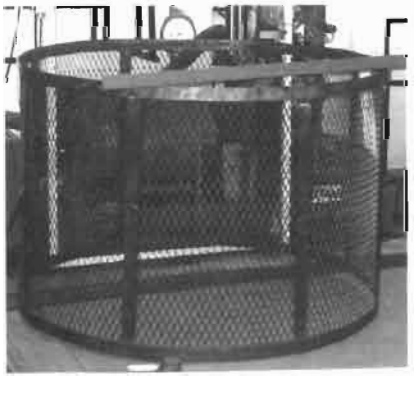

Figure A.8: Complete Inner Ring

Figures A.6 to A.8 above show the wire mesh being attached to the circular fittings. These fittings were specially made out of flat bar. The supporting struts joining two fittings was fitted at the workshop.

Terminating Fitting

A 6 mm thick steel plate was used to make the end fitting for the conductor terminals. One end fitting would have a turn-buckle in order to tension the conductor and insulator string in the cage. The end fitting would be bolted to the insulating clamps.

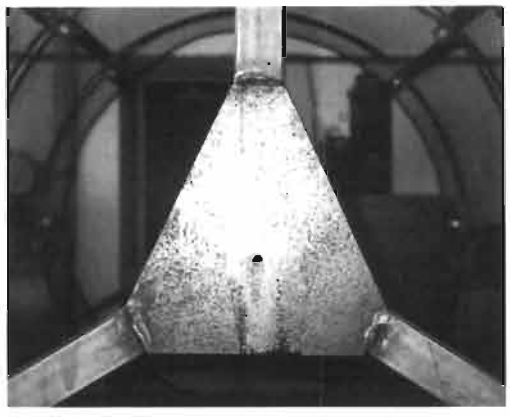

Figure A.9: End Fitting

Cage Support

Angle iron was also bought to suspend the outer cages from the support structure. As well as to join the A-frame end structures to the rest of the support structure. The cage was constructed in such a way that it could easily be dismantled and moved to another location.

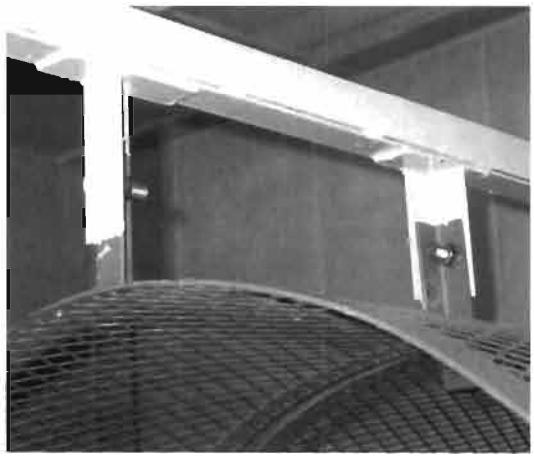

Figure A.10: Top Cage Support

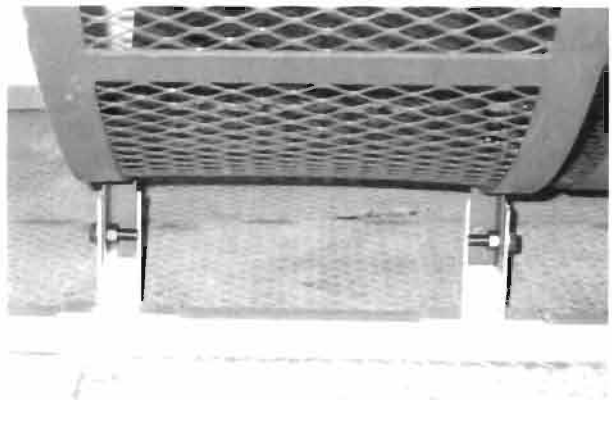

Figure A.11: Bottom Cage Support

Insulators used to support the cage

The sixteen, 10mm insulators were used to connect the inner ring to the two outer rings.

Figure A.12: Initial Connecting Insulator

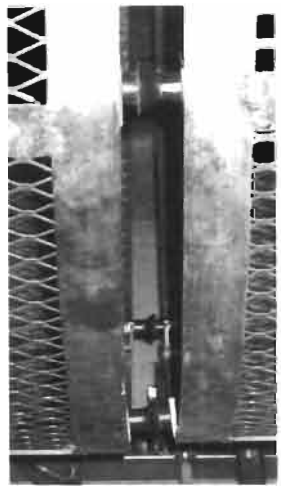

Figure A.13: Rings Attached by Insulators

The cage was left in the workshop overnight, with the inner ring suspended by the insulators attached to the outer rings. The next morning it was discovered that these insulators could not withstand the shearing force exerted upon them and a lot of them failed.

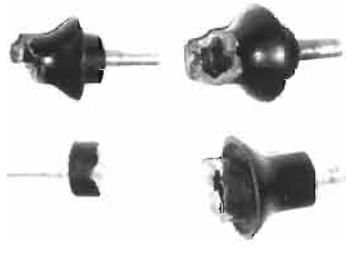

Figure A.14: Failed Insulators

After these insulators failed, it was decided that we would design the insulators to be used in the cage. These new insulators are made of Vesconite. They are very strong and non-conducting. They flashed over at 28 kV DC.

Figure A.15: New Insulators

Conductors used for testing

The initial conductors to be tested were obtained from Mr. Tony Britten who supplied a conductor with a diameter of 1.36cm. Mr. Ian Ferguson from Eskom in New Germany kindly supplied the mink conductor (1 cm diameter). Arthur Burger supplied the earthwire which, was used on the Cahora Bassa Line (1.76 cm diameter).

Support Structure Insulators

The insulators used during testing were obtained from Fabio bologna at ESKOM TSI.

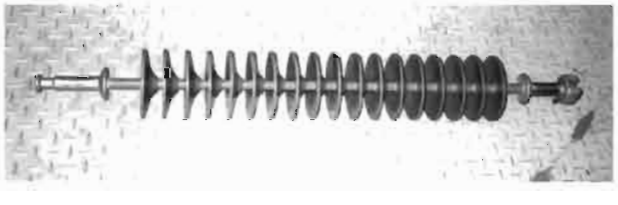

Figure A.16: Conductor Support Insulator

Figure A.17: Conductor Attached to Corona Cage Via the Insulator

The main criterion for the choice of insulators was that the length between conducting parts of the insulator should be greater than 75 cm, which is the greatest cage to conductor distance. This would ensure that the shortest distance between the energised conductor and ground would be through the cage.

Installation in the laboratory

Once the cage and support structure had been assembled in the workshop, it was dis-assembled and taken down to the HVDC laboratory where the technicians re-assembled it. Assembly and dis-assembly was made easy due to the fact that the cage was designed and built in parts which are easily joined together. This is shown in figure A.18 below.

Figure A.18: Laboratory Technicians attaching Cage Rings to Support Structure

Figure A.19: Completed Corona Cage in HVDC Laboratory

APPENDIX B

HVDC LABORATORY CONSTRUCTION

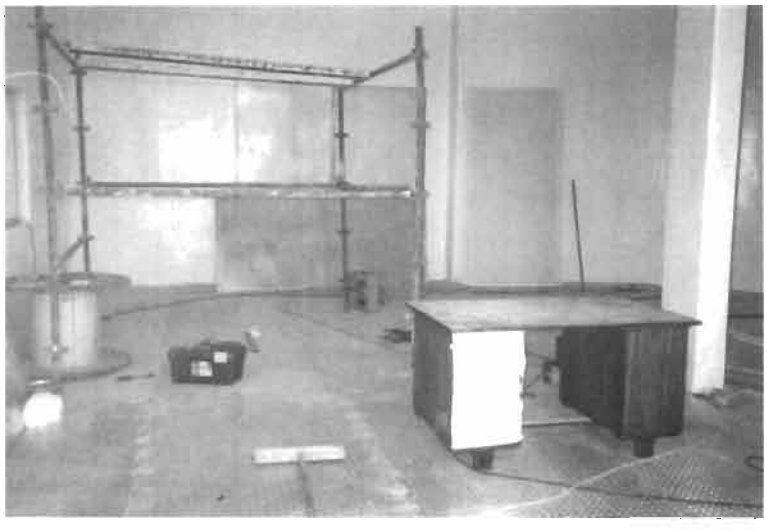

Figure B.1 HVDC Laboratory Under construction

Figure B.2: Installation of the shielding mesh

Figure B.3: Outside view of HVDC Laboratory under Construction

Figure B.4: Outside View of Completed HVDC Laboratory

Figure B.5: HVDC test kit being Assembled

APPENDIX C

MEASUREMENT INSTRUMENTS

C.1 Ammeter

The ammeter used during testing was discussed in chapter five. Below follows a detailed diagram of the controls and jacks of this ammeter as well as a photograph of it.

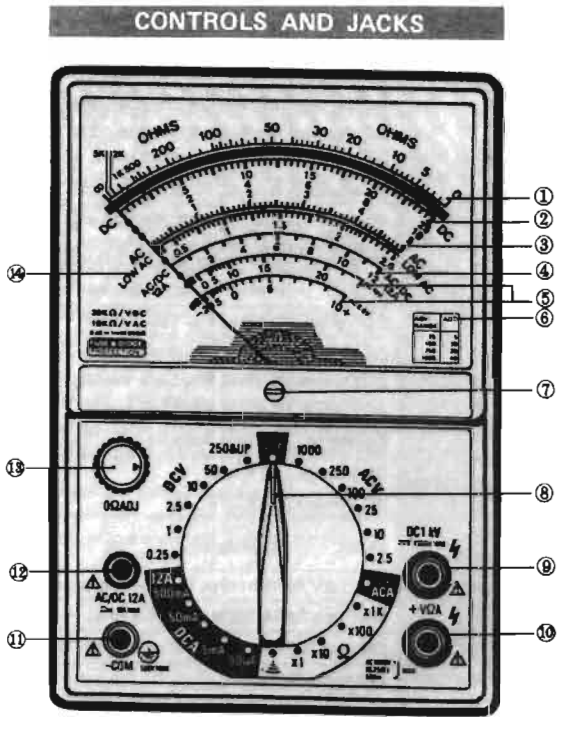

Figure C.1: Diagram of Ammeter used

1. Ohms Scale
2. DC Volts, DC Ampere Scale
3. AC Volts Scale
4. AC/DC 12 A Scale
5. dB (Decibel Scale)
6. dB Add number chart refer ACV Scale
7. Meter Zero Adjusting Screw

8. Range Selector Knob
9. For only DC 1000V (DC 1 kV) jack terminal plug-in connection for red test lead.
10. +AC/DC Voltages, DC Amperes and Ohms Jack Terminal, Except DC 1000V and AC/DC 12 A measurement.
11. COM Jack Terminal, Plug-in connection for black test lead.
12. For only AC/DC 12A Jack terminal. Plug-in connection for red test lead.
13. Ohms zero adjusting knob.
14. Low AC volts Scale for AC 2.5 V range.

APPENDIX D

Direct Integration of Laplace's Equation: Field Between Coaxial Cylinders with Two Dielectrics

The following is a solution for the voltage of co-axial cylinders with two dielectrics which was modified from Ramo, Whinnery and Van Duzer [Ramo, Whinnery, Van Duzer, 1994]

Figure D.1 below is a representation of coaxial cylinders with two dielectrics.

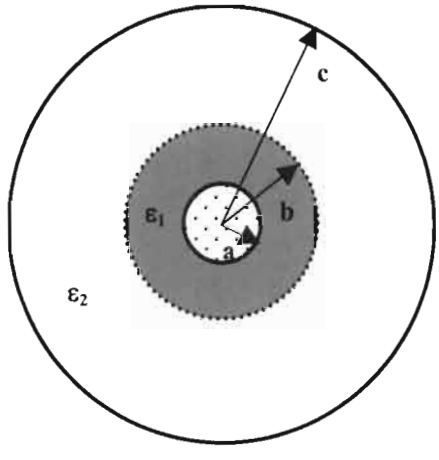

Figure D.1: Coaxial Cylinders with Two Dielectrics

a = conductor radius

b = a + thickness of coating

c = radius of cage

ε_1 = permitivity of silicone

ε_2 = permitivity of air

The inner potential at a, is V_0 and the outer potential at b is 0 V.

Laplaces equation in cylindrical coordinates is as follows:

$$\nabla^2\Phi = \frac{1}{r}\frac{\partial}{\partial r}\left(r\frac{\partial\Phi}{\partial r}\right) + \frac{1}{r^2}\frac{\partial^2\Phi}{\partial\phi^2} + \frac{\partial^2\Phi}{\partial z^2} = 0 \qquad (D.1)$$

As stated in chapter four, due to the symmetry of the coaxial configuration the problem reduces to a one-dimensional problem. Equation D.1 therefore becomes:

$$\frac{1}{r}\frac{\partial}{\partial r}\left(r\frac{\partial\Phi}{\partial r}\right) = 0 \qquad (D.2)$$

Now multiplying by r on both sides and integrating we get:

$$\left(r\frac{\partial\Phi}{\partial r}\right) = C_1 \quad \text{(D.3)}$$

Integrating again we have:

$$\Phi_1 = C_1 \ln r + C_2 \qquad \text{(D.4)}$$

This solution is valid in the first dielectric region (ε_1), where a < r < b. The same equations can be used for the second dielectric region (ε_2). This resultant equation is as follows:

$$\Phi_2 = C_3 \ln r + C_4 \qquad \text{(D.5)}$$

This solution is valid region 2 where b < r < c.

Now applying the boundary conditions:

A: $\Phi_1 = V_0$ at r = a

B: $\Phi_2 = 0$ at r = c

These are two equations required to solve equations D.4 and D.5 simultaneously. Since we have four unknowns (C_1, ... C_4) in these two equations we will need another two equations to compliment A and B.

Continuity conditions apply at the boundary between the two dielectric media. This says that the potential and normal component of electric flux density must be continuous across the charge-free boundary. Therefore we have the following:

C: $\Phi_1 = \Phi_2$ at r = b

D: $\varepsilon_1\left(\partial\Phi_1/\partial r\right) = \varepsilon_2\left(\partial\Phi_2/\partial r\right)$ at r = b

D therefore implies that $\varepsilon_1 C_1 = \varepsilon_2 C_2$ at r = b.

Now substituting A into D.4 we get:

$$V_0 = C_1 \ln a + C_2$$

This implies that:

$$\underline{C_2 = V_0 - C_1 \ln a} \qquad \text{(i)}$$

Now substituting B into D.5 we get:

$$0 = C_3 \ln r + C_4$$

this implies that:

$$\underline{C_4 = -C_3 \ln r} \quad \text{(ii)}$$

Now substituting C into D.4 and D.5 we get:

$$C_1 \ln b + C_2 = C_3 \ln b + C_4$$

This gives us:

$$\underline{C_3 = (C_1 \ln b + C_2 - C_4)/\ln b} \quad \text{(iii)}$$

Substituting D into D.4 and D.5 we get:

$$\varepsilon_1 C_1 = \varepsilon_2 C_3$$

$$\underline{C1 = \varepsilon_2 C_3/\varepsilon_1} \quad \text{(iv)}$$

Manipulating (iii) and equating to (iv):

$$C_3 = (C_1 \ln b + C_2 - C_4)/\ln b$$

$$\Rightarrow C_1 = (C_3 \ln b + C_4 - C_2)/\ln b$$

So:

$$(C_3 \ln b + C_4 - C_2)/\ln b = \varepsilon_2 C_3/\varepsilon_1$$

Making C_3 the subject of the formula:

$$C_3 = \frac{C_4 - C_2}{\ln b \times \left(\frac{\varepsilon_2}{\varepsilon_1} - 1\right)}$$

Substituting (i) and (ii) into the above equation:

$$C_3 = \frac{-C_3 \ln c - \left(V_0 - C_1 \ln a\right)}{\ln b \times \left(\frac{\varepsilon_2}{\varepsilon_1} - 1\right)}$$

After some algebraic manipulation we get:

$$C_3 = \frac{-V_0}{\ln b \times \left(\frac{\varepsilon_2}{\varepsilon_1} - 1\right) + \ln c - \ln a \times \left(\frac{\varepsilon_2}{\varepsilon_1}\right)} \qquad (*)$$

Once we have obtained C3 the other constants C1, C2 and C4 are quite easy to get, they are as follows:

$$C_1 = \frac{-V_0\left(\frac{\varepsilon_2}{\varepsilon_1}\right)}{\ln b \times \left(\frac{\varepsilon_2}{\varepsilon_1} - 1\right) + \ln c - \ln a \times \left(\frac{\varepsilon_2}{\varepsilon_1}\right)} \qquad (**)$$

$$C_2 = V_0 - \frac{-V_0\left(\frac{\varepsilon_2}{\varepsilon_1}\right)\ln a}{\ln b \times \left(\frac{\varepsilon_2}{\varepsilon_1} - 1\right) + \ln c - \ln a \times \left(\frac{\varepsilon_2}{\varepsilon_1}\right)} \qquad (***)$$

$$C_4 = \frac{V_0 \ln c}{\ln b \times \left(\frac{\varepsilon_2}{\varepsilon_1} - 1\right) + \ln c - \ln a \times \left(\frac{\varepsilon_2}{\varepsilon_1}\right)} \qquad (****)$$

Now the initial equations can be easily solved by, substituting the known variables into the equations for C_1, C_2, C_3 and C_4. Then substitute these variables back into the original equations.

Now: a = 0.88 cm, b = 0.8825 cm, c = 75 cm, $\varepsilon_1 = 1$, $\varepsilon_2 = 2.4$ and $V_0 = 150$ kV. This implies that C1 = -14.065, C2 = 148.202, C3 = -33.756, C4 = 145.741.

So the voltage at the surface of the coating is 149.77 kV, this means a volt drop of 0.223 kV or 230 V. So the maximum electric field gradient in the coating is 92 kV/cm.

APPENDIX E

Analysis of Silicone Coating for Corona Reduction

Coatings of Silicone rubber material are being evaluated to determine if their use can reduce the problem of corona discharge. Three samples were submitted for scanning electron microscope (SEM) analysis. They were marked as follows:

1. Mid-section small conductor (1.00 cm diameter)
2. Mid-section large conductor (1.76 cm diameter)
3. Mid-section medium sized conductor (1.36 cm diameter)

In the evaluations use is made of the material behaviour when an electron beam accelerated to 20KV is focussed onto the sample as target. This beam is normally under high vacuum (less than 10^{-4} mbar) and produces a surface charge on the sample depending on the interaction of the beam on the sample and the capacitative and conductive discharge mechanisms. The methods employed are not fully researched and do not give clear quantitative data, but could help in identifying and highlighting differences in behaviour.

EDX analysis of the samples

The samples were analysed by energy dispersive X-ray spectroscopy (EDX). The spectra show high silicone peaks with few contaminants except aluminium (probably from the conductor) and titanium (probably a pigment). Figure1 shows two spectra taken on samples 1 and 2. Except for a possible small variation in titanium content, the composition showed no significant differences in the three samples. The at the high end of the spectrum the cut-off potential was in the range 14KV to 16KV indicating a beam energy loss due to sample charging of about 4 to 6KV. The cut-off potential was not clearly defined, making a comparison between the samples subjective.

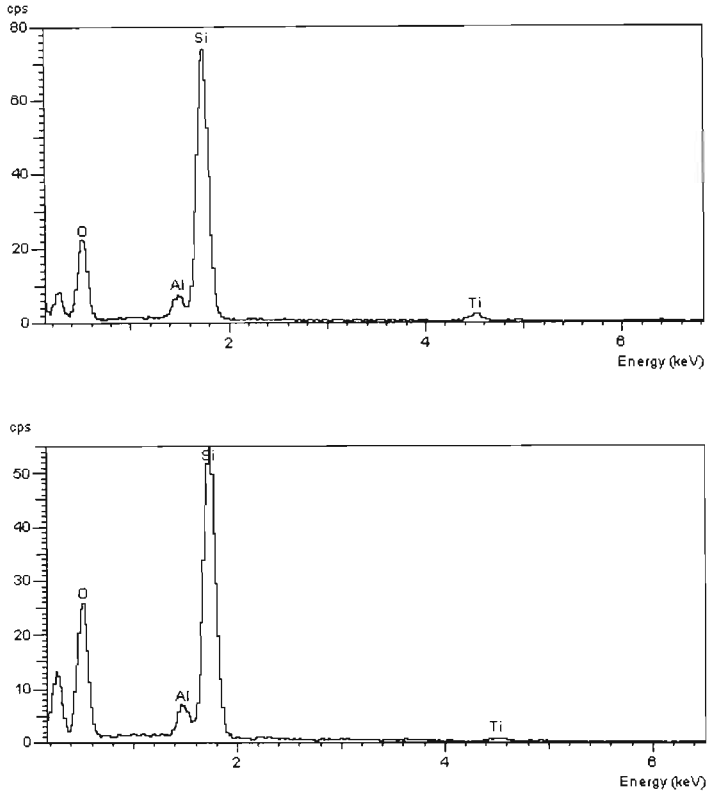

Figure E1. EDX spectra of coatings.

Charging:

Samples were imaged by an electron beam at 20KV at a constant beam current, not measured but estimated at a few micro-Amps. The images of all three samples at the magnification setting of 10X were stable in all cases. At 50 times magnification, corresponding to about a square millimetre image area, the image was distorted and unstable. Figure 1 shows the images of the three samples at the two magnification settings.

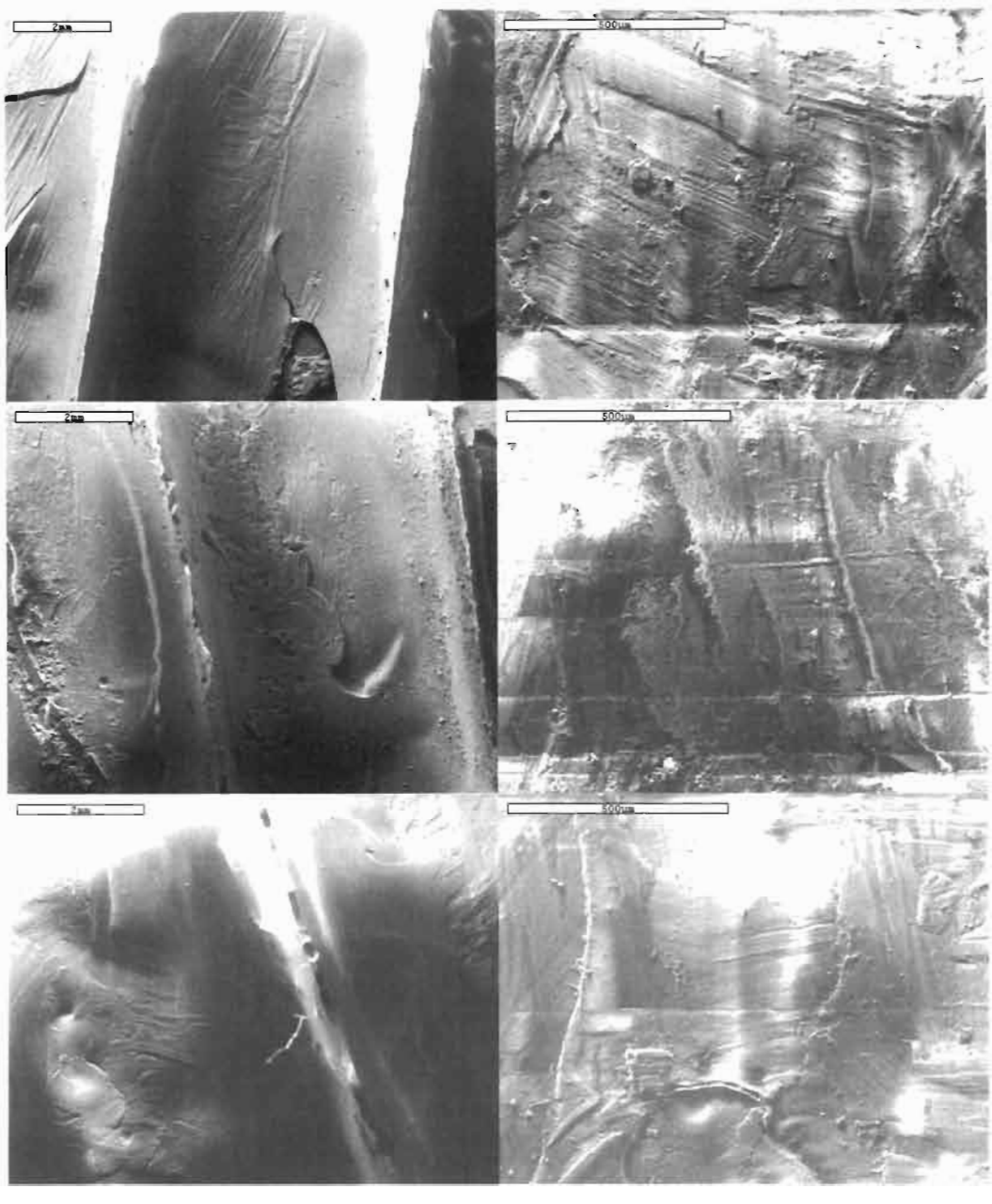

Figure E2. Images at 20KV. From top to bottom samples 1 to 3. Left image at 10x magnification, right image at 50x magnification.

Sample 2 was the least stable (most charged) image. This trend was confirmed when the voltage was then reduced to determine the effect of the residual charge.

Sample 2 remained fully charged, deflecting the beam towards the internals of the specimen chamber for at least 30 minutes. The deflected image was stable and undistorted at low voltages and remained stable at voltages up to 7KV. Figures 2a to 2c show images of the secondary detector taken at 1.2KV, 2KV and 5KV. Figure 2d shows an image of Sample 1 at 2KV. The latter image was highly distorted stable for only a few minutes. The image from Sample 3 was similar. It is concluded that a

significant difference exists between the discharge of the three samples with Sample 2 discharging less readily than the other two.

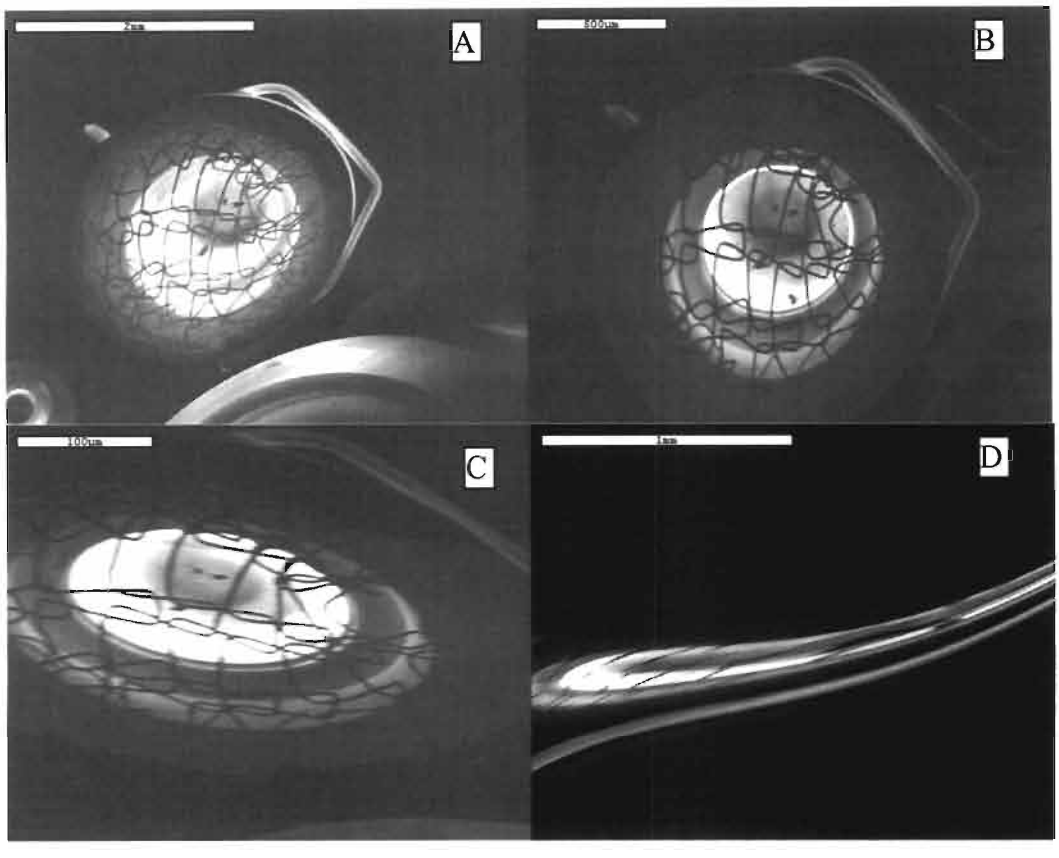

Figure E3. Images of secondary electron detector reflected from charged sample. Sample 2: A: 1.2KV B: 2KV C: 5KV D: Sample 1 at 2KV.

Ionic discharge

The sample chamber was filled with air at controlled pressure using the environmental SEM facilities. This has the effect of discharging the sample due to ionic conduction (corona discharge). The specimen charge typically dissipates as the pressure in the partial vacuum increases beyond a particular value. These values are tabled below:

Sample number	Pressure (mbar)
1	2.4
2	1.8
3	2.2

Table E.1 Pressure exerted on samples.

It can be seen that sample 2 discharged most readily in air, even though the charging in high vacuum as determined above was more severe and more stable.

APPENDIX F

ELECTRIC AND MAGNETIC FIELDS

F.1 ELECTRIC FIELDS

In order to understand electric fields and field theory, it is important to understand charge theory.

F.1.1 Electric Charge

The phenomena of two objects sticking together can be explained by the notion that objects, when rubbed together, can gain a net **electric charge**. There are two types of charge, labeled positive (+) and negative (-), with the following basic properties:

- Like charges of the same sign, repel each other.
- Unlike charges of the opposite sign, attract each other.

Detailed experiments have established the following fundamental characteristics of electric charge:

- Charge is never created nor destroyed - it is *conserved.*
- Charge always comes in an integral multiple of a basic unit - it is *quantized.*

This basic unit of charge is conventionally denoted by e:

$$e = 1.602 \times 10^{-19}\, Coulombs(C)$$

From Newton's Universal Law of Gravitation, it is known that a gravitational force field is associated with material bodies due to their physical property, known as mass. Newton showed that the gravitational force of attraction between two bodies of masses, m_1 and m_2, separated by a distance R, which is large compared to their sizes, is equal to:

$$\frac{m_1 m_2 G}{R^2} \qquad \text{(F.1)}$$

Where: m_1 and m_2 are the masses of the objects

G is the universal gravitational constant

In a similar manner, a force field known as the electric field is associated with bodies that are charged. A material body may be charged positively or negatively or may possess no net charge at all [9].

Alternatively, we can say that an electric charge creates an electric field in the space surrounding it. When a second charged particle approaches the first, it reacts with it, indirectly, through the fields created by both particles. The accepted unit of charge, from the SI (International System), is the Coulomb (C) which, compared to the charge of an electron (-1.60219E-19 C), is high. In fact $6.24*10^{18}$ electrons represent a charge in one negative coulomb.

From experiments conducted by Coulomb it was shown that for two charged bodies, which are small in size compared to their separation so that they can be considered as point charges:

- The magnitude of the force is proportional to the square of the distance between the charges.
- The magnitude of this force depends on the medium.
- The direction of the force is along the line joining the charges.

For free space, the constant of proportionality is $1/4\pi\varepsilon_0$ where ε_0 is known as the permittivity of free space, having a value of $8.854*10^{-12}$. Now, if we consider two point charges Q_1C and Q_2C separated R m in free space as shown in figure F.1, then the forces $\mathbf{F}_1$ and $\mathbf{F}_2$ experienced by Q_1 and Q_2 respectively are given by

$$F_1 = \frac{Q_1 Q_2}{4\pi\varepsilon_0 R^2} i_{21} \qquad \text{(F.2)}$$

$$F_2 = \frac{Q_2 Q_1}{4\pi\varepsilon_0 R^2} i_{12} \qquad \text{(F.3)}$$

Where $\mathbf{i}_{21}$ and $\mathbf{i}_{12}$ are unit vectors along the line joining Q_1 and Q_2 as shown in the figure below. Equations 2.2 and 2.3 represent Coulomb's law.

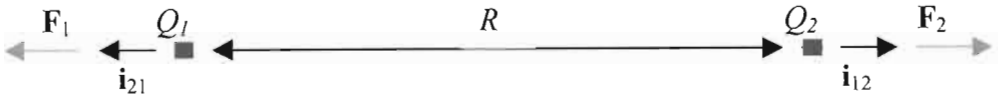

Figure F.1: Forces Acting on a Particle

F.1.2 Electric Field Definition

For the case of the gravitational field of a material body, we define the gravitational field intensity as the force per unit mass experienced by a small test mass placed in that field. Similarly, the force per unit charge experienced by a small test charge placed in an electric field is known as the electric field intensity. This is denoted by the symbol **E**. Alternatively, if in a region of space, a test charge q experiences a force **F**, then the region is said to be characterized by an electric field of intensity **E** given by:

$$E = \frac{F}{q} \qquad \text{(F.4)}$$

The unit of the electric field intensity is Newton per coulomb, or more commonly volt per meter, where a volt is Newton-meter per coulomb.

The electric field is in the same direction as that of the force acting upon a positive test charge or in the opposite direction as the force acting on a negative test charge. In this manner the field lines (or lines of force) are directed from positive charges to negative charges. The electric field produced by a charge Q is:

$$E = \frac{Q}{4\pi\varepsilon_0 R^2} i_R \qquad \text{(F.5)}$$

Q = value of the static charge creating the field.

R = distance from the charge

i_R= The unit vector uniting the two points under consideration.

To calculate the electric field of a system of charges at a given point, we first calculate the field of each charge in that point and then do the summation. This is known as the principle of Superposition:

$$E = \frac{Q_1}{4\pi\varepsilon_0 R_1^2} i_{R_1} + \frac{Q_2}{4\pi\varepsilon_0 R_2^2} i_{R_2} + \cdots + \frac{Q_n}{4\pi\varepsilon_0 R_n^2} i_{R_n} \qquad \text{(F.6)}$$

A way of visualizing an electric field is to spread grass seeds over a liquid, like oil, and place two electrodes (a positive and negative) into the oil. You will see the seeds align with the electric field.

An electric field could be defined as: "The region of space surrounding static electric charges, which may be mapped by drawing lines of electric flux and orthogonal equipotential lines". These lines delineate the electric field surrounding the charges [2, 310].

F.1.3 Conductor Surface Electric Fields

The most important influencing factor in the occurrence and characteristic of corona discharges on transmission lines conductors is the electric field distribution in the region surrounding the conductor surfaces. In analyzing corona performance, information, on the variation of the electric field around the conductor as well as in the space just outside the conductor surface, is required. Electrostatic field principles have been applied to develop accurate methods for the determination of conductor surface electric fields of transmission lines, particularly for lines using bundled conductors.

The corona performance of a transmission line which, is defined by effects such as,

- Corona Loss
- Radio Interference and
- Audible Noise

Depends mainly on two sets of factors:

- Line Design
- Ambient Weather Conditions

The line design factors of interest are the type and dimensions of the conductor, phase spacing in the case of AC lines and pole spacing in the case of DC lines, and height above ground of the conductors. The most important factor that influences the generation of corona, however, is the electric field distribution in the vicinity of the conductor surface.

Ambient weather conditions influence the corona performance in two ways: firstly the temperature, pressure and relative humidity of the ambient air affect the basic ionization processes involved in corona discharges; and secondly any precipitation

such as rain or snow deposited, on the conductor surface, distorts the electric field in the vicinity.

F.1.4 The Differences between AC and DC Electric Fields

DC electric fields are different to their AC counterparts due mainly to the following factors: DC lines generate electric fields that are constant by nature, whereas AC lines produce electric fields, which oscillate in accordance with the frequency at which the system operates.

AC electric fields are independent of season, climate, weather and wind, depending only on the geometry and voltage of the conductors because they are determined only by the charge residing on the conductors [10, 1-63]. In the case of AC lines, electric induction effects on people and objects located near the line are produced mainly due to capacitive coupling, and corona [5].

Due to the constant nature of the voltage on DC lines, capacitive coupling is almost non-existent, while corona on the conductors and the resulting space charges play a dominant role in the induction effects produced [5]. The DC electric field causes charged particles to migrate to ground and to other objects. Voltages can therefore be induced on insulated objects to this ionic flow [30].

DC electric fields depend in a large part on the space. The DC field though undirectional, may slowly change as the space charge is moved by the wind. These fields vary, greatly with weather, season and climate. The electric field at ground potential has the polarity of the nearest conductor [10, 1-64].

The generation of air ions is peculiar to HVDC; these ions can reach concentrations significantly above ambient values near ground, both within and outside the right of way. This aspect of the HVDC environmental line performance is potentially the greatest constraint on line design [10, 1-64].

Two zones surround "live" DC conductors: [12, 73]

- Ionization zone and the
- Interelectrode zone.

The ionization zone is usually 2 cm thick for pole spacings' and conductor heights of about 15m.

The presence of the corona generated Space Charge phenomenon makes the electric field and charge environment in the vicinity of DC transmission lines complex and dynamic [6].

F.1.5 Electric Fields Between Various Electrode Configurations

The formulae for calculating the electric field strength for various electrode configurations are well known, some of them are given below.

- **Parallel Plate Electrodes:** If a voltage is applied between parallel plates the electrostatic field between them will be uniform. In general the electric field strength for this configuration is given by the following:

$$E = \frac{V}{d}$$

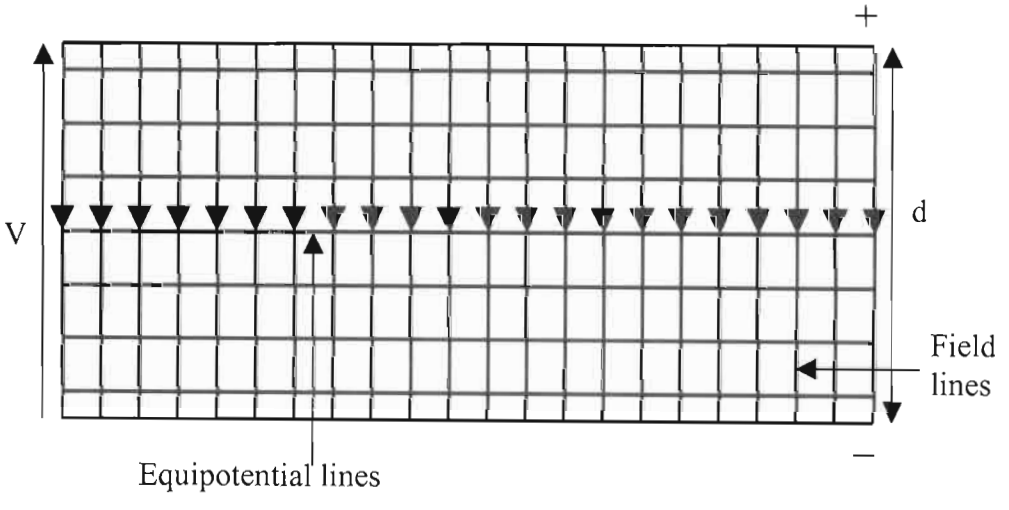

Figure F.2 Parallel Plate Electrode Configuration

Figure F.2 above shows us the parallel plate configuration. Since the field is uniform the electric field strength will be constant throughout the inter-electrode region. In practical cases the field strength will be higher at the edges of the electrodes due to the end or fringing effects.

- **Concentric cylinders:** If curved electrodes are used the electric field strength will not be constant throughout the interelectrode region. In this configuration the equipotential lines are much closer together near the inner conductor than at the outer conductor. This type of electric field is known as a non-uniform electric field.

  The electric field at any point between the inner and outer electrodes is given by the following formula:

$$E_r = \frac{V}{r \ln\left(\frac{b}{r}\right)}$$

  Where a < r < b

  a = inner radius

  b = outer radius

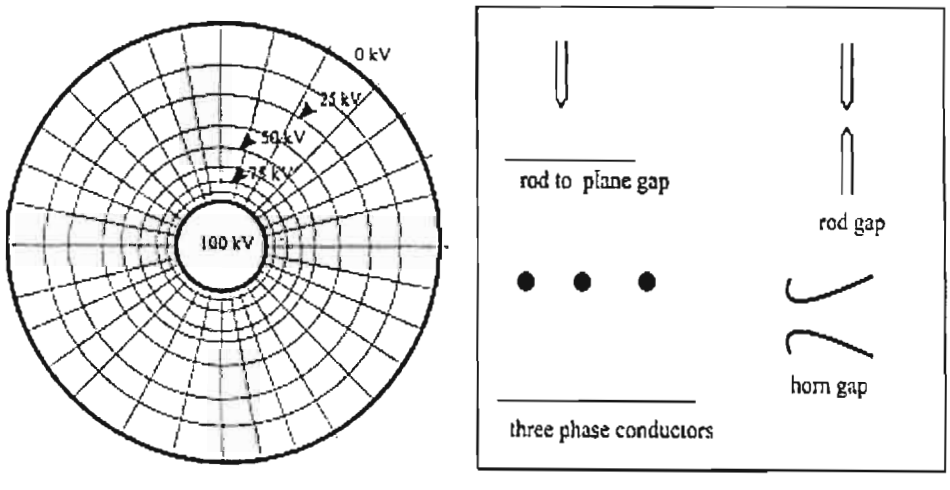

a) b)

Figure F.3: a) Field Between concentric cylinders, b) Other configurations which lead to non-uniform fields [17].

- **Concentric Spheres:** If a voltage V is applied between two concentric spheres the maximum electric field strength can be found using Gauss' Law and is as follows:

$$E_a = \frac{V}{a^2\left(\frac{1}{a} - \frac{1}{b}\right)}$$

When b $\rightarrow \infty$, that is if the sphere is isolated, then $E_a = \frac{V}{a}$.

F.2 Magnetic Fields

F.2.1 Definition of a Magnetic Field

A magnetized bar has its power concentrated at two ends, its poles; they are known as its north (N) and south (S) poles, because if the bar is hung by its middle from a string, its N end tends to point northwards and its S end southwards. The N end will repel the N end of another magnet, S will repel S, but N and S attract each other, shown in the figure below. The region where this is observed is loosely called a magnetic field.

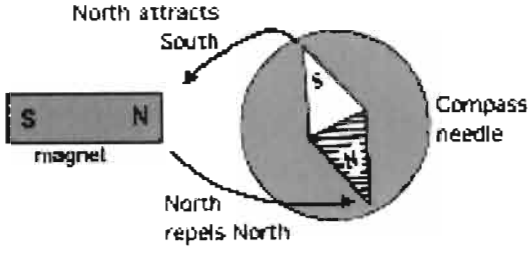

Figure F.4: Effect of Magnetic Poles [20].

Either pole can also attract iron objects such as pins and paper clips. That is because under the influence of a nearby magnet, each pin or paper clip becomes itself a temporary magnet, with its poles arranged in a way appropriate to magnetic attraction. But this property of iron is a very special type of magnetism, almost an accident of nature!

Out in space there is no magnetic iron, yet magnetism is widespread. For instance, sunspots consist of glowing hot gas, yet they are all intensely magnetic. The Earth's own magnetic powers arise deep in its interior, and temperatures there are too high for iron magnets, which lose all their power when heated to a red glow.

F.2.2 Electromagnetism

Matter consists of electrically charged particles: each atom consists of light, negative electrons swarming around a positive nucleus as seen in figure F.5. Objects with extra electrons are negatively (-) charged, while those missing some electrons are positively (+) charged.

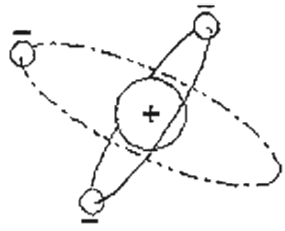

Figure F.5: The atom [20].

Such charging with "static electricity" may happen (sometimes unintentionally!) when objects are brushed with cloth or fur on a dry day. Experiments in the 1700s have shown that (+) repels (+), (-) repels (-), while (+) and (-) attract each other.

Close to 1800 it was found that when the ends of a chemical "battery" were connected by a metal wire, a steady stream of electric charges flowed in that wire and heated it. That flow became known as an electric current. In a simplified view, what happens is that electrons hop from atom to atom in the metal [20].

In 1821 Hans Christian Oersted in Denmark found, unexpectedly, that such an electric current caused a compass needle to move. An electric current produced a magnetic force [20].

Andre-Marie Ampere in France soon unraveled the meaning. The fundamental nature of magnetism was not associated with magnetic poles or iron magnets, but with electric currents. The magnetic force was basically a force between electric currents (figure below):

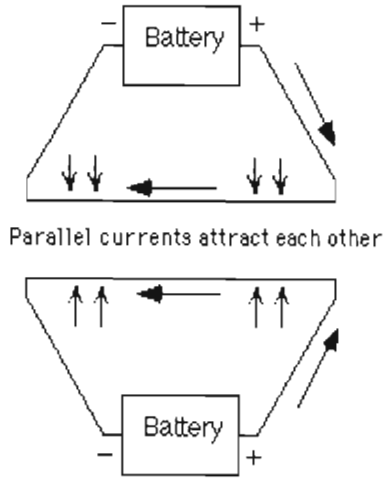

Figure F.6: Force Between Two Electric Currents [20].

Two parallel currents in the same direction attract each other

Two parallel currents in opposite directions repel each other.

Here is how this can lead to the notion of magnetic poles. Bend the wires into circles with constant separation:

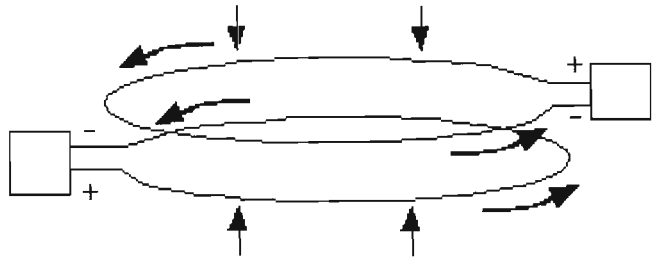

Figure F.7: Two Magnetic Loops [20].

- Two circular currents in the **same** direction **attract** each other.
- Two circular currents in **opposite** directions **repel** each other.

Replace each circle with a coil of 10, 100 or more turns, carrying the same current (figure below): the attraction or repulsion increases by an appropriate factor.

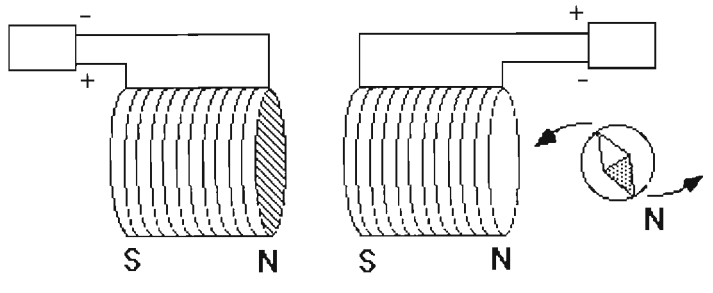

Figure F.8: Magnetic Coils [20].

In fact, each coil acts very much like a magnet with magnetic poles at each end (an "electromagnet"). Ampere guessed that each atom of iron contained a circulating current, turning it into a small magnet, and that in an iron magnet all these atomic magnets were lined up in the same direction, allowing their magnetic forces to add up.

The magnetic property becomes even stronger if a core of iron is placed inside the coils, creating an "electromagnet"; that requires enlisting the help of iron, but is not essential. In fact, some of the world's strongest magnets contain no iron, because the added benefit of iron inside an electromagnet has a definite limit, whereas the strength

of the magnetic force produced directly by an electric current is only limited by engineering considerations.

In space, on the Sun and in the Earth's core, electric currents are the only source of magnetism. We loosely refer to the region of their influence as their magnetic field.

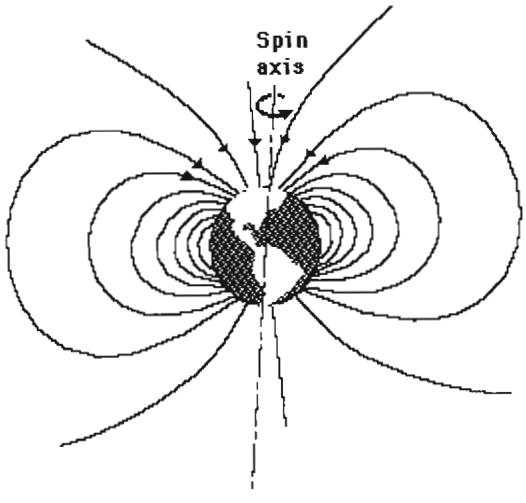

Figure F.9: The Earth's Rotation Inducing a Magnetic Field [20].

F.2.3 Differences between AC and DC magnetic fields

AC magnetic fields are alternating in nature and capable of inducing currents in circuits and conductive bodies. The magnetic field of DC lines is similar to the earth's magnetic field. These magnetic field values generally, do not exceed the value of the earth's field and have not been associated with any biological or health effects for people [10, 1-64].

The earth's natural magnetic field, ranges from 30 to 70 μTeslas(T) depending on the location of the measurement. Magnetic fields under HVDC transmission lines, which are static in nature, are typically of the order of 20 μT [13, 3].

F.3 SUMMARY

Electric charge is never created or destroyed, electric charge always comes in an integral multiple of a basic unit. Like charges repel each other and unlike charges attract each other. The basic unit of charge is the Coulomb (C).

Electric field intensity is measured in Newtons per Coulomb or more commonly in Volts per Meter. The electric field is in the same direction as that of the force acting upon a positive test charge or in the opposite direction of the force acting upon a

negative test charge. This means that field lines are directed from the positive charge to the negative charge.

Electric field distribution in the region surrounding the conductor is the most important factor, influencing the occurrence and characteristics of corona discharges on transmission lines.

DC electric fields differ from AC electric fields in that DC transmission lines generate electric fields which are static in nature whereas AC transmission lines generate electric fields which oscillate in accordance with the frequency at which the system in question operates.

Electric fields can be broken up into two sets, these are:

- Uniform fields and
- Non-uniform fields

Electric currents can cause magnetic fields to occur. Two parallel currents in the same direction attract each other and two parallel currents in the opposite direction repel each other.

AC magnetic fields are alternating in nature and capable of inducing currents in circuits and conductive bodies. DC magnetic fields are similar to the earth's magnetic field. The DC field magnitude generally does not exceed the earth's magnetic field values.